DISSERTATION

Submitted to the
Combined Faculty of Natural Sciences and Mathematics
of the Ruperto Carola University Heidelberg, Germany
for the degree of
Doctor of Natural Sciences

Presented by
M.Sc. Shubhankar Sood
Born in: Chandigarh, India
Oral examination: 11th August 2021

Characterization of Bone Marrow Mesenchymal Stem Cell Niche Dynamics upon Stress, with Focus on Clinical Translation

Referees:

Prof. Dr. Andreas Trumpp

Prof. Dr. med. Daniel Nowak

"The important thing is not to stop questioning. Curiosity has its own reason for existence. One cannot help but be in awe when he contemplates the mysteries of eternity, of life, of the marvelous structure of reality. It is enough if one tries merely to comprehend a little of this mystery each day."

Albert Einstein

ABSTRACT

The bone marrow niche is a complex organ system, which has classically been studied for its role as the seedbed of hematopoiesis. Recent research has highlighted the complexity of the bone marrow at the cellular level unraveling Mesenchymal Stem Cells (MSC) as critical supporting cells for Hematopoietic Stem Cells (HSCs). However, little is known about the role of MSCs in physiological and pathophysiological states of the bone marrow. Therefore, in the first part of this thesis, we studied the engagement of MSCs in the stress response of the murine bone marrow niche over time. In the second part of this thesis, the HSC expansion potential of MSCs was studied and translated into a human system in order to overcome the limitations of HSC transplantation for regenerative medicine. Taken together, my thesis deals with the **"Characterization of Bone Marrow Mesenchymal Stem Cell Niche Dynamics upon Stress, with Focus on Clinical Translation".**

Inflammation is a key component in the complex biological response of the body to harmful stimuli. In the context of the bone marrow, inflammation is an overarching process central to most if not all forms of stress challenges and disease settings. Current research in the field is focused on understanding the response of HSCs to inflammation. While such research provides descriptive understanding of the HSC niche with its stromal compartment, it falls short in translating this into functional applications confounded by a single marker approach of classifying the niche cell diversity. In this thesis, we utilized the power of single-cell sequencing coupled with a functional proliferation readout to investigate inflammation response over time of an unbiased bone marrow niche. Further, we identified and described a novel inflammation-responding MSC (iMSC) population which, unlike its stromal counterpart, responded directly and dynamically to IFNα stimulation. We showed that iMSCs uniquely produce key inflammation cytokines and secreted factors at the onset of the IFNα response while they

markedly downregulated extracellular matrix (ECM) factors and, thus, facilitated niche remodeling at a late time point. Using ligand-receptor mapping, we further identified pivotal inflammation-specific interactions between iMSCs and HSCs within the bone marrow. Hence, we concluded the first part of my thesis with a novel iMSC signature with direct application in unravelling inflammation dynamics of the bone marrow niche. The proposed iMSC signature has the potential to significantly contribute to our understanding of bone marrow niche perturbations in disease settings, like leukemia and immunodeficiencies.

Bone marrow transplants (BMTs) have highlighted the HSC potential to restore a new functional hematopoietic system in diseased recipients. However, a major roadblock for this scientific breakthrough is our limited potential for *ex vivo* HSC expansion. In the second part of my thesis, we propose a potent *ex vivo* HSC expansion system based on bone lining-derived reinvigorating Mesenchymal Stem Cells (rMSCs). Using a functional approach, we created a robust pipeline for the fluorescence-activated cell sorting (FACS)-based isolation and *ex vivo* expansion of rMSCs from both murine and patient-individualized human samples. The bulk and single-HSC long-term expansion using rMSCs maintained phenotypic stemness over multiple cell differentiation cycles and provided functional bone marrow reconstitution capabilities upon transplant. Notably, our rMSC co-culture system outperformed existing alternatives for HSC expansion including systems using stromal cells, non-cellular coating factors, or different medium compositions. Further, using our donor-individualized experimental strategy, we isolated and analyzed both plastic-adherent stromal cells (PASCs) and rMSCs from the same patient sample highlighting more favorable gene expression profiles in rMSCs compared to PASCs for HSC expansion. Thus, with the second part of this thesis, we showed that our rMSC-based system for HSC expansion can play a pivotal role in research to reduce the number of mice used for *ex vivo* experiments. Moreover, our patient-individualized

rMSC-based HSC expansion system could potentially be used for curative and personalized gene therapy in numerous diseases.

In summary, with my thesis, I deciphered functional subsets of murine stromal cells regulating the *in vivo* inflammatory response of the bone marrow and promoting *ex vivo* HSC expansion. Our functional approach of stromal cell characterization revised the current understanding of the bone marrow niche and holds the promise for clinical breakthrough.

Keywords: Bone marrow niche, Murine mesenchymal stromal/stem cells, Microenvironment, Inflammation, Interferon-alpha, Single-cell transcriptomics, Hematopoietic stem cells, *ex vivo* expansion, Human mesenchymal stromal/stem cells, Bone marrow transplant, Personalized medicine.

ZUSAMMENFASSUNG

Die Nische des Knochenmarks ist ein komplexes Organsystem, das klassischerweise für seine Rolle als Keimzelle der Hämatopoese untersucht wurde. Neuere Forschungen haben die Komplexität des Knochenmarks auf zellulärer Ebene hervorgehoben und mesenchymale Stromazellen (MSC) als kritische Unterstützungsfaktoren für hämatopoetische Stammzellen (HSCs) entschlüsselt. Allerdings ist wenig über die Rolle von MSCs in physiologischen und pathophysiologischen Zuständen des Knochenmarks bekannt. Deshalb haben wir im ersten Teil dieser Arbeit das Mitwirken von MSCs in der Stressantwort der murinen Knochenmarksnische im Zeitverlauf untersucht. Im zweiten Teil dieser Arbeit wurde das HSC-Expansionspotential von MSCs untersucht und auf ein humanes System übertragen, um die Grenzen der HSC-Transplantation für die regenerative Medizin zu überwinden. Insgesamt befasst sich meine Arbeit mit der **"Charakterisierung der Stress-Dynamik von mesenchymalen Stromazellen der Knochenmarknische, mit Fokus auf klinische Translation".**

Entzündungen sind eine Schlüsselkomponente in der komplexen biologischen Antwort des Körpers auf schädliche Reize. Im Kontext des Knochenmarks ist die Entzündung ein übergreifender Prozess, der für die meisten, wenn nicht sogar alle Formen von Stressherausforderungen und Krankheitssituationen zentral ist. Die aktuelle Forschung auf diesem Gebiet konzentriert sich auf das Verständnis der Antwort von HSCs auf Entzündungen. Die Forschung liefert daher ein deskriptives Verständnis der HSC-Nische mit ihrem stromalen Kompartiment. Dies kann jedoch nicht in funktionelle Anwendungen übertragen werden, da der Ein-Marker-Ansatz zur Klassifizierung der Zellvielfalt in der Nische dies verhindert. In dieser Arbeit haben wir die Leistungsfähigkeit der Einzelzellsequenzierung in Verbindung mit einer funktionellen Proliferationsmessung genutzt, um die Entzündungsreaktion einer unverfälschten Knochenmarksnische im Zeitverlauf zu untersuchen. Darüber hinaus

identifizierten und beschrieben wir eine neuartige, auf Entzündungen reagierende MSC-Population (iMSC), die im Gegensatz zu ihrem stromalen Gegenstück direkt und dynamisch auf die IFNα-Stimulation reagierte. Wir konnten zeigen, dass iMSCs wichtige Entzündungszytokine und sezernierte Faktoren zu Beginn der IFNα-Antwort produzieren, während sie extrazelluläre Matrix (ECM)-Faktoren deutlich herunterregulieren und somit die Nischenumstrukturierung zu einem späten Zeitpunkt erleichtern. Mittels Liganden-Rezeptor-Mapping konnten wir darüber hinaus entscheidende entzündungsspezifische Interaktionen zwischen iMSCs und HSCs im Knochenmark identifizieren. Damit schlossen wir den ersten Teil meiner Dissertation mit einer neuartigen iMSC-Signatur ab, die eine direkte Anwendung bei der Entschlüsselung der Entzündungsdynamik in der Nische des Knochenmarks ermöglicht. Die vorgeschlagene iMSC-Signatur hat das Potenzial, wesentlich zu unserem Verständnis von Störungen der Knochenmarksnische bei Krankheiten wie Leukämie und Immundefekten beizutragen.

Knochenmarktransplantationen (BMTs) ermöglichen die Wiederherstellung eines neuen funktionellen hämatopoetischen Systems in erkrankten Empfängern. Ein großes Hindernis für diesen wissenschaftlichen Durchbruch ist jedoch unsere begrenzte Fähigkeit für die *ex vivo* HSC-Expansion. Im zweiten Teil meiner Dissertation schlagen wir ein sehr wirksames *ex vivo*-HSC-Expansionssystem vor, das auf reinvigorierenden mesenchymalen Stromazellen (rMSCs) basiert, die von der Knochenoberfläche, dem Übergang zwischen Knochenmark und Knochengewebe, stammen. Unter Verwendung eines funktionellen Ansatzes haben wir eine robuste Pipeline für die Fluoreszenz-aktivierte Zellsortierung (FACS)-basierte Isolierung und *ex vivo*-Expansion von rMSCs sowohl aus murinen als auch aus menschlichen Patientenproben entwickelt. Die Langzeitexpansion von rMSCs als Bulk- und Einzel-HSCs behielt den phänotypischen Stammzustand über mehrere Zelldifferenzierungszyklen bei und ermöglichte eine funktionelle Knochenmarkrekonstitution

nach Transplantation. Insbesondere übertraf unser rMSC-Kokultursystem bestehende Alternativen für die HSC-Expansion, einschließlich Systemen, die Stromazellen, nicht-zelluläre Beschichtungsfaktoren oder unterschiedliche Medienzusammensetzungen verwenden. Darüber hinaus haben wir mit unserer patientenindividuellen experimentellen Strategie sowohl plastikadhärente Stromazellen (PASCs) als auch rMSCs aus derselben Patientenprobe isoliert und analysiert und dabei günstigere Genexpressionsprofile bei rMSCs im Vergleich zu PASCs für die HSC-Expansion festgestellt. Somit haben wir mit dem zweiten Teil dieser Arbeit gezeigt, dass unser rMSC-basiertes System für die HSC-Expansion eine zentrale Rolle in der Forschung spielen kann, um die Anzahl der für *ex vivo*-Experimente verwendeten Mäuse zu reduzieren. Darüber hinaus könnte unser patientenindividualisiertes rMSC-basiertes HSC-Expansionssystem potenziell für eine kurative und personalisierte Gentherapie bei zahlreichen Krankheiten eingesetzt werden.

Zusammenfassend lässt sich sagen, dass wir mit meiner Arbeit funktionelle Untergruppen von murinen Stromazellen entschlüsselt haben, die die Entzündungsreaktion des Knochenmarks *in vivo* regulieren und die HSC-Expansion *ex vivo* fördern. Unser funktioneller Ansatz der Stromazellcharakterisierung revidiert das aktuelle Verständnis der Knochenmarksnische und verspricht einen klinischen Durchbruch.

Stichwörter: Knochenmark-Nische, Murine mesenchymale Stromal-/Stammzellen, Mikroumgebung, Entzündung, Interferon-alpha, Einzelzell-Transkriptomik, Hämatopoetische Stammzellen, *ex vivo* Expansion, Humane mesenchymale Stromal-/Stammzellen, Knochenmarktransplantation, Personalisierte Medizin.

TABLE OF CONTENT

1 INTRODUCTION

1.1 A brief history of the bone marrow

The bone marrow is currently defined as the primary site for blood production, through a process termed hematopoiesis (1). The human bone marrow has an incredible turn-over rate, producing around 350 billion platelets, 180 billion erythrocytes and 12 billion lymphocytes on a daily basis (2). However, to understand the current narrative of the field we need to connect with the past conceptualization of the bone marrow.

While literature from the 17th century describes erythrocytes for the first time, it was not until the 19th century that researchers questioned the function and origin of the bone marrow (3). Hippocrates of Kos (460-370 BC), regarded as the *Father of Medicine* (4), and Aelius Galenus (129-210 BC), a pioneering medical researcher of his era (5), considered the bone marrow the nutrition source for the bone (6). Aristotle (384-322 BC) had a contradictory opinion and claimed that the bone marrow was a waste by-product (6). It was not until 1872 when Charles Robin reported the bone marrow to be highly vascular and formed after the bone during development, suggesting the bone marrow was not a nutritious source for the bone and rather had an independent function (3).

Ernst Christian Neumann (1834-1918) was a professor at the Pathological Institute at Konigsberg. He was the first to unravel the presence of nucleated erythrocytes and postulated the concept of erythropoiesis occurring in the human bone marrow (7). Further, Neumann published work describing the process of leukopoiesis and proposing the concept of a common stem cell for all hematopoietic cells (8). Neumann believed that all hematopoietic cells in an adult originated from post-embryonic stem cells that where formed in the bone marrow by reticulum cells (9), unaware of the concept of a 'hematopoietic inductive niche' which was not postulated until the 20th century (10).

Giulio Bizzozero (1846-1901), regarded as a pioneer of histology, was a professor of general pathology at the university of Turin. He not only went on to confirm Neumann's claims regarding erythrocytes and leucocytes in his two publications, but also identified platelets as the third constituent of the blood (11). Bizzozero put forth the concept of hemostasis or arresting the flow of blood to be the major function of the platelets. He went on to build on his bone marrow model by suggesting that the platelets represented an independent cell lineage and hemostasis was not synonymous to blood coagulation (12).

Sir William Osler (1849-1919) was one of the founding professors of the Johns Hopkins Hospital and is regarded as the *Father of Modern Medicine* (13). He gave a series of three lectures in New York combining his own research with the likes of Neumann and Bizzozero, proposing a detailed model of the bone marrow. In his book titled *The Principles and Practices of Medicine* published in 1892, Osler postulates the concept of a hematopoietic differentiation tree with a common stem cell at the top of the hierarchy branching out into distinct lineages (14). Interestingly, this early concept with its original idea still holds true until today. Though, it was only towards the end of the 19th century that this concept of hematopoiesis could be experimentally proved thanks to advancements in cell histology techniques. James Homer Wright developed the staining of the megakaryocytes and Paul Ehrlich's the aniline dye on heat-fixed bone marrow smears which allowed the analysis of the composition and changes in the bone marrow (15).

In the late 20th century, the bone marrow transplant became the landmark for hematological advancement (16). Once again highlighting how the model of the bone marrow has evolved over the course of history, pitted with controversial concepts and challenging ideas, along with evolution in scientific technology.

1.2 The beauty in the complexity of the bone marrow

The bone along with its marrow is a vital and complex organ. It is unique in its mechanical composition with a gradient of hard calcified bone tissue on the outside to viscous bone marrow as we move inwards (17). In part due to its mechanically optimized structure, the bone also has a marked hypoxia gradient (18,19). This unique balance between its structure and composition is reflected in its two important functions: provide mechanical integrity for the body to enable mobility and serve as the primary site for hematopoiesis (20). The bone marrow niche in itself has a complex biological makeup with numerous cell types interacting with each other through both juxtracrine and paracrine signaling (21). Adding to the apparent complexity, the bone marrow is both highly vascularized and rich in secreted factors all of which harmoniously work together making the bone marrow a unique organ system.

1.2.1 Cellular components

A number of cell types have been suggested to be part of the bone marrow niche including hematopoietic stem cell (HSCs), osteoblasts, endothelial cells, perivascular cells, megakaryocytes, sympathetic nerve cells and mesenchymal stem/stromal cells (MSCs) (22). HSCs are a small population of hematopoietic cells responsible for the lifelong production of blood and immune cells (23). Arguably one of the most well studied stem cell types, HSCs reside in a specialized microenvironment in the bone marrow termed as the HSC niche (24). At homeostasis, HSCs are maintained in a long-term quiescence state in part by its niche and are activated to cycle on demand (25).

The bone marrow niche is shown to be perivascular, created in part by MSCs and lined by endothelial cells and often, but not always, located near trabecular bone (26). Early studies shed light on the crucial role of the bone marrow niche and HSC interaction. Osteolineage cells in particular osteoblasts have been identified as a key component of the endosteal HSC niche

(27) . *In vitro*, HSC growth is supported by osteoblastic cells and *in vivo* ablation of osteolineage cells markedly disrupts hematopoiesis (28). In addition, transgenic mouse models and intermittent parathyroid hormone (PTH) administration systems have been used to study important hematopoietic factors expressed by osteolineage cells (29,30).

Throughout embryogenesis the hematopoietic system dynamically interacts with the vasculature, with endothelial structures giving rise to the first definitive HSCs during fetal development (31,32). The blood vessels not only play a critical role in adult bone remodeling but also in trafficking hematopoietic stem and progenitor cells (HSPCs) between the bone and the bloodstream (33). Blocking angiogenesis signaling via endothelial cells in the bone marrow has shown to have detrimental effects on the engraftment of HSCs post-transplant (34,35). Endothelial cells have also been shown to directly affect HSC proliferation by expressing endothelial cell-specific adhesion molecule E-selectin (36), and the lack of endothelial-specific factors like vascular endothelial growth factor (VEGF) causes bone marrow failure (35,37). With the arteriole running along the length of the long bones and sinusoids traversing perpendicular to the long axis, the bone marrow vasculature thus constitutes a rather large and crucial cellular component of the adult bone marrow (38,39).

Perhaps the most controversial addition to this list are the bone marrow MSCs. Even though multiple high impact research publications highlight the spatial association of the HSCs with the MSC niche in the bone marrow, this cell population has been difficult to characterize (26,40). Classically the MSCs are defined as multipotent stromal cells with the potential to give rise to adipocyte, chondrocytes and osteogenic lineage (41). However, in part due to their heterogeneity and lack of consensus on their defining features the MSCs still remain a black-box. Recent advancement in deep bone imaging complemented with sophisticated transgenic mouse models have contributed to our understanding of the MSCs as an active bone marrow niche component (21,42). Studies show significant improvement in donor engraftment upon co-transplantation of MSCs with HSPCs and enhanced murine HSC self-renewal potential

(43,44). The field has defined MSCs based on the active HSC niche factor they express *e.g.* Nestin^{+} stromal cells, CXCL12-abundant reticular cells, SCF-expressing cells and Leptin receptor-expressing cells, to name the well-studied MSC types (26,42,45–47).

1.2.2 Biochemical properties

The bone marrow due to its cellular diversity is very rich in biochemical signaling molecules, including growth factors, cytokines, chemokines, morphogens and adhesion molecules (48,49). These biochemical molecules have been shown to contribute both directly and indirectly to the bone marrow niche function, by providing paracrine and juxtracrine signaling (50). Thrombopoietin (TPO) and osteoblast derived factor angiopoietic-1 (ANGPT1) bind to their respective receptors MPL and TIE2 on the HSCPs to regulate quiescence (51–53). Whereas, C-X-C motif chemokine receptor 4 (CXCR4) signaling via C-X-C motif chemokine 12 (CXCL12) abundant reticular cells (CAR cells) are pivotal in HSPC pool maintenance and expansion potential (42,46).

Growth factors like Stem Cell Factor (SCF) and C-X-C chemokine ligand 12 (CXCL12) are known to be non-cell-autonomously required for HSC microenvironment maintenance (54–58). SCF as a biomolecule is present in both soluble and membrane-bound forms in the bone marrow. SCF binds to its receptor KIT, expressed by hematopoietic cells and most importantly HSCs (59–61). Though, the role of SCF in HSC maintenance has been well documented, the source of the secreted factor is linked to multiple MSC types with distinct spatial localization across the bone marrow (62–64). Similarly, CXCL12-CXCR4 signaling is also crucial for the maintenance of a stable bone marrow microenvironment. Conditional deletion of Cxcr4 or Cxcl12, either globally or in a cell type-specific manner, depleted HSCs from the bone marrow and affected the proliferation of multiple restricted progenitors (42,65). Owing to this central

role of CXCL12 in the adult bone marrow, a sub-set of MSCs are defined solely based on this factor as CXCL12-abundant reticular cells or CAR cells (66,67).

Other important molecular components of the bone marrow niche include locally acting factors such as Notch ligands, Wnt/b Catenin signaling, VEGF signaling, BMPs, N-Cadherin and IL-6 that are all shown to modulate niche function but may be dispensable for adult HSC maintenance (34,48,68–70). Biochemical factors acting over a long-range to regulate the bone marrow niche include estrogen (source: ovaries), leptin (source: adipocytes) and thrombopoietin (source: liver and kidney, but bone marrow source unknown) (71–73).

1.2.3 Cell-to-cell interaction

Numerous cell-to-cell interaction participate in driving bone marrow niche behavior, under homeostasis. As an example, CAR cells have been shown to be in direct contact with the HSCs and play an important role in cell orientation during HSC division (46,66,74). Further studies have shown that HSPC survival and self-renewal is correlated with the transfer of reactive oxygen spices (ROS) to MSCs through connexin-43 (Cx43)-dependent gap junctions (75). Using whole-mount immunofluorescent imaging of the bone marrow vasculature, endothelial cells are reported to form sub-niches with direct contact with the leptin+ stromal cells and HSCs (42,45). Recent reports speculate on the role of the sympathetic nervous system in maintaining steady state homeostasis of the bone marrow (76). With non-myelinated Schwann cells interacting not only with the endothelial cells but also with the stromal cells to maintain HSC hibernation (77). In addition, autocrine ligand-receptor signals regulate a balance between proliferation and differentiation in the bone marrow. Including ANGPTI with its receptor TIE2, IGF-1 with its receptor IGF-1R and TNFα with its receptor TNFR (78–80). Molecular signals are further enhanced by positive feedback loops, such as hypoxia-inducible factor 1 alpha (HIF-1-α) and TPO driven transcription of VEGF by the endothelial cells with

profound downstream impact on the global bone marrow microenvironment (51,52,81–83). Multipotent stromal cells defined by their Leptin expression, residing at the cortical bone lining, directly interact with their osteoblastic progenitors to maintain steady bone turnover rate and adult bone mass (67,84). Moreover, in recent years, nestin^{+} stromal cells have been shown to interact with immature-adipocytes and play a role in HSC homing to the bone marrow niche post transplantation (85,86).

1.2.4 Biomaterial properties

The bone marrow niche is a complex multi-dimensional system that not only includes cellular and biochemical factors but also possess unique biomechanical properties. Bone marrow stiffness and extracellular matrix (ECM) representation, along with other physiochemical properties regulate the HSC quiescence, activation, proliferation and differentiation (87–89). Often overlooked, the extracellular matrix provides a mechanical scaffold and serves as a source of proteases and growth factors for the bone marrow microenvironment (90). Analysis of the bone marrow both *in vivo* and *in vitro* has identified the presence of fibronectin, laminin, collagenase (mostly I, IV, V & VI) and other large molecules such as syndecan, biglycan, hyaluronan and glycosaminoglycan (91–95). The bone marrow MSCs are labelled as the chief producers of most of these ECM factors, followed by osteoblasts and endothelial cells (96–99). The extent of ECM effect on the MSCs and the osteo-lineage can be elucidated by a study of mice lacking the ECM component biglycan. These knock-out mice exhibit defects in the ability of marrow derived progenitors to differentiate into mature osteoblasts (100,101). In the context of hematopoiesis, the ECM has been reported to directly or indirectly modulate HSC physiology (102–104). In particular, the ECM proteins play an important role in HSC mobilization from the niche. For example, hyaluronic acid has been shown to be anchoring HSCs to the bone marrow which can be cleaved by CD44 to partially

mobilize the stem cells into circulation (105,106). In myeloma patients, it has been observed that the bone marrow niche is significantly stiffer in comparison to healthy individuals. Further, this increased stiffness was linked to the disease progress with the myeloma niche being preferential to myeloma stem cells homing (107,108).

1.2.5 Gas concentration

The physiological role of oxygen, and thus lack thereof, in the context of cellular respiration is well documented. Although hypoxia is not common in most healthy human tissue, the bone marrow is somewhat unique with a distinct hypoxia gradient (109,110). The importance of hypoxia and hypoxia-inducible-factor-1 (HIF-1) was studied using an elegant osteoblast-specific genetic deletion of *Hif1α* mouse model. The study demonstrated the direct effect of hypoxia on bone development and turnover rate (111). Further, data suggests a broader role of hypoxia in regulating multiple niche populations including MSCs and HSCs. *In vitro* data suggests that osteo-primed stromal cells are more supportive of HSPC culture under hypoxia, with HIF being stabilized in these osteo-stromal cells (112,113). On the contrary, deletion of *Hif1α* gene on the HSCs causes their rapid exit from dormancy and results in myelosuppression (111). Moreover, pharmacological stabilization of HIF-1α protein in HSCs results in lower metabolic activity and quiescence (114). Studies have also linked a typical feature of the HSCs to preferentially home at the endosteal region of the bone marrow, which is characterized by low perfusion and distinctive hypoxia (115,116). Further, recent technologically advanced research uses sensitive oxygen sensors to better quantify the *in vivo* hypoxia gradient in the bone marrow niche (117–119). The molecular response of the cellular components to the oxygen gradient in the bone marrow was a crucial discovery, which won the 2019 Nobel prize in physiology or medicine, and has broadened our understanding of gas exchange in the bone marrow (120).

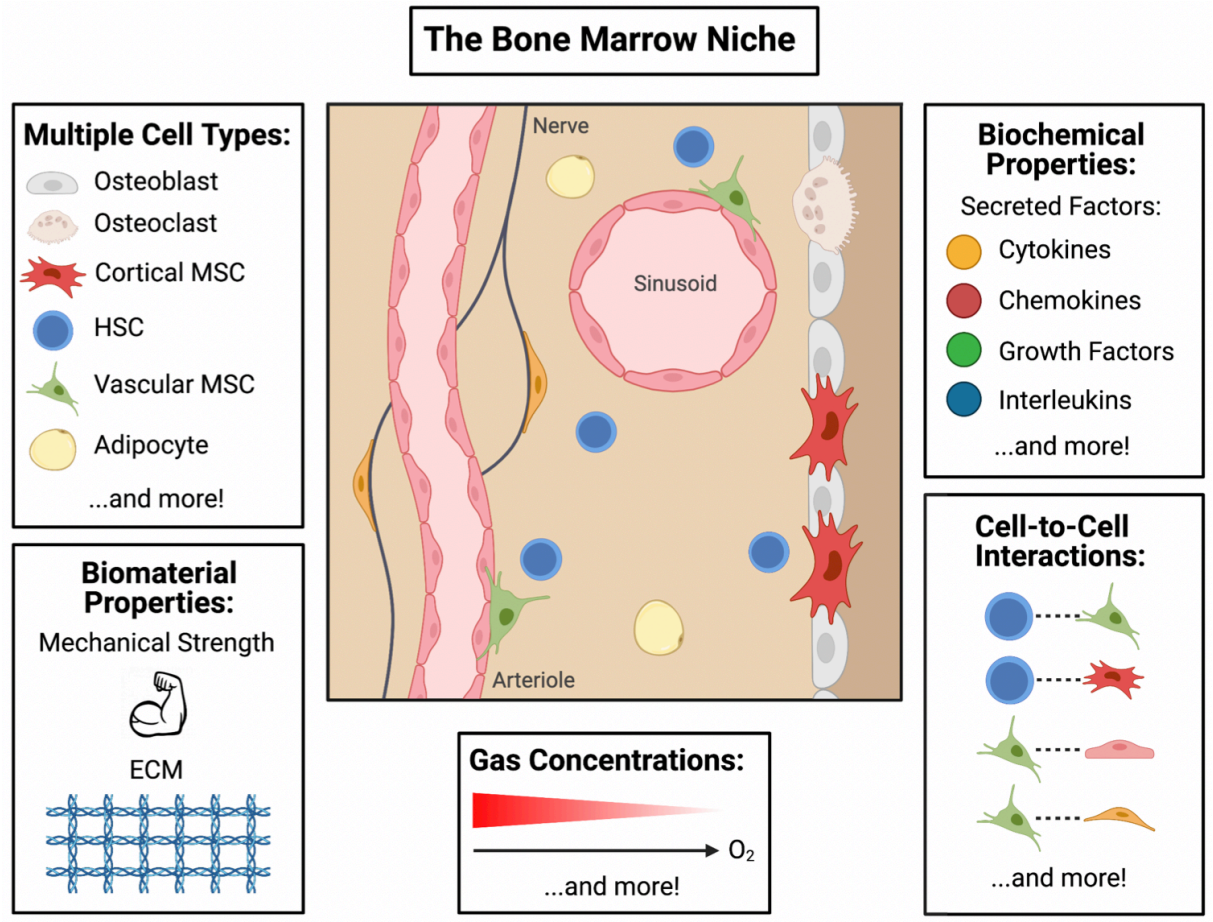

Figure 1. The components of an adult bone marrow niche. The bone marrow is a complex organ system with multiple cell types, interacting with each other both directly or through the production of numerous secreted molecules. Adding an additional layer of complexity, the bone marrow has a dynamic physiochemical architecture along with a characteristic hypoxia gradient. A combination of these factors makes the bone marrow niche a complex yet unique structure.

1.3 The bone marrow Mesenchymal Stem/Stromal Cells

The MSCs are a rare population of multipotent cells, as stated previously, and are characterized by their *in vitro* tri-lineage differentiation potential *i.e.* adipocytes, chondrocytes and osteocytes (121,122). Within the bone marrow, MSCs typically make up about 0.01% of total cells and 0.1% of stromal cells, not accounting for the variability due to digestion (86,123). While bone marrow MSC research has gained a lot of traction in the last decade, both in murine and human system, this cell type has been particularly difficult to define, in part due to lack of consensus on its critical characteristic be it plastic adherence *in vitro,* functional *in vivo* readout

or variable cell surface markers. Nonetheless, numerous studies have utilized elegant transgenic murine models supplemented with advanced whole-bone imaging technique to demonstrate the important role of MSCs as an active component of the bone marrow niche (26,41,88).

In the murine system, groups have focused on defining MSCs based on their expression of critical HSC signaling molecules like CXCL12 and SCF. Morrison's group, among others, used a *Cxcl12* conditional deletion model to propose leptin as a bona-fide marker for MSCs (67). Using leptin receptor-Cre to specifically delete *Cxcl12* expression, they further went on to show that the HSCs were mobilized from their niche but with no effect on their function (124). Prior studies from the Frenette's group identified MSCs based on their expression of nestin using a GFP-tagged system (26,125). These nestin-GFP+ MSCs where enriched for colony forming unit-fibroblast (CFU-F) activity and expressed high levels of Kit ligand and CXCL12, classical HSC maintenance factors (26). A broader classification of MSCs are under the umbrella term CXCL12-abundant reticular cells (CAR cells) based on the assumption that they express the highest amount CXCL12 chemokine in the bone marrow (42,66,126). Deletion of *Cxcl12* gene in CAR cells using osterix-cre results in dysregulation of HSC quiescence and has deleterious effect on their repopulation capacity (127,128). Another rather recent model of MSCs suggests the Ng2-CreER^{+} cells to be the main source of CXCL12 and SCF in the bone marrow (125). However, this model is still under debate as conditional deletion of *Scf* using Ng2-CreER has no effect on HSC numbers and adult hematopoiesis (45,129–131).

For the human system, the International Society for Cellular Therapy (ISCT) proposed minimal criteria to define MSCs. Human MSCs must be plastic-adherent when maintained in 2D *in vitro* culture conditions. They must express CD73, CD90 and CD105 on their surface while lacking the expression of CD34, CD45, CD14, CD19 and HLA-DR surface molecules. In addition, human MSCs must also differentiate into adipocytes, osteoblast and chondroblasts in culture (132). While the criteria proposed by ISCT aim at standardizing human MSC clinical translation, new reports suggest an unaccounted heterogeneity in the MSC pool (133). Using

latest transcriptional profiling techniques at the single-cell level, researchers are now unravelling the complexity of the human stromal system (40,134).

1.4 The Mesenchymal Stem/Stromal Cell niche concept

According to the niche hypothesis, biochemical signals and physiochemical properties of the microenvironment governs the stem cells response and fate (135). In the context of the bone marrow, the majority of the studies have focused on the HSC microenvironment termed HSC-niche or HSC instructive niche (41,136,137). Newer models look at the bone marrow niche from the MSC perspective, postulating distinct MSC-HSC niche concepts (26,86). Broadly, the MSC niche concept can be subdivided into two major categories *i.e.* macro-vascular niches and micro-HSC specific niches.

The vascular-MSC niche concept stems from the observation that HSCs preferentially home in proximity of the sinusoid and arteriole within the bone marrow (125). This gave rise to the peri-sinusoidal and peri-arteriolar niche models (26,125,138,139). Studies suggest the peri-sinusoidal niche to be nestin^{+} MSC-dominant in contrast to the peri-arteriolar niche which is leptin^{+} MSC-specific, with both serving as active HSC niches (46,137,140). The peri-sinusoidal and peri-arteriolar microenvironment differ with respect to vessel wall permeability, oxygen tension and the capacity of HSCs to migrate through the vessel walls (118,139,141,142).

The newer and controversial micro-niche concept builds on the immediate HSC instructive surrounding, including directly associated MSCs and endothelial cells along with local molecular signals produced by them (39,88,136). This model assumes the long-term HSC (LT-HSC) at its center and characterizes the local cellular and non-cellular microenvironment around it (26,143). Using Saturn-Capture microdissection technique and cutting-edge single-cell spatial transcriptomics, new studies have been able to substantiate the micro-niche model in liver, brain and to a certain degree in the bone marrow (134,144–147).

1.5 The bone marrow niche under stress

Exposure to stress stimuli such as blood loss, pathogens, chemotherapeutics agents and irradiation induces potent inflammation response in the bone marrow (148,149). The hemopoietic system goes through dramatic alteration to compensate for the increased demand for blood and immune cells (150). Studies have demonstrated that HSCs can not only sense but also directly respond to inflammatory cytokines (151,152). In response to inflammatory stress, the HSCs can alter their cell cycle properties, function and mobilization (153–157). Quiescent HSCs have been shown to be triggered into active cell cycle upon both type I and type II IFNα stimuli (151,154). Acute IFNα type I induces cell cycle activation of HSCs via IFNAR-STAT1 signaling, whereas chronic IFN exposure leads to LT-HSC exhaustion and accumulation of DNA damage (151,152).

Bone marrow endothelial cells line the vasculature and serves as a protective barrier against inflammation and immune response (158). Data suggests that in acute inflammation response of mice to IFNα the endothelial cells proliferate and leads to downstream vessel remodeling (159). This remodeling is mediated by increased production of vascular endothelial growth factor (VEGF) by both the HSCs and MSCs in the bone marrow. Further, immune response data to bacterial stress suggests increased vascular permeability by the direct response of endothelial cells to the stimuli (160).

Multiple sub-types of MSCs have also been shown to recognize and alter the niche response upon infection (45,46,125,128). MSCs can directly respond to insults via pathogen-specific receptors and produce microenvironment-modifying chemokines and cytokines (161). Moreover, in an acute infection model the MSCs have been shown to cause the expansion of myeloid progenitors and mature myeloid cells via increased secretion of interlukine-6 (IL-6) (162,163). Further, CAR cells cause increased mobilization of HSCs into circulation, upon infection, by suppressing the production of CXCL12 chemokine (58,75). In contrast, CAR cells

upregulate the production of C-C motif chemokine ligand 2 (CCL2) upon *Listeria* infection resulting in significant increase in circulating monocytes (161).

1.6 Interferons and downstream signaling

Interferons (IFNs) are a group of polypeptide cytokines that are secreted in response to viral infection (164,165). They have several important functions for both the host cell and its microenvironment. Importantly, IFNs induce both cell-intrinsic and cell-extrinsic antiviral state by causing the up-regulation of IFN stimulated genes (ISGs) (166). Further, they modulate the innate immune response of their neighboring cells by pro-inflammatory pathways and cytokine production (167,168). Moreover, IFNs also play a role in adaptive immunity as they can promote the production of antigen-specific B and T cells (164).

Based on the receptor through which they signal, IFNs can been categorized as type I (IFN-I), type II (IFN-II) and type III (IFN-III). IFN-I family can further be sub-categorized as IFNα, IFNβ, IFNε, IFNκ and IFKω. Though all IFN-I molecules signal through the same cell surface heterodimeric receptor IFNα/β (IFNAR). Most cell types in the body express IFNβ, whereas IFNα is somewhat unique to hematopoietic cells noticeably the HSCs and dendritic cells. The IFN-II family on the other hand consists only of IFNγ and is sensed by the IFNγ receptor (IFNGR). Predominately T-cells and natural killer cells secrete IFNγ. IFN-III is mainly restricted to epithelial cells and hepatocytes. IFNλ1 (IL-29), IFNλ2 (IL-28A), IFNλ3 (IL28B) and IFNλ4 make up the IFN-III family (169–172).

Secreted IFN-I cytokine binds to the transmembrane IFNAR receptor and triggers the receptor dimerization. In the canonical IFN-I-induced signaling pathway, IFNAR engagement causes the activation of tyrosine kinases Janus kinase 1 (JAK1) and tyrosine kinase 2 (TYK2), which leads to the phosphorylation of cytoplasmic signal transducer and activator of transcription 1 (STAT1) and signal transducer and activator of transcription 2 (STAT2).

Phosphorylated STAT1 and STAT2 translocate to the nucleus to from a tri-molecular complex with IFN-regulatory factor 9 (IRF9) termed IFN-stimulated gene factor 3 (ISGF3). ISGF3 in turn binds to the IFN-stimulated response elements (ISRE) leading to the direct transcription of the ISGs. Studies show that ISG-encoded proteins inhibit viral transcription, translation and replication. Furthermore, they are also reported to degrade the viral nucleic acid and modulate the cellular lipid metabolism (164,171,172).

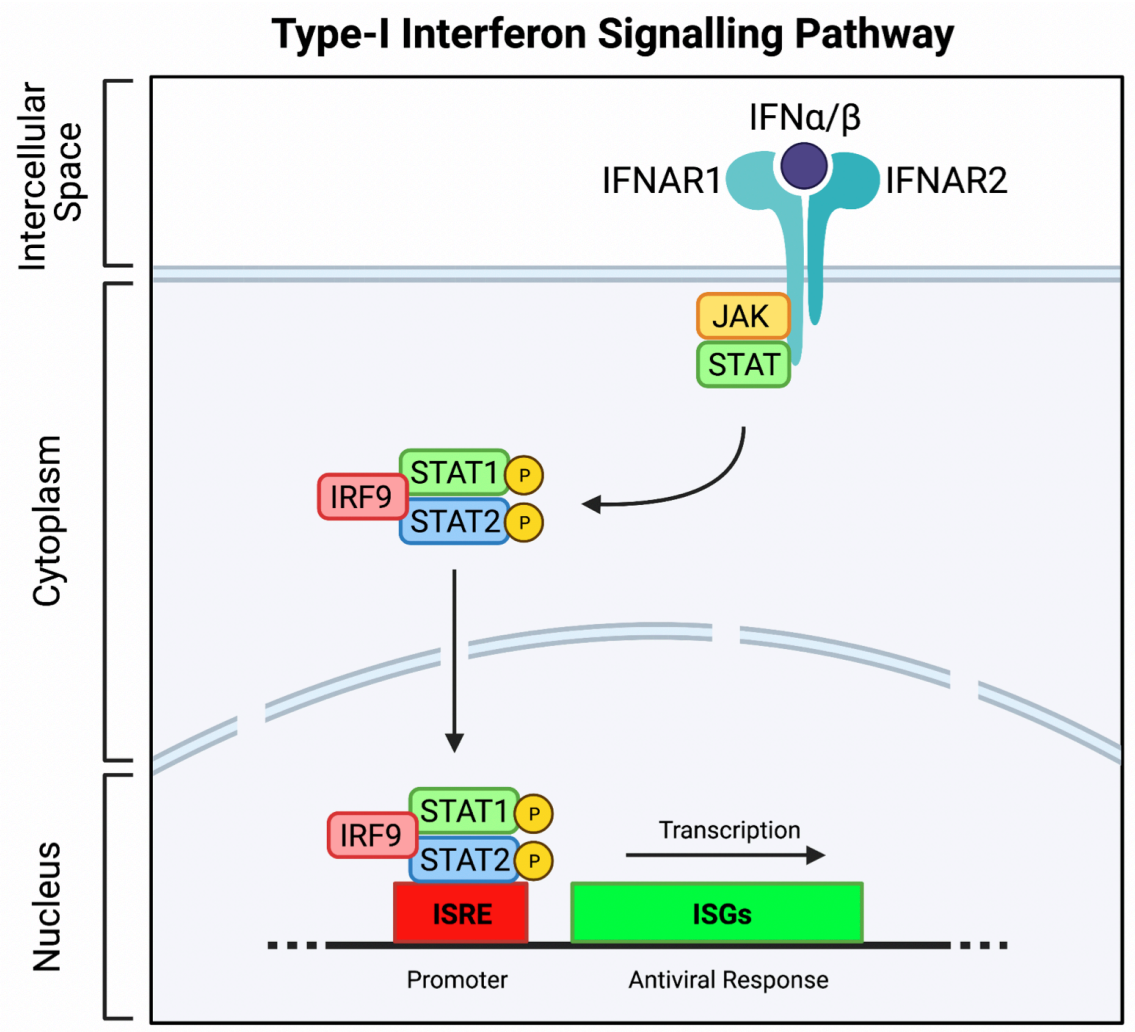

Figure 2. The canonical type-I interferon signaling pathway. Secreted IFNα and IFNβ binds the heterodimeric receptor IFNα receptor (IFNAR), composed of IFNAR1 and IFNAR2 subunits. Resulting in the activation of receptor associated Janus kinase 1 (JAK1), which in turn phosphorylates signal transducer and activator of transcription 1 (STAT1) and signal transducer and activator of transcription 2 (STAT2). The heterodimeric STAT1 and STAT2 translocate to the nucleus to associated with IFN-regulatory factor 9 (IRF9), forming the tri-molecular IFN-stimulated gene factor 3 (ISGF3). ISGF3 specifically binds to the IFN stimulated response element (ISRE) and induces the transcription of IFN stimulated genes (ISGs).

1.7 The malignant bone marrow niche

The historic notion of leukemia being a genetic disease has changed after the realization that leukemic stem cell (LSC) activity is influenced by microenvironmental cues (88,173,174). This discovery has encouraged research on extrinsic regulators of leukemia and has built a model of the malignant bone marrow niche.

Hematopoietic malignancies are characterized by abnormal bone marrow vasculature and angiogenesis (17,88). Thus, endothelial cell research in the context of leukemia has driven strong clinical interest (35,45,175). Malignant bone marrow studies have linked the endothelial cell specific pro-angiogenic VEGF pathway to disease progression, with anti-VEGF therapy in clinical trials (176,177). In the context of acute myeloid leukemia (AML), the bone marrow endothelial cells cause increased vascular permeability, reduced perfusion, and downstream remodeling of the vasculature (178,179). Further, the endothelial cells have also been suggested to dramatically increase the production of ROS and nitric oxide in a murine leukemia model resulting in loss of barrier function and cell death (148,180).

Clinical data suggests that hematopoietic malignances profoundly perturb the MSC bone marrow niche (143,181,182). Numerous studies highlight the MSC-dependent microenvironment remodeling upon leukemia (173). The most popular model suggests that the bone marrow stromal niche becomes more supportive of LSC, thus malignant hematopoiesis, and discourages HSC homing, thus health hematopoiesis (148,173). MSCs of the bone marrow of patients with myelodysplastic syndrome (MDS) have revealed increased methylation profiles compared to MSCs from healthy donors. In contrast, AML patients show a global hypo-methylation pattern in their MSCs (173,182). Myeloproliferative neoplasia (MPN) studies have shown that MSCs promote homing of LSCs through the expression of CXCL10, fibroblast growth factor (FGF) and IL-6 (183). Moreover, in patients with chronic myelogenous leukemia

(CML) the MSCs have been shown to have protective function over LSCs through the CXCL12-CXCR4 signaling pathway (184).

1.8 The Bone marrow niche in the clinic

A promising clinical application of the bone marrow niche is in context of bone marrow transplants (BMTs) and gene therapy (16). Bone marrow transplant as a concept was pioneered using stem cells derived from the bone marrow by Prof E. Donnall Thomas and his team, and was awarded the Nobel Prize in 1990 (185). This has led to the emergence of BMTs as the new paradigm, with the potential to restore a new functional hematopoietic system in diseased recipients (16,43,186). In most cases, BMTs are preceded by radiation therapy, chemotherapy or immunotherapy to reduce the malignant burden of the bone marrow and improve healthy HSC engraftment potential.

Radiation exposure is suggested to increase the mutation burden on the HSCs and cause serious damage to the bone marrow microenvironment (187). Studies comparing the micro-computed tomography analysis of the murine bone marrow post-irradiation to healthy controls show dramatic reduction in bone volume and compromised bone tissue (188). This deleterious effect of irradiation on the bone marrow architecture has been linked to a marked increase in osteoclasts, cells responsible for bone resorption (189). Further reports also highlight the destruction of collagen-depended ECM within irradiated murine bone marrow (190). On the contrary, radiation therapy has shown to increase bone marrow adipocytes which serve as a source of SCF for the HSCs to regenerate (191). Of note, there is controversial data on the MSCs being the direct source of the increased adipocytes in the irradiated marrow (192,193). Another comprehensive study on murine MSCs upon irradiation suggests differentiation skewing towards increased adipogenic and reduced osteogenic output (194,195).

Chemotherapy, a major branch of medical oncology, uses chemotherapeutic agents like cisplatin and 5-flurouracil (5-FU) causing myelo-ablation in a malignant bone marrow (196). Globally chemotherapy also results in the destruction of bone marrow architecture, including the stromal and vascular tissues (40,148). Studies suggest that 5-FU leads to the activation of quiescent HSCs and promoted their expansion in a FGF1-dependent manner (197,198). Conversely, 5-FU treatment has been linked to endothelial cell function by causing massive vasculature damage and leakiness (198,199). Furthermore, reports suggest that chemotherapy hampers the cross-talk between nestin+ MSCs and sympathetic nerves resulting in impaired HSC mobilization and compromised hematopoietic recovery (200).

In recent years, immunotherapy has become of great interest in the clinical setting as it promises fewer side effect by targeting malignant cells more specifically than radiation therapy or chemotherapy(148,201). As immunotherapy relies on either eliciting or amplifying the patient's immune response, it causes a significant increase in pro-inflammatory cytokine levels that can results in potentially lethal Cytokine Response Syndrome (CRS) (201,202). Murine CRS models show greatly elevated bone marrow serum levels of IL-10, IL-6 and IFNγ long after immunotherapy (203,204). Resulting in impaired HSC regeneration and a compromised bone marrow niche.

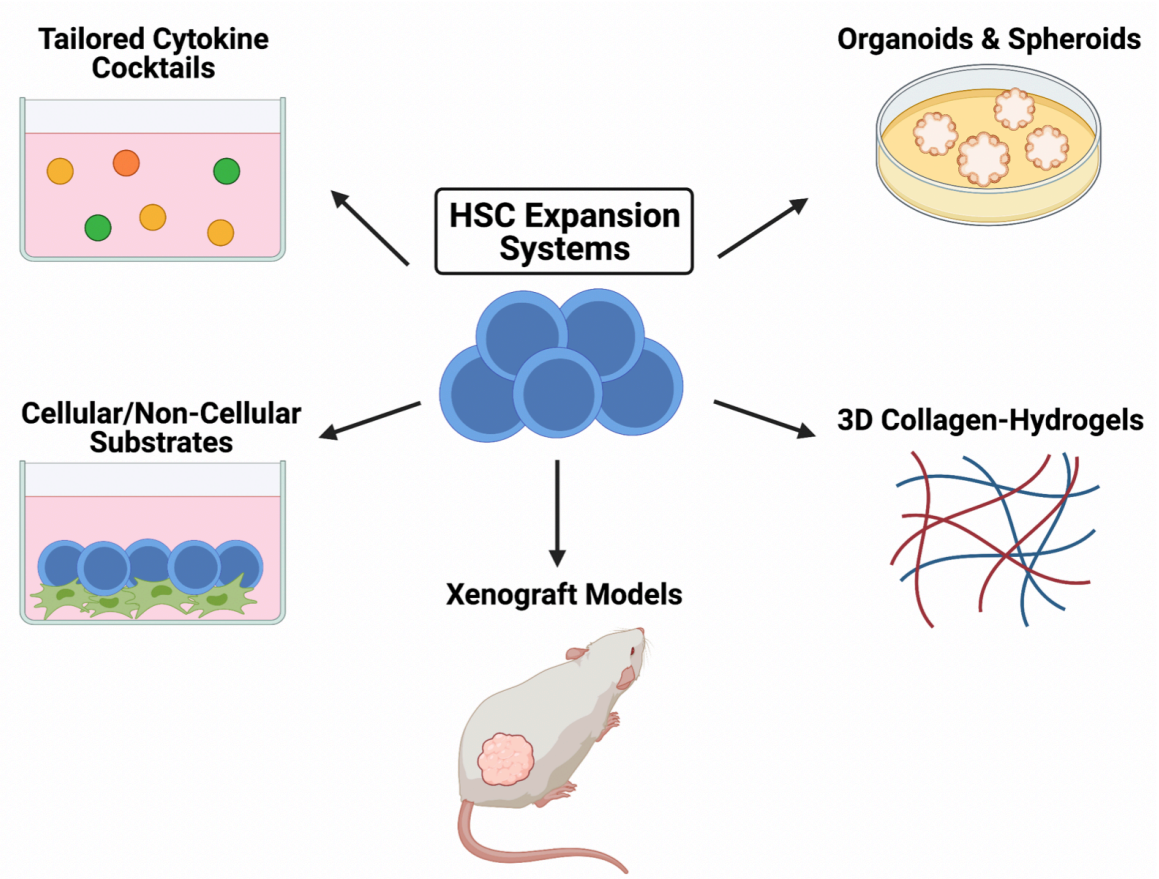

Figure 3. *Ex vivo* Hematopoietic Stem Cell (HSC) expansion systems. The bone marrow HSCs makeup the majority of stem cells used for clinical applications. There are numerous different *ex vivo* HSC expansion systems, each with their own merits and limitations. Some well-established expansion systems include, 2D *in vitro* tailored cytokine cocktail media and bone marrow ECM derived non-cellular/cellular coatings, 3D organoids and spheroids along with collagen-associated hydrogels, and murine xenograft models.

1.9 Stem cell expansion systems

A major roadblock in clinical application of the HSCs is the limited expansion of HSCs *ex vivo* with currently available techniques (23,205). Though, this concept of HSC expansion in itself is not new, with multiple studies proposing innovative solutions and companies providing optimized media, these approaches only offer limited success with no advancement in clinical transplants (206–210). On the other hand, even with our detailed understanding of the bone marrow stromal compartment, we fall short of a patient-specific stromal cell isolation and thus

genetic manipulation tools (23). Nonetheless, improvements in techniques from 2D cultures to 3D culture *in vitro* along with xenograft murine models are supporting advanced medical application (96,211,212).

Most HSC *ex vivo* expansion methods are tailored around either human CD34+ cells or murine LSK cells, both populations include stem and progenitor cells. Such expansion systems are required in clinic to provide both progenitors in the short-term and generate robust long-term reconstitution (23,205,212). *Boitano et al.* paved the way for human HSC expansion by their high-throughput screen of 100,000 small molecules and serum-free expansion medium with varying cytokine cocktails. They proposed an aryl hydrocarbon receptor antagonist, StemRegenin (SR1) to promote a 50-fold *ex vivo* expansion of human cord-blood derived $CD34^+$ cells (207). Further, Cooke's group demonstrated a striking 17-fold increase in long-term human HSC engraftment in immunodeficient mice (208). In the murine system, Yamazaki's group recently proposed a high TPO with low SCF media supplemented with polyvinyl alcohol (PVA) for long-term *ex vivo* HSC expansion. Under their media conditions the HSCs where shown to functionally expand between 236 and 899-folds over one month in culture (213).

In addition to soluble factors like cytokines, the bone marrow niche provides a complex ECM and a 3D scaffolding to the HSCs *in vivo.* Building on the biophysical properties of the HSC microenvironment, multiple studies have tested different ECM substrates including tissue culture polystyrene (TCPS), polyethylene terephthalate (PET) and polyether sulfone (PES) as HSC *ex vivo* expansion systems (214–218). Further, cellular coating with OP9 cells, fibroblasts and MSCs have shown a limited short-term expansion and survival potential on the HSCs (219–222). Advanced 3D HSPC culture systems using Matrigel supplemented with fibronectin suggests a 5-7-fold expansion at the expense of differentiation of the HSPCs into progenitors (212,223). Another study reported significant enhancement in engraftment of human cord-

blood $CD34^+$ cells in a murine xenograft model using GSK-3b inhibitor pretreatment regime (224,225).

These different strategies for the expansion of HSCs *ex vivo* or *in vitro* exploit the most current knowledge that HSCs rely on the bone microenvironment for proliferation, expansion and differentiation. Still the approaches cannot fulfill the objective of sufficiently high HSC numbers of clinical grade quality for transplantation. With my PhD project, I have further investigated the role of MSCs in the maintenance and expansion of HSCs in order to come up with an improved protocol to provide sufficient numbers of HSCs for clinical applications.

2 AIM OF THE THESIS

The bone marrow niche has been classically studied in great detail in the context of maintenance of hemopoietic stem cells. More recent research has elucidated the importance of the mesenchymal stem cells within the homeostatic bone marrow microenvironment. However, little is known regarding the impact of stress on the bone marrow niche over time. This in part, along with difficulty in defining an HSC supportive MSC cell population has limited our regenerative medicine applications. Therefore, the aim of this thesis is the "**Characterization of bone marrow mesenchymal stem cell niche dynamics upon stress, with focus on clinical translation"**.

In the context of the bone marrow, inflammation is an overarching process central to most if not all forms of stress challenges and disease setting. Current research in the field is focused on understanding inflammation in the context of the HSC. While such research provides a descriptive understanding of the microenvironment, it falls short in translating it to functional applications confounded by a single marker approach of classifying the microenvironment cell diversity. Therefore, in this project we aimed to utilize the power of single-cell sequencing coupled with functional proliferation readout to investigate inflammation response overtime of the bone marrow microenvironment in an unbiased approach. This study is described under the project, **"Inflammatory-responding Mesenchymal Stem Cells (iMSCs) dynamically modulate the bone marrow microenvironment response to stress".**

Bone marrow transplants (BMTs) in the last decade have emerged as a novel paradigm in healthcare, with potential to restore a new functional hematopoietic system in recipients in cases where the system of the recipient is not functional. However, a major roadblock for this

scientific breakthrough is our limited potential for *ex-vivo* HSC expansion. Due to availability of low HSC numbers often successful transplant is frequently a big challenge. To address this unmet clinical challenge, we aimed to develop a personalized medicine concept for improved *ex vivo* HSC expansion using novel donor-specific MSC population. This study is described under the project, **"Ex *vivo* Hematopoietic Stem Cell (HSC) expansion using reinvigorating Mesenchymal Stem Cells (rMSCs) for personalized medicine".**

3 RESULTS

3.1 Inflammation-responding Mesenchymal Stem Cells (iMSCs) dynamically modulate the bone marrow microenvironment response to stress

In this project we systematically characterized the native murine bone marrow niche upon inflammation stress over-time, ascribing cellular identity based on the functional potential of the bone marrow cellular compartments to respond upon perturbation.

3.1.1 Bone lining-derived iMSCs are the major responder to IFNα-mediated inflammatory stress

To study the response dynamics of an unbiased bone marrow microenvironment upon inflammatory stress, an *in vivo* BrdU cell proliferation immunoassay was used. Acute inflammation was triggered through the administration of a single dose of IFNα per mouse over a time-course, followed by a single injection of BrdU 16 hours before sacrifice (Figure 4A). As we had previously reported, HSCs and endothelial cells (Endo) showed known kinetics to inflammation response with a peak in proliferation at 24 h and 3 h, respectively (Figure 4B) (151,159). Further, bone marrow derived stromal cells (SC) showed a response but with slower kinetics with a maximum of 27% of cells proliferating at 72 h post stimulation. Interestingly, bone lining-derived iMSCs stood out as the major responders to IFNα in comparison to all other cell types. These iMSCs exhibited a rapid response with 69% of cells proliferating at 3 h and the peak proliferation response at 24 h post IFNα injection.

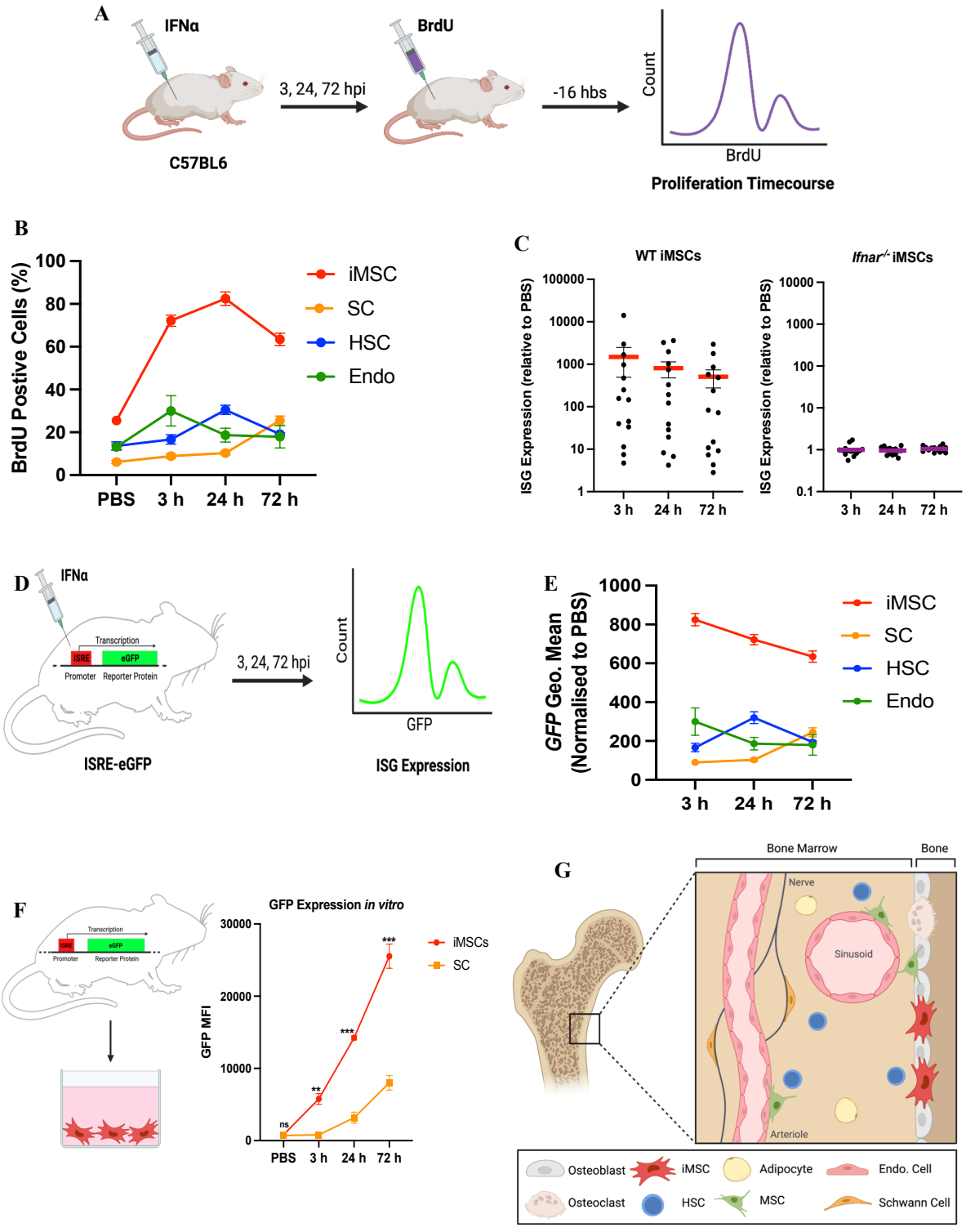

Figure 4. Identification of inflammation-responding bone lining-derived MSCs (iMSCs)

(A) Schematic of *in vivo* BrdU proliferation assay upon a single dose of IFNα ($5x10^6$ units/kg) at 3, 24 and 72 hours post injection (hpi) in C57Bl/6 (WT) mice. BrdU (100µg/g) is administered 16 hours before sacrifice (hbs). (B) The proportion of $BrdU^+$ proliferating cells within the BM niche at 3, 24, and 72 hpi IFNα stimulation, iMSC: inflammation-responding mesenchymal stem cells ($CD45^-$, $Ter119^-$, $CD31^-$, $PDGFR\alpha^+$, $CD51^+$), SC: bone-marrow-derived stromal cells ($CD45^-$, $Ter119^-$, $CD31^-$), HSC: hematopoietic stem cells ($Lineage^-$ $cKIT^+$ $Sca1^+$ $CD48^-$ $CD150^+$ & $CD34^-$) and Endo: endothelial cells

($CD45^-$, $Ter119^-$, $CD31^+$). (mean ± SEM, n ≥ 3). (C) Transcriptional levels of Interferon Stimulated Genes (ISGs: refer material and methods for gene list) relative to its PBS control, in iMSCs from either WT or *Ifnar*$^{-/-}$ mice treated with IFNα. (mean ± SEM, n ≥ 3). (D) ISRE-eGFP reporter mice are used to assess dynamic ISG changes 3, 24, and 72 hours post injection with IFNα ($5x10^6$ units/kg). (E) ISRE-eGFP expression kinetics of BM niche cell populations 3, 24 or 72 post IFNα injection, visualized as eGFP intensity normalized to PBS control. iMSC: inflammation-responding mesenchymal stem cells, SC: bone-marrow derived stromal cells, HSC: hematopoietic stem cells and Endo: endothelial cells. (mean ± SEM, n ≥ 3). (F) ISRE-eGFP expression dynamics of iMSCs and SCs 3, 24 and 72h post addition of IFNα (1000 IU/ml.) *in vitro*. (mean ± SEM, n ≥ 3, unpaired two-tailed student's t-test performed between SCs and iMSCs: * $p \leq 0.05$, ** $p \leq 0.01$, *** $p \leq 0.001$, **** $p \leq 0.0001$, ns: non-significant). (G) Graphical visualization of the bone-lining-derived iMSC's microenvironment in the bone marrow.

We characterized these inflammation-responding MSCs (iMSCs) via fluorescence-activated cell sorting (FACS) negatively selecting for surface marker expression of CD31 (endothelial cell marker), CD45 (pan hematopoietic marker) and Ter119 (mature erythrocyte marker), and positively selecting for the established stromal cell markers CD51 and PDGFR (226). Comparing the iMSC fraction between digested bone lining (BL iMSCs) *vs.* bone marrow (BM iMSCs), the bone lining contained 2800 iMSCs per mouse in contrast to 120 iMSCs in the bone marrow (Figure 5A). Moreover, fluorescence-sorted BL iMSCs possessed tri-lineage differentiation potential and colony-forming unit-fibroblasts (CFU-F) capability *in vitro*, unlike its BM counterpart which were nonviable in culture (Figure 5B).

To study whether the IFNα response of the iMSCs was signaled via its receptors and mediated through the downstream canonical JAK-STAT pathway, we made use of knockout mice for either type-I IFN receptors (*Ifnar*$^{-/-}$) or cytoplasmic transcription factor STAT1 (*Stat*$^{-/-}$*)*. The iMSCs from the *Ifnar*$^{-/-}$ mice showed impaired proliferation capacity and cell cycle activation upon inflammatory stress (Figure 5C & D). Further, the iMSC response to type-I IFN was processed through the downstream transcriptional activation of associated ISGs (Figure 4C & Figure 6B). This effect was lost in *Ifnar*$^{-/-}$ and *Stat*$^{-/-}$ iMSCs. This IFNAR and STAT-mediated, and ISG-driven response of iMSCs also led to proliferation of these cells *in vitro*,

revealing that iMSCs directly and independently responded to IFNα stimuli (Figure 5E & F). The direct response of iMSCs to IFNα in culture was both dose-dependent and time-specific, as was shown by a dose-dependent and time-specific increase in protein expression levels of the ISG, Sca-1 (Figure 5H & 6A). In contrast to increased proliferation, the CFU-F potential of WT iMSC significantly decreased with increasing IFNα concentration *in vitro*. This decrease in colony formation activity was lost *Ifnar*$^{-/-}$ and *Stat*$^{-/-}$ iMSCs (Figure 5G).

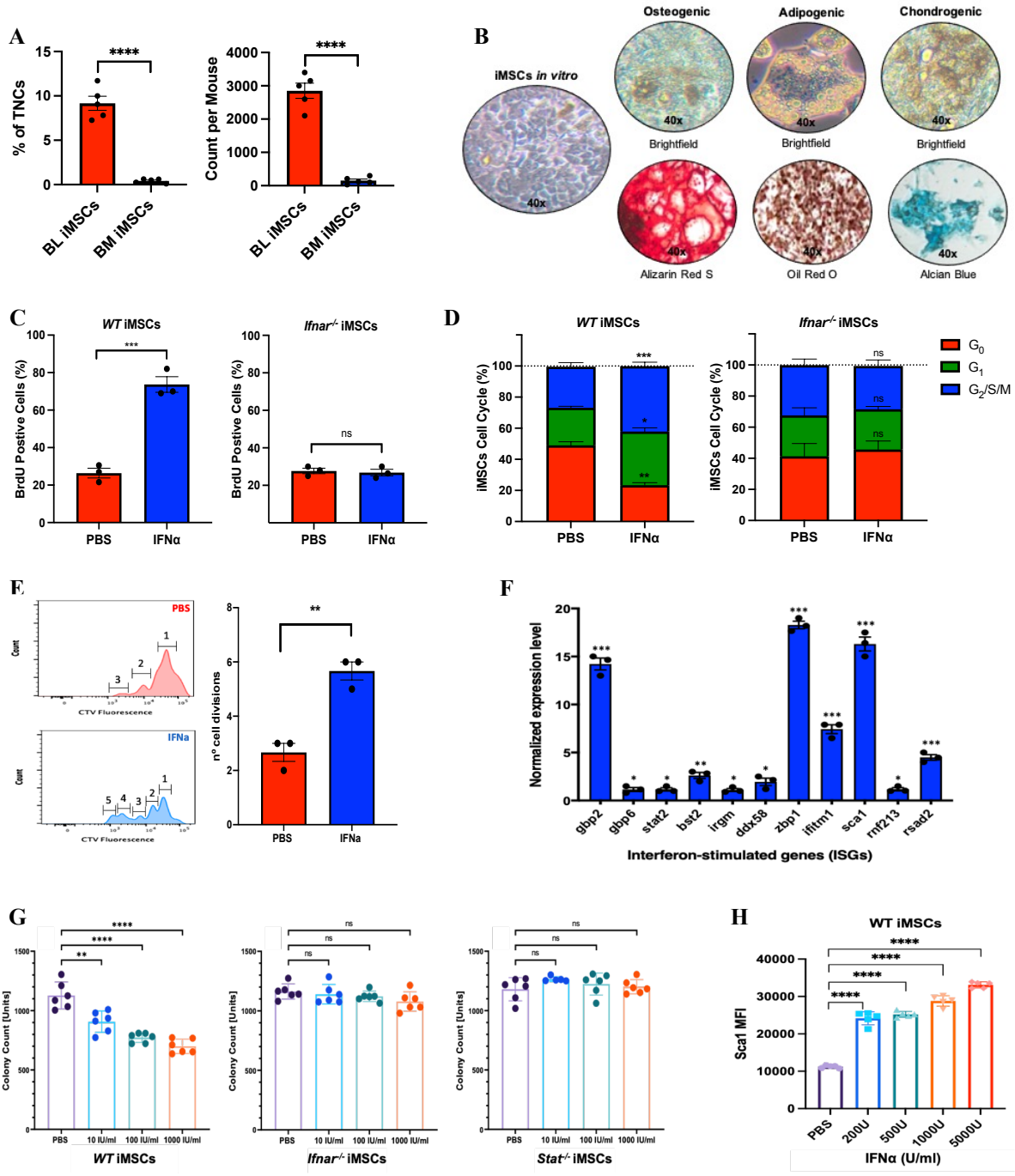

Figure 5. See legend on following page

Figure 5. The bone lining-derived iMSCs directly respond to IFNα stress via their IFN receptor
(A) Plot representing the proportion and absolute cell numbers of phenotypic iMSC isolated from either total digested bone marrow (BM) or bone chips (BL) using the surface marker panel: $CD45^-$ $Ter119^-$ $CD31^-$ (TNCs: Triple negative cells) along with $CD51^+$ and $PDGFRa^+$, gated within alive cells. (Mean ± SEM, n ≥ 3, unpaired two-tailed student's t-test performed between BL-iMSCs and BM-iMSCs: * p ≤ 0.05, ** p ≤ 0.01, *** p ≤ 0.001, **** p ≤ 0.0001, ns: non-significant). (B) Tri-lineage differentiation potential of the BL-iMSCs in culture into osteocytes, adipocytes and chondrocytes. (magnification = 40x, n ≥ 3). (C) IFNAR dependent increase in $BrdU^+$ proliferating iMSCs 24 h post IFNα ($5x10^6$ units/kg) treatment *in vitro*. The BL-iMSCs were FACS-sorted from either WT or *Ifnar-/-* mice and in culture for 24 h. (Mean ± SEM, n ≥ 3, unpaired two-tailed student's t-test performed between IFNα treated and PBS control iMSCs independently for WT and $Ifnar^{-/-}$ iMSCs: * p ≤ 0.05, ** p ≤ 0.01, *** p ≤ 0.001, **** p ≤ 0.0001, ns: non-significant). (D) Cell cycle analysis of WT or $Ifnar^{-/-}$ iMSCs post 24 h IFNα ($5x10^6$ units/kg) stimulation, using Ki67 and DAPI. (Mean ± SEM, n ≥ 3, unpaired two-tailed student's t-test performed between PBS and IFNα treatment in a cell-cycle phase specific manner: * p ≤ 0.05, ** p ≤ 0.01, *** p ≤ 0.001, **** p ≤ 0.0001, ns: non-significant). (E) Cell trace violet (CTV) label dilution assay upon 24 h IFNα (1000 IU/ml) treatment of iMSCs in culture. (Mean ± SEM, n ≥ 3, unpaired two-tailed student's t-test performed between PBS and IFNα treated iMSCs: * p ≤ 0.05, ** p ≤ 0.01, *** p ≤ 0.001, **** p ≤ 0.0001, ns: non-significant). (F) qPCR transcriptional levels of ISGs represented as PBS control normalized expression values from 24 h in vitro IFNα stimulated iMSCs. (Mean ± SEM, n ≥ 3, unpaired two-tailed student's t-test performed between individual ISG and its respective PBS control: * p ≤ 0.05, ** p ≤ 0.01, *** p ≤ 0.001, **** p ≤ 0.0001, ns: non-significant). (G) Colony-forming unit-fibroblasts (CFU-F) potential of WT, $Ifnar^{-/-}$ or $Stat1^{-/-}$ iMSCs treated with increasing IFNα concentration for 24 h *in vitro*. (Mean ± SEM, n = 5, unpaired two-tailed student's t-test performed between PBS and individual IFNα concentration: * p ≤ 0.05, ** p ≤ 0.01, *** p ≤ 0.001, **** p ≤ 0.0001, ns: non-significant). (H) Sca1 protein expression, measured using FACS, on iMSCs treated for 24 h with increasing IFNα concentration *in vitro*. (Mean ± SEM, n ≥ 3, unpaired two-tailed student's t-test performed between PBS and individual IFNα concentration: * p ≤ 0.05, ** p ≤ 0.01, *** p ≤ 0.001, **** p ≤ 0.0001, ns: non-significant).

To compare iMSC's transcriptional dynamics to other bone marrow cellular components *in vivo*, an eGFP reporter mouse model tagging the ISRE promoter (ISRE-eGFP) was used (Figure 4D). Upon IFNα stimulation, HSCs, endothelial cells and stromal cells showed eGFP kinetics that were similar to their proliferation profiles (Figure 4B &E) suggesting that the transcriptional upregulation of ISGs in these cell types was correlated to their functional proliferative response upon inflammation. Notably, iMSCs did not follow the

same trend as there was an uncoupled early transcriptional response of ISGs at 3 h followed by progressively increasing cell proliferation until 72 h post stimulation (Figure 4E and Figure 6C to M). Furthermore, fluorescence-sorted ISRE-eGFP iMSCs exhibited significantly higher GFP induction in comparison to SCs over time *in vitro* (Figure 4F) highlighting that the bone lining-derived iMSCs served as the major responders to acute IFNα stress (Figure 4G).

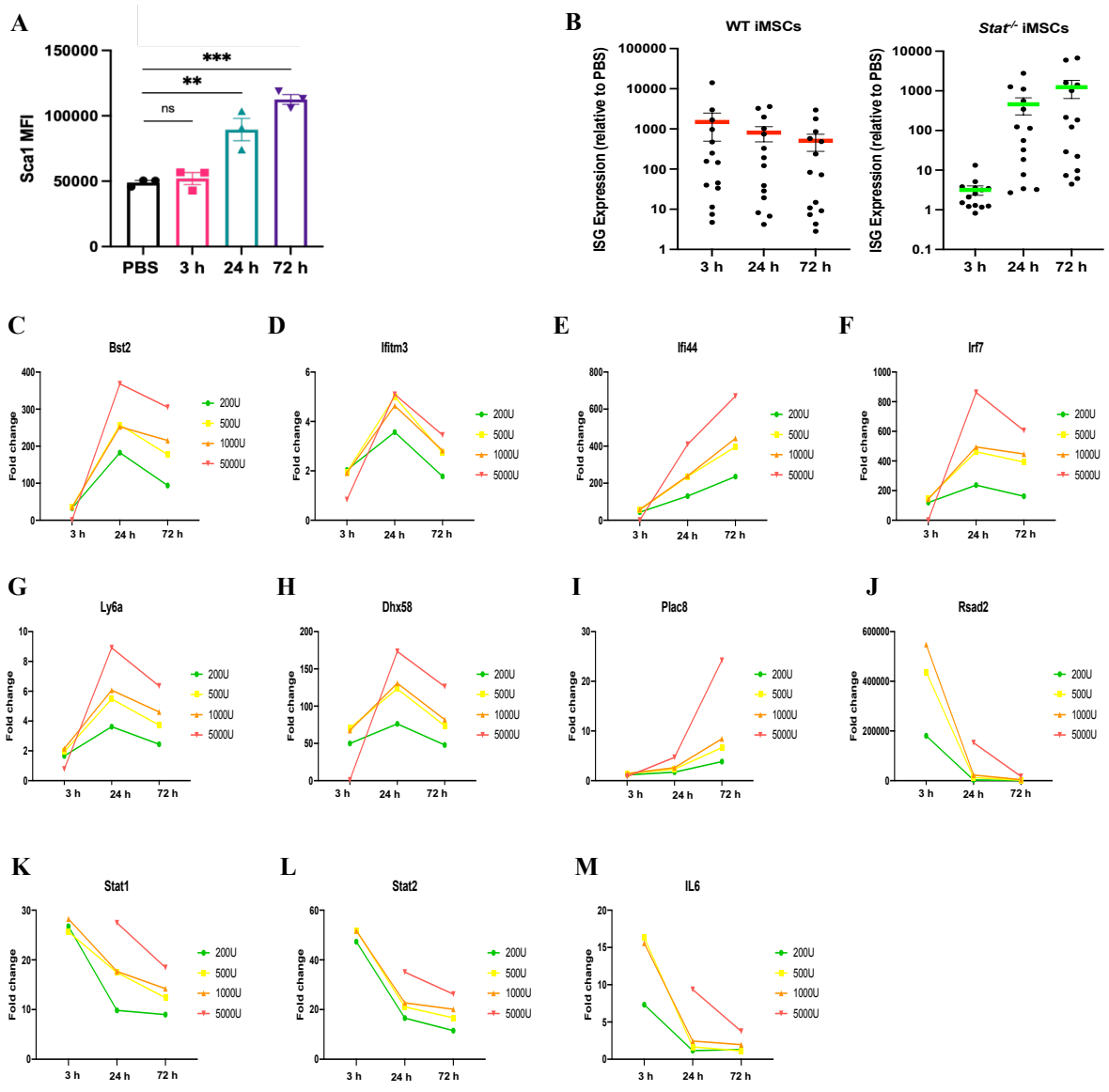

Figure 6. Interferon stimulated gene expression in iMSCs show temporal kinetics upon IFNα stimulation

(A) Sca1 protein expression of *in vitro IFNα treated* iMSCs over time. (Mean ± SEM, n ≥ 3, unpaired two-tailed student's t-test performed between PBS and individual IFNα treatment timepoint: * $p \leq 0.05$, ** $p \leq 0.01$, *** $p \leq 0.001$, **** $p \leq 0.0001$, ns: non-significant). (B) qPCR transcriptional levels of ISGs relative to its PBS control, in WT or *Stat1*$^{-/-}$ iMSCs over the *in vitro* IFNα time-course. (mean ± SEM, n ≥ 3). (C) To (M) qPCR transcriptional temporal kinetics of individual ISGs relative to its PBS

control *in vitro*, for WT iMSCs, over the time-course with increasing concentrations of IFNα. (mean ± SEM, n ≥ 3).

3.1.2 The iMSCs exhibit distinct transcriptional states throughout the course of the IFNα response

To study the transcriptional dynamics of the functionally characterized iMSC population, we performed bulk RNA sequencing of mouse-matched digested BL-iMSCs and BM-HSCs (Figure 7A). Unsupervised hierarchical clustering and principal component analysis revealed iMSCs clusters based on the temporal dynamics of the stress response with the first dimension constituting 14.2% of variance in the dataset, which separated the 3 h time point from all others (Figure 7B & Supplementary Figure 8A). The second dimension (accounting for 12.3% of variance) separated the response at 24 h furthest away from the PBS control, and showed that the response at 72 h was closest to the homeostatic PBS control. Using a published ISG dataset as a reference (227–229), we showed that the iMSC response was type-I IFN pathway-mediated (Figure 7C and Figure 8B). Strikingly, gene set enrichment analysis (GSEA) revealed three distinct temporal transcriptional states for the response which are an early (3 h) pro-inflammatory and immunomodulatory signature, a metabolic and proliferative signature at 24 h, and a late (72 h) ECM re-modulating signature (Figure 7D & Figure 8C). In addition, unsupervised enrichment maps confirmed distinct time-point-specific biological processes for iMSCs upon response to IFNα (Figure 8D to F).

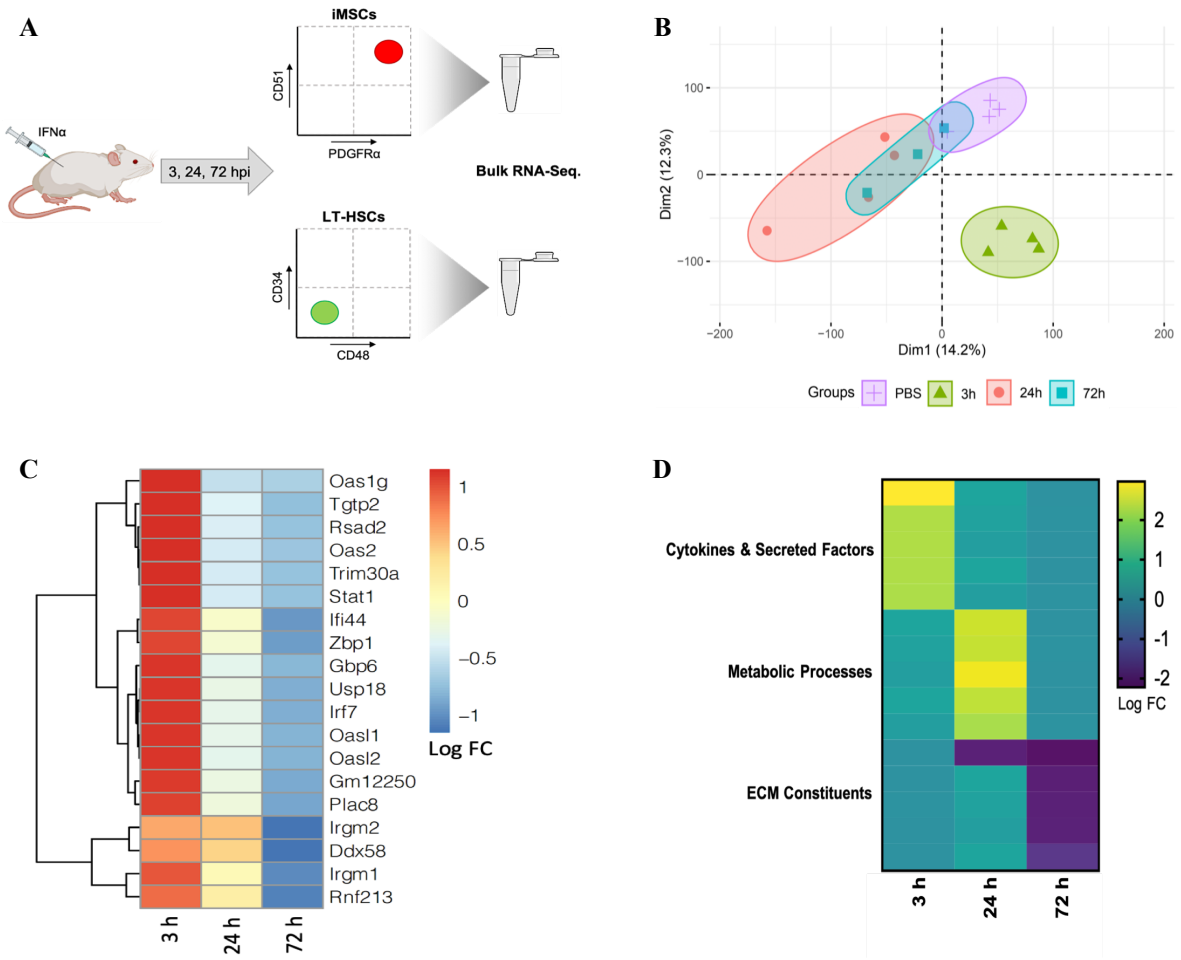

Figure 7. Global transcriptomic analysis of the iMSC response to acute inflammation over time

(A) Experimental setup displaying the IFNα stimulation regime followed by RNA-seq of two mouse-matched FACS sorted populations: iMSCs ($CD45^-$, $Ter119^-$, $CD31^-$, $PDGFR\alpha^+$, $CD51^+$) and Long Term (LT) HSCs ($Lineage^-$ $cKIT^+$ $Sca1^+$ $CD48^-$ $CD150^+$ & $CD34^-$). (B) Principal component analysis (PCA) of the 4 treatment datasets of iMSCs based on expression values of all detected genes. (n = 3/4). (C) Heatmap of ISG expression in iMSCs at the different timepoints post IFNα injection, represented as fold change (Log FC) normalized to PBS control dataset (FDR ≤ 0.05). (D) GSEA-based iMSC heatmap representing major biological processes altered during IFNα time course (Scale: Log FC, FDR ≤ 0.05).

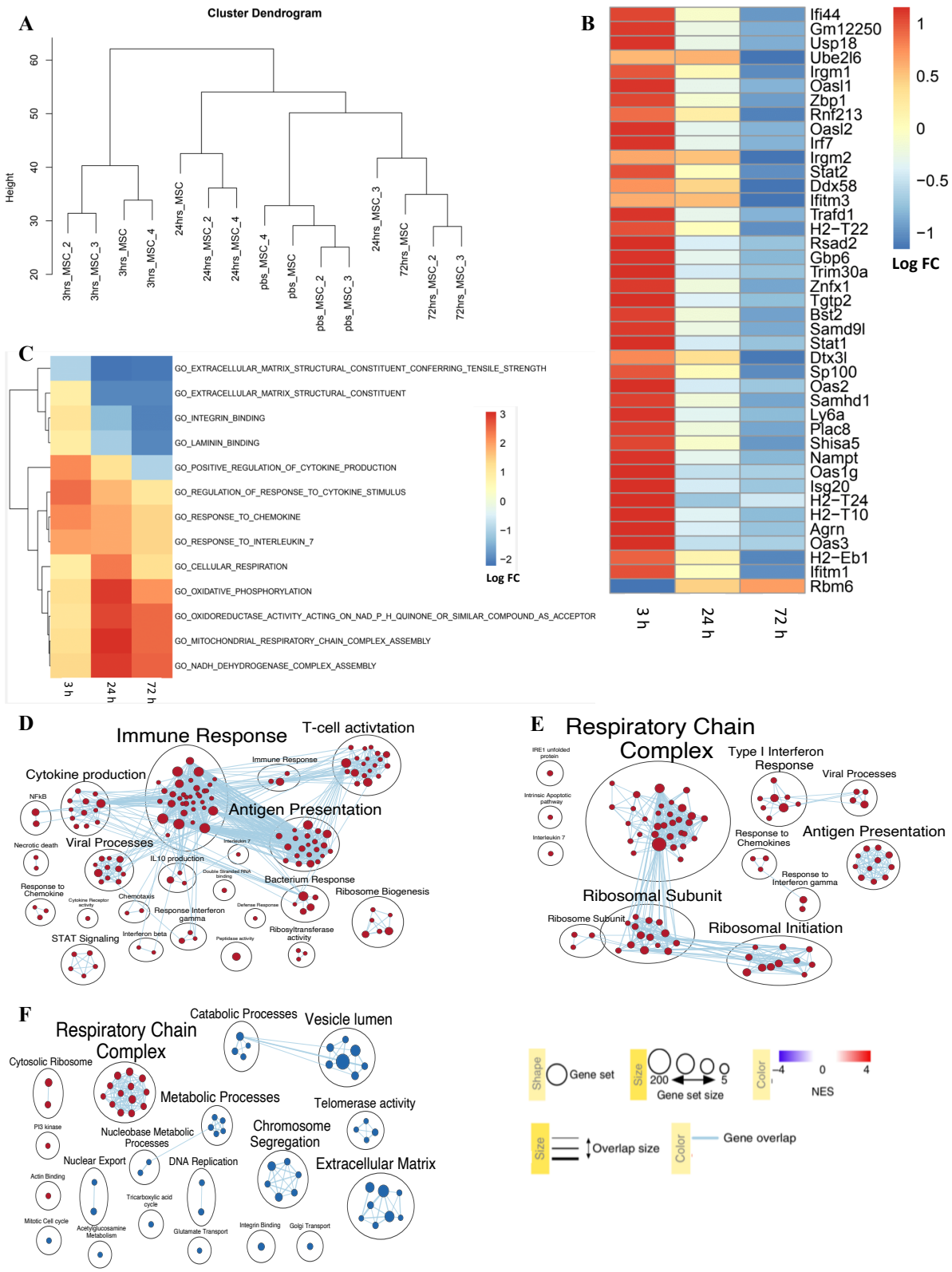

Figure 8. iMSCs exhibit distinct time-point specific transcriptional changes upon inflammatory stress

(A) Unsupervised hierarchical clustering (dendrogram) of the PBS and 3 IFNα ($5x10^6$ units/kg) treatment datasets (3, 24 and 72h) for iMSCs based on expression values of all detected genes in the RNAseq dataset. (n = 3/4). (B) Heatmap of ISG expression kinetics, represented as fold change (Log

FC) normalized to PBS control dataset, for iMSC upon IFNα stimulation (FDR ≤ 0.05). (C) GSEA-based heatmap representing major biological processes changed in iMSCs during IFNα time course (Scale: Log FC, FDR ≤ 0.05). (D) Unsupervised enrichment map visualization of major biological pathways changed in iMSCs at 3 h post IFNα stimulation. (n = 3/4, FDR ≤ 0.05). (E) Unsupervised enrichment map visualization of major biological pathways changed in iMSCs at 24 h post IFNα stimulation. (n = 3/4, FDR ≤ 0.05). (F) Unsupervised enrichment map visualization of major biological pathways changed in iMSCs at 72 h post IFNα stimulation. (n = 3/4, FDR ≤ 0.05).

3.1.3 The iMSCs show an early pro-inflammatory and immunomodulatory state

To better understand the early pro-inflammatory state of iMSCs, the RNA-seq data was further analyzed. We uncovered that secreted pro-inflammatory factors were significantly upregulated in the 3 h sample compared to the PBS control (Figure 9A). Further, GSEA using the Gene Ontology system of classification (GO term analysis) revealed pro-inflammatory and immunomodulatory pathways being significantly enriched only at 3 h post stimulation of iMSCs (Figure 10A & B).

Next, we compared this early pro-inflammatory signature of iMSCs to BM-derived SCs and endothelial cells, both recognized as stress-responding and cytokine-producing cell types. Our qPCR validation of the 3 h iMSC signature identified distinct cytokine and secreted factor profiles for iMSCs, endothelial cells and SCs (Figure 9B). The BL-iMSCs were shown to be the predominant stromal source for *C-X-C Motif Chemokine Ligand 5 (Cxcl5), C-C motif chemokine 9 (Ccl9)* and *Bone Morphogenic Protein 5 (Bmp5),* whereas the BM-SCs specifically produced *TNF Superfamily Member 10 (Tnfsf10)* and *Guanylate Binding Protein 7 (Gbp7)*. BM-endothelial cells secreted *C-X-C Motif Chemokine Ligand 9 (Cxcl9)* and *C-X-C Motif Chemokine Ligand 10 (Cxcl10).* This shows that all of the different bone marrow cellular constituents showed a response post-stimulation, but different genes were upregulated by the different cell types. Interestingly, we show that the previously described crucial pro-inflammatory factors of the stress response were produced by the iMSCs.

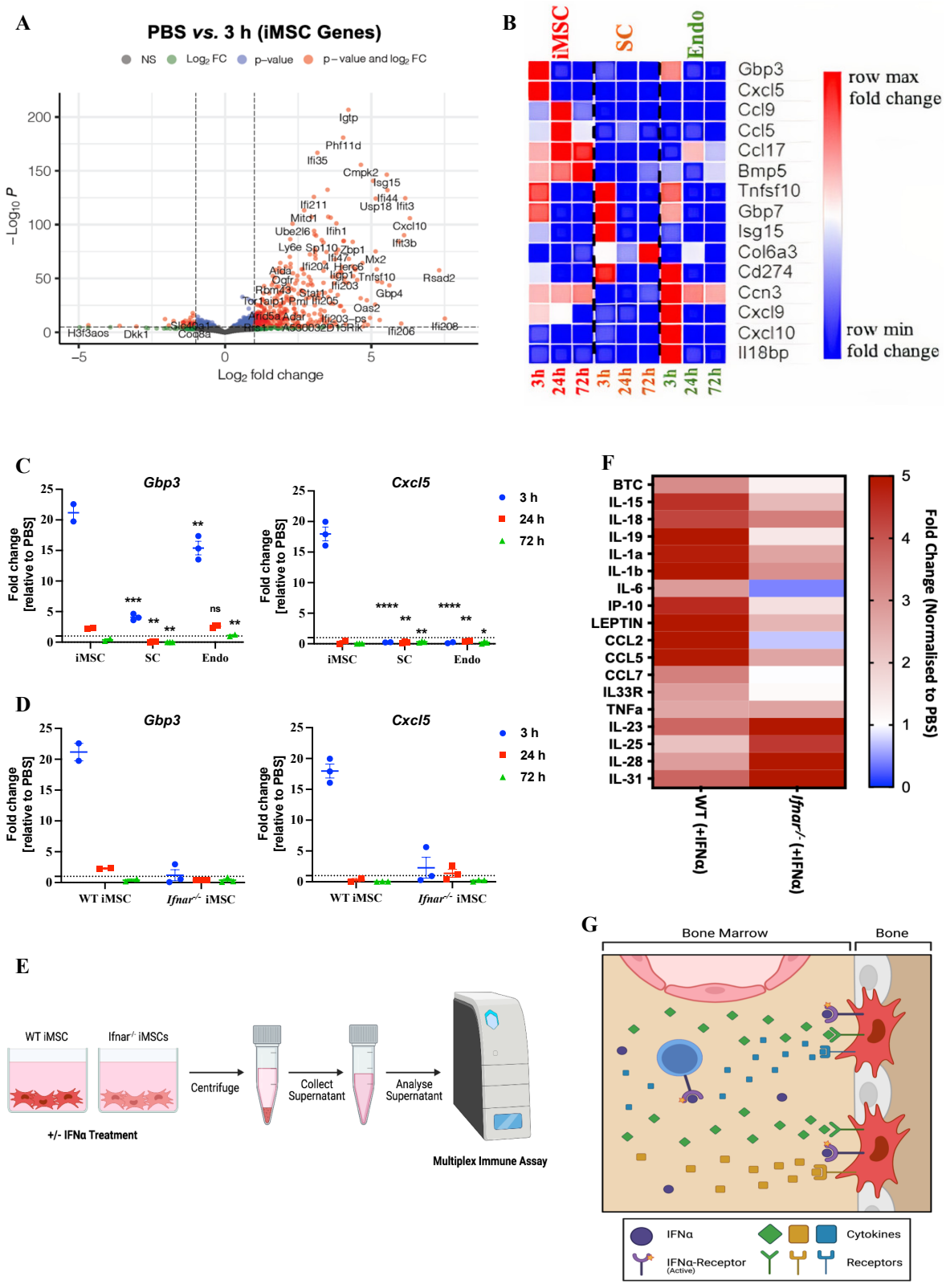

Figure 9. iMSCs show an early pro-inflammatory response upon IFNα treatment

(A) Volcano plot of PBS vs. 3 h iMSC gene-set with $\log_2$ fold change and p-value cut-off of 1 and 0.05 respectively. (Total variables plotted = 29936, n = 3/4). (B) Heatmap comparing qPCR transcriptional expression of the top pro-inflammatory secreted factor genes, identified in iMSCs in the the RNA-sequencing dataset, between iMSCs, SCs and Endothelial cells at different timepoints post IFNα

injection. (Scale: row normalized units, mean from n = 5). (C) Temporal kinetics of qPCR transcriptional levels of cytokines *Gpb3* and *Cxcl5* upon IFNα stimulation *in vivo*, across iMSCs, SCs and Endothelial cells. (Mean ± SEM, n ≥ 3, Three-way-ANOVA test comparing time-point specific cell type response to its respective iMSC time-point: * $p \leq 0.05$, ** $p \leq 0.01$, *** $p \leq 0.001$, **** $p \leq 0.0001$, ns: non-significant). (D) qPCR transcriptional levels of *Gpb3* and *Cxcl5* genes plotted as fold change normalized to PBS control in iMSCs from WT and *Ifnar*$^{-/-}$ mice at different timepoints post IFNα injection. (Mean ± SEM, n ≥ 3). (E) Experimental setup for *in vitro* protein multiplex assay on supernatant of cultured WT or *Ifnar*$^{-/-}$ iMSCs treated with IFNα (1000IU/ml). (F) Heatmap representing fold changes in protein levels of cytokines in supernatant upon in vitro IFNα treatment of WT and *Ifnar*$^{-/-}$ iMSC Represented data is normalized to iMSC PBS control expression levels. (Mean of n = 3). (G) Graphical representation of early pro-inflammatory response of the iMSCs 3h post IFNα treatment.

Even though, all iMSC-specific cytokines and secreted factors were upregulated 3 h post IFNα stimulation, some of them reached even higher expression levels at later time points. This suggested that the individual genes fulfill different functions in the temporal IFNα response and these fine-tuned expression changes were not detected using bulk RNA sequencing. *Guanylate Binding Protein 3* (*Gbp3*) and *Cxl5* had the highest fold change in expression at 3 h post stimulation relative to the PBS control (Figure 9C). *Ccl9* and *C-C motif chemokine 5 (Ccl5)* reached peak transcriptional expression at 24 h, *C-C motif chemokine (Ccl17)* and *Bmp5* were significantly upregulated throughout the whole-time course with a maximum expression at the 72 h time-point (Figure 10C). Furthermore, these changes were depended on the IFN signaling, since IFNα stimulation of *Ifnar*$^{-/-}$ iMSCs did not result in any detectable changes in the pro-inflammatory gene signature (Figure 9D and Figure 10D). We also validated the iMSC's early inflammation response signature at the protein level using a multiplex immune assay technique to measure changes in cytokine levels in culture supernatants of WT and *Ifnar*$^{-/-}$ iMSCs treated with IFNα or PBS *in vitro* were assessed (Figure 9E). The treated WT iMSCs produced pro-inflammatory cytokines in the monoculture *in vitro* system confirming that iMSCs directly responded to IFNα treatment via the IFNAR-mediated pathway by producing and releasing pro-inflammatory cytokines (Figure 9F & G).

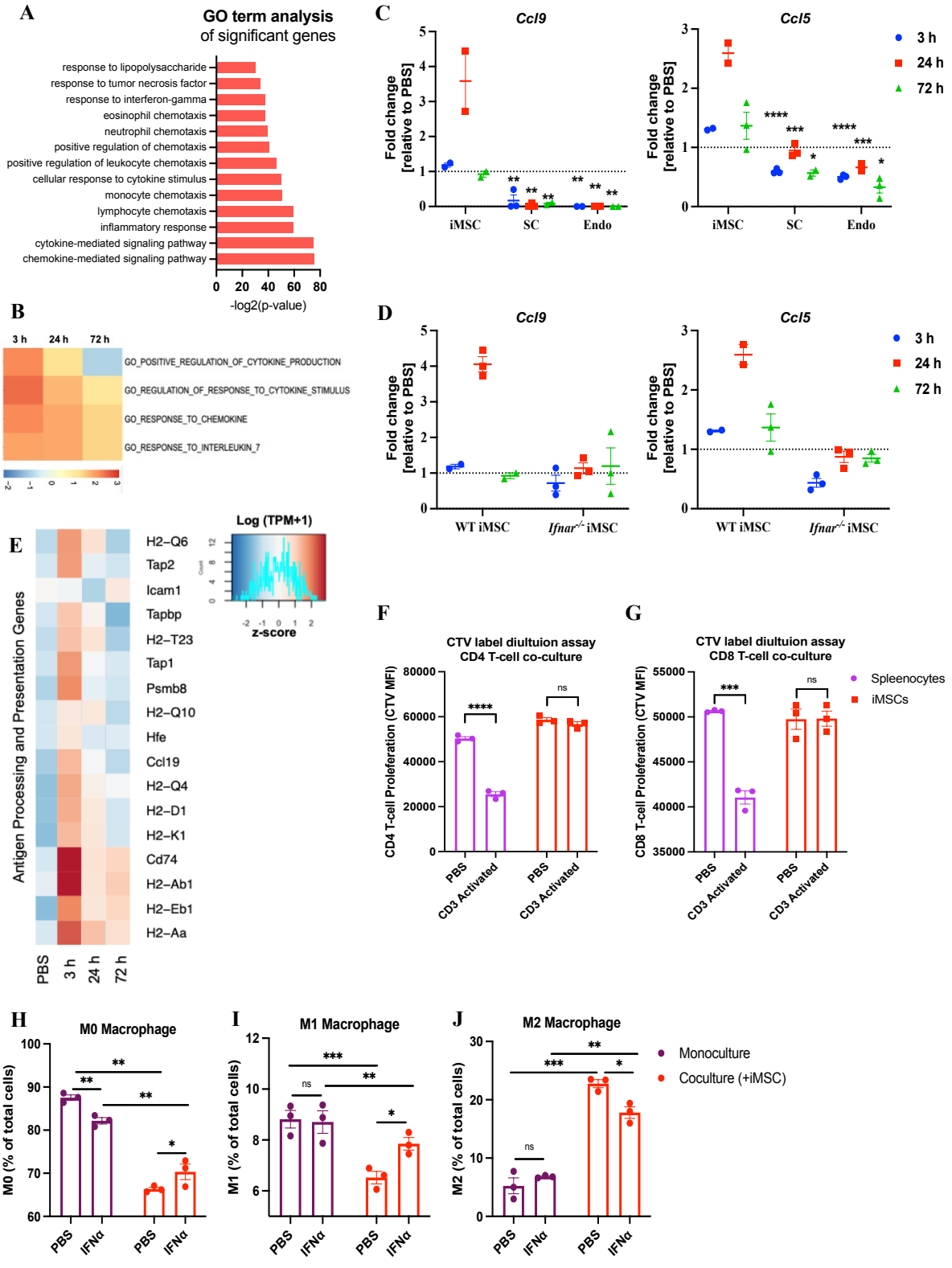

Figure 10. Immunomodulatory effect of iMSCs in the early phase of the bone marrow IFNα response

(A) Representation of the top GO terms pathways significantly upregulated in iMSCs 3 h post IFNα injection. (p-value cut-off = 0.05, n = 3/4) (B) GSEA-based heatmap showing cytokine-related biological processes being upregulated in iMSCs at the 3 h time point of IFNα response (Scale: Log FC, FDR ≤ 0.05). (C) Temporal kinetics of qPCR transcriptional levels of cytokines *Ccl9* and *Ccl5* upon

IFNα ($5x10^6$ units/kg) stimulation *in vivo*, in iMSCs, SCs and Endothelial cells. (Mean ± SEM, n ≥ 3, Three-way-ANOVA test comparing time-point specific cell type response to its respective iMSC time-point: * p ≤ 0.05, ** p ≤ 0.01, *** p ≤ 0.001, **** p ≤ 0.0001, ns: non-significant). (D) qPCR transcriptional levels of *Ccl9* and *Ccl5* genes plotted as fold change normalized to PBS control for WT and *Ifnar*$^{-/-}$ iMSCs over IFNα time-course. (Mean ± SEM, n ≥ 3). (E) Heatmap representing crucial antigen processing and presentation genes modulated in the iMSCs throughout the IFNα time course. (Log (TPM+1), Scale: z-score, n = 3/4). (F) Cell trace violet (CTV) label dilution assay performed on CD4+ T cells *in vitro* upon CD3 antibody activation either as co-culture with spleenocytes or iMSCs. (Mean ± SEM, n ≥ 3, unpaired two-tailed student's t-test performed between the two individual datasets as indicated on the graph: * p ≤ 0.05, ** p ≤ 0.01, *** p ≤ 0.001, **** p ≤ 0.0001, ns: non-significant). (G) Cell trace violet (CTV) label dilution assay performed on CD8+ T cells *in vitro* upon CD3 antibody activation either as co-culture with spleenocytes or iMSCs. (Mean ± SEM, n ≥ 3, unpaired two-tailed student's t-test performed between the two individual datasets as indicated on the graph: * p ≤ 0.05, ** p ≤ 0.01, *** p ≤ 0.001, **** p ≤ 0.0001, ns: non-significant). (H) Non-activated (M0) macrophage, represented as percentage of total cells, 24 h post *in vitro* IFNα (1000 IU/ml) stimulation either as monoculture or co-cultured with iMSCs. (Mean ± SEM, n ≥ 3, unpaired two-tailed student's t-test performed between the two individual datasets as indicated on the graph: * p ≤ 0.05, ** p ≤ 0.01, *** p ≤ 0.001, **** p ≤ 0.0001, ns: non-significant). (I) Pro-inflammatory (M1) macrophage, represented as percentage of total cells, 24 h post *in vitro* IFNα (1000 IU/ml) stimulation either as monoculture or co-cultured with iMSCs. (Mean ± SEM, n ≥ 3, unpaired two-tailed student's t-test performed between the two individual datasets as indicated on the graph: * p ≤ 0.05, ** p ≤ 0.01, *** p ≤ 0.001, **** p ≤ 0.0001, ns: non-significant). (J) Anti-inflammatory (M2) macrophage, represented as percentage of total cells, 24 h post *in vitro* IFNα (1000 IU/ml) stimulation either as monoculture or co-cultured with iMSCs. (Mean ± SEM, n ≥ 3, unpaired two-tailed student's t-test performed between the two individual datasets as indicated on the graph: * p ≤ 0.05, ** p ≤ 0.01, *** p ≤ 0.001, **** p ≤ 0.0001, ns: non-significant).

In addition to cytokine gene sets, the GSEA analysis also indicated immune response and antigen processing pathways to be significantly upregulated by the iMSCs at the 3 h time-point (Figure 8D). With regard to the role of iMSCs in the immune response of the bone marrow microenvironment, our data showed that the iMSCs significantly upregulated the antigen-processing and presenting gene sets at the 3 h time point (Figure 10E). To functionally validate the immunomodulator effect of the iMSCs, we co-cultured them with mouse-matched BM-macrophages (non-activated: M0, pro-inflammatory: M1, anti-inflammatory: M2) or T cells (CD4 helper T cells) isolated from the bone marrow. The iMSCs caused a significant decrease

in the proportion of M0 and M1 macrophages of the total cells compared to the respective cells in mono-culture (Figure 10H & I). In contrast, the percentage of M2 macrophages of the total cells increased five-fold when co-cultured with iMSCs compared to being in monoculture (Figure 10J). Interestingly, upon IFNα stimulation both M0 and M1 macrophages exhibited positive trends towards increased cell numbers when co-cultured with iMSCs, and the M2 macrophages showed the opposite trend with a decrease in cellular proportion upon IFNα treatment in co-culture. These changes were not significantly different. To assess the effect of iMSCs on CD4 helper T cells, we used Cell Trace Violet (CTV) label dilution assay. Comparing spleenocyte co-culture (positive control) to iMSC co-culture with anti-CD3 antibody-activated CD4 T cells, there was a significant suppression in the proliferation of the T cells (Figure 10F & G).

Taken together, we showed for the first time that the iMSCs produced many of the most important pro-inflammatory cytokines and that this response occurred very early upon stress induction. In addition, our data suggests a potential role of the iMSCs in the modulation of the immune cells in the bone marrow.

3.1.4 The iMSCs exhibit a late bone marrow extracellular matrix re-modulatory state

Next, we characterized the down-regulated ECM signature observed in the overall temporal dynamics of the iMSC response to acute inflammation (Figure 7D, Figure 8C & F). At the late (72 h) time-point post IFNα stimulation, the iMSCs significantly down-regulated genes contributing to the bone marrow structural composition in comparison to the homeostatic PBS control (Figure 11A). Further, global GO term analysis of the complete iMSC dataset revealed that multiple ECM components, such as laminin and integrin, and BM architecture-related pathways were down-regulated specifically at the 72 h time-point (Figure 11B). To obtain a global view on the matrisomal signature of the iMSCs upon stress, we used a published

ECM gene set as a refence (107,230) and found that the iMSCs had a marked transcriptional reduction in ECM genes at the 72 h time-point (Figure 12A). Hence, our data suggests a role of BL-iMSCs in ECM re-modulation upon acute inflammation which was previously unknown.

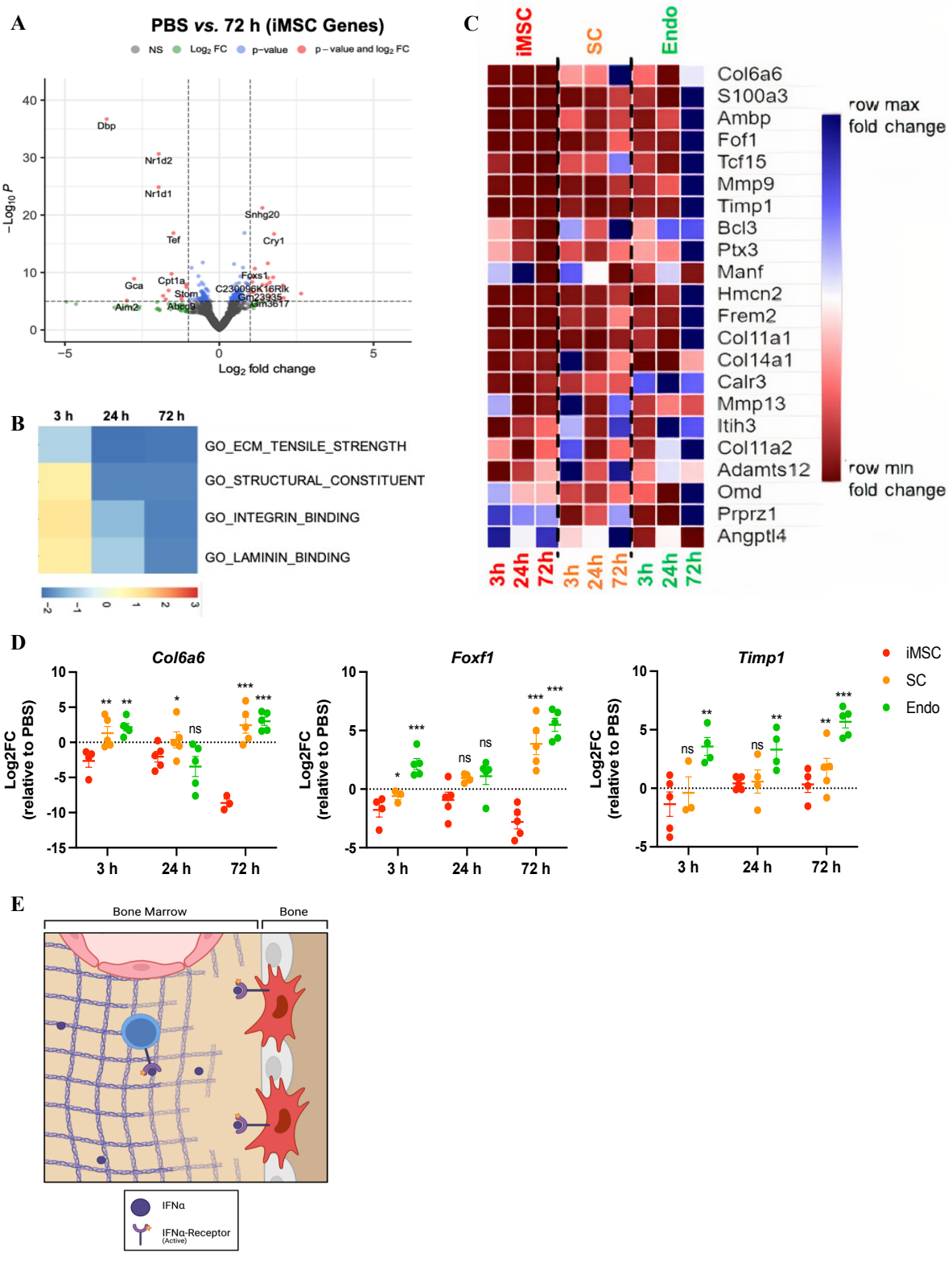

Figure 11. See legend on following page

Figure 11. Extracellular matrix re-modulatory function of the iMSCs in the recovery phase of the IFNα response

(A) Volcano plot of PBS vs. 72 h iMSC gene-set with $\log_2$ fold change and p-value cut-off of 1 and 0.05 respectively. (Total variables plotted = 29936, n = 3/4). (B) GSEA-based iMSC heatmap showing BM structural and ECM processes being downregulated at the 72 h time point of IFNα response (Scale: Log FC, FDR ≤ 0.05). (C) Heatmap comparing the qPCR transcriptional expression of the most down-regulated ECM genes, found in the RNA-sequencing dataset, between iMSCs, SCs and Endothelial cells over the IFNα time-course. (Scale: row normalized units, mean from n = 5). (D) Temporal kinetics of qPCR transcriptional levels of ECM genes *Col6a6, Foxf1* and *Timp1* upon IFNα stimulation *in vivo*, across iMSCs, SCs and Endothelial cells. (Mean ± SEM, n ≥ 3, Three-way-ANOVA test comparing time-point specific cell type response to its respective iMSC time-point: * p ≤ 0.05, ** p ≤ 0.01, *** p ≤ 0.001, **** p ≤ 0.0001, ns: non-significant). (E) Graphical representation of the iMSC bone-marrow niche response 72 h post-acute inflammation, highlighting the local ECM re-modulatory function of the iMSCs.

To determine the specificity of the iMSC's ECM re-modulatory transcriptional profile, we performed qPCR analysis comparing iMSCs to the BM-SCs and endothelial cells. All three cell types downregulated some important ECM-related genes including *Ambp*, *Tcf15*, *Col11a1*, and *Col14a1* upon IFNα treatment (Figure 11C). Among these three cell types, iMSCs showed down-regulation of the highest number of gene and to the highest degree. Furthermore, the different ECM genes from the three cell types showed specific kinetics when followed over time. For instance, *Col6a6* was progressively down regulated in iMSCs but did not significantly change in the SCs and endothelial cells over time (Figure 11D). In contrast, *Timp1* remained stable for iMSCs over time but showed significant upregulation at 72 h for the SCs and endothelial cells. Interestingly at the 72 h time-point, the iMSCs showed significant down-regulation of ECM genes, including *Foxf1, Tcf15, S100a3, Ptx3* and *Mmp9,* while the SCs and endothelial cells showed an increased transcriptional expression of these same genes (Figure 11D & Figure 12B-E).

In summary, we observed that the cellular components of the BM locally alter the expression of ECM components, suggesting cellular compartmentalization of matrisome

regulation in the BM, with iMSCs playing a central role in the re-structuring of the BM upon acute stress insult (Figure 11E).

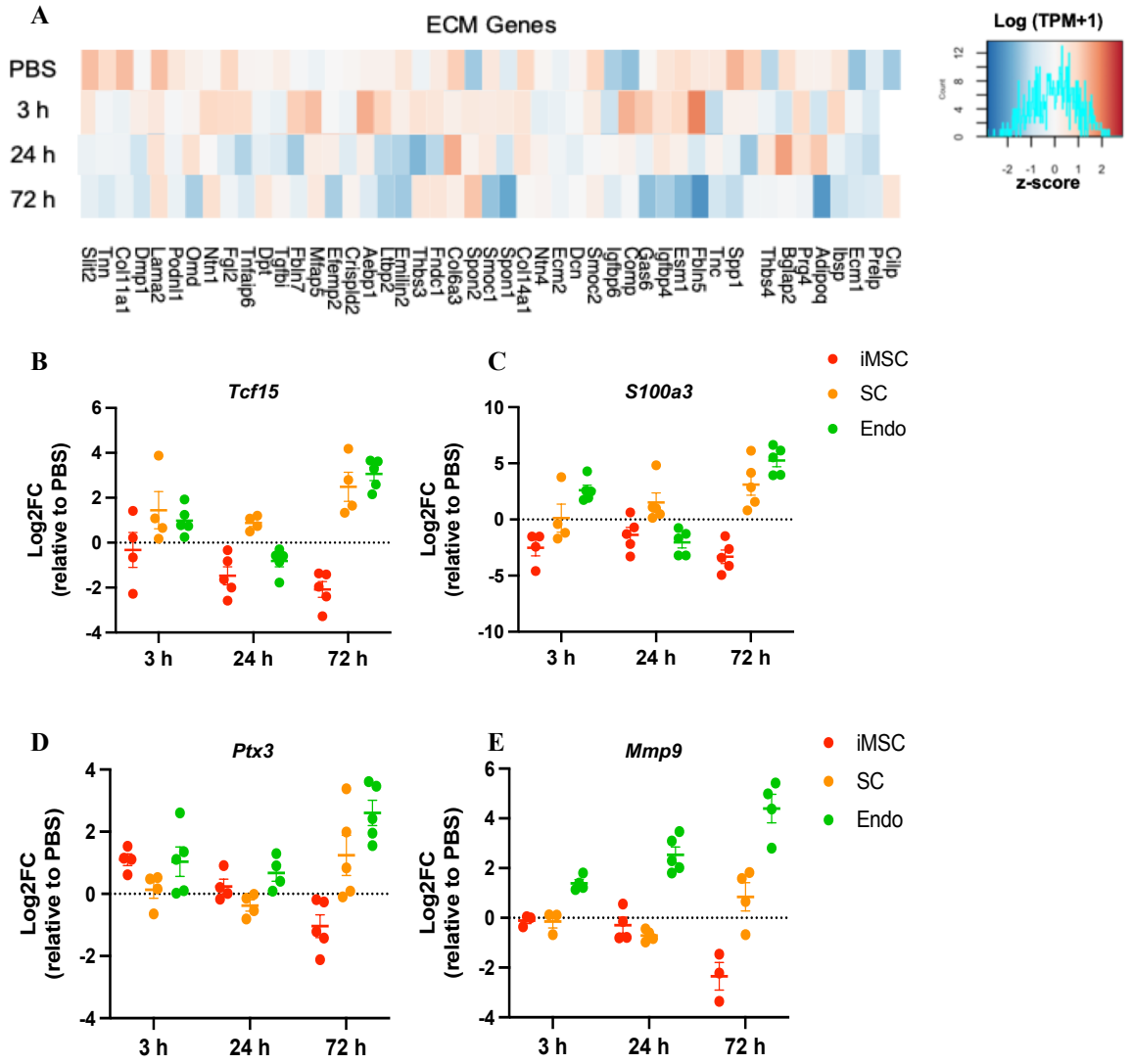

Figure 12. Downregulation of extracellular matrix transcriptional signature in iMSCs at the recovery phase of the IFNα response

(A) Heatmap representing changes in ECM gene expression in iMSCs throughout the IFNα time course. (Log (TPM+1), Scale: z-score, n = 3/4). (B) To (E) Temporal kinetics of the qPCR transcriptional expression of ECM genes *Tcf15, S100a3, Ptx3* and *Mmp9* upon IFNα () stimulation *in vivo* in iMSCs, SCs and Endothelial cells. (Mean ± SEM, n ≥ 3).

3.1.5 The iMSCs directly modulate the HSC response dynamics to acute inflammation

So far, iMSCs among the different constituents of the bone marrow niche are suggested to have the strongest response to IFNα stimulation with regard to proliferation, cytokine production, and ECM modulation. Therefore, we hypothesized that iMSCs influence the BM HSC response in the context of acute inflammation (Figure 13A). To infer direct molecular interaction between these two cells types, we collaborated with Adrien S. Jolly and Thomas Höfer to use a used a self-established receptor-ligand interaction dataset. In brief, our interactome dataset consisted of 1863 receptor-ligand pairs supported by primary research literature and itinerated by compiling different datasets (Fantom-V human receptor-ligand interactions, InnateDB, IntactDB, and EBI-GOA NonIntact) along with other publicly available protein-protein interaction datasets (123). We scored the likelihood of a receptor-ligand pair interaction, termed as mean interaction score (MIS), between HSCs and the iMSCs from 0: "very unlikely" to 1: "very likely" based on the individual transcriptional profiles of the two cell types. Plotting the MIS between HSCs and iMSCs *vs.* variance in a merged time-point dataset, revealed crucial known HSC-specific interaction pairs including *Cxcr4-Cxcl14, Cxcr4-Cxcl12,* and *Kit-Kitl* (Figure 13B). Interestingly, these receptor-ligand pairs did not show a significant change in interaction between HSCs and iMSCs over the course of acute IFNα response. In contrast, three interaction pairs composed of iMSC ligands *Col5a3, Col5a1* and *Mdk* and their common HSC receptor *Sdc3* showed a very high degree of variance over the stress response time-course (Figure 13C & Figure 14A). In addition, the major changes in interaction throughout the IFNα response were accounted for the HSC receptors *Sell, Axl* and *Itgb6* binding to their iMSC ligands *Cfh, Gas6* and *Fn1,* respectively. This suggested a pivotal role of previously unexplored receptor-ligand interactions in modulating the iMSC-driven HSC response to acute inflammation (Figure 13A).

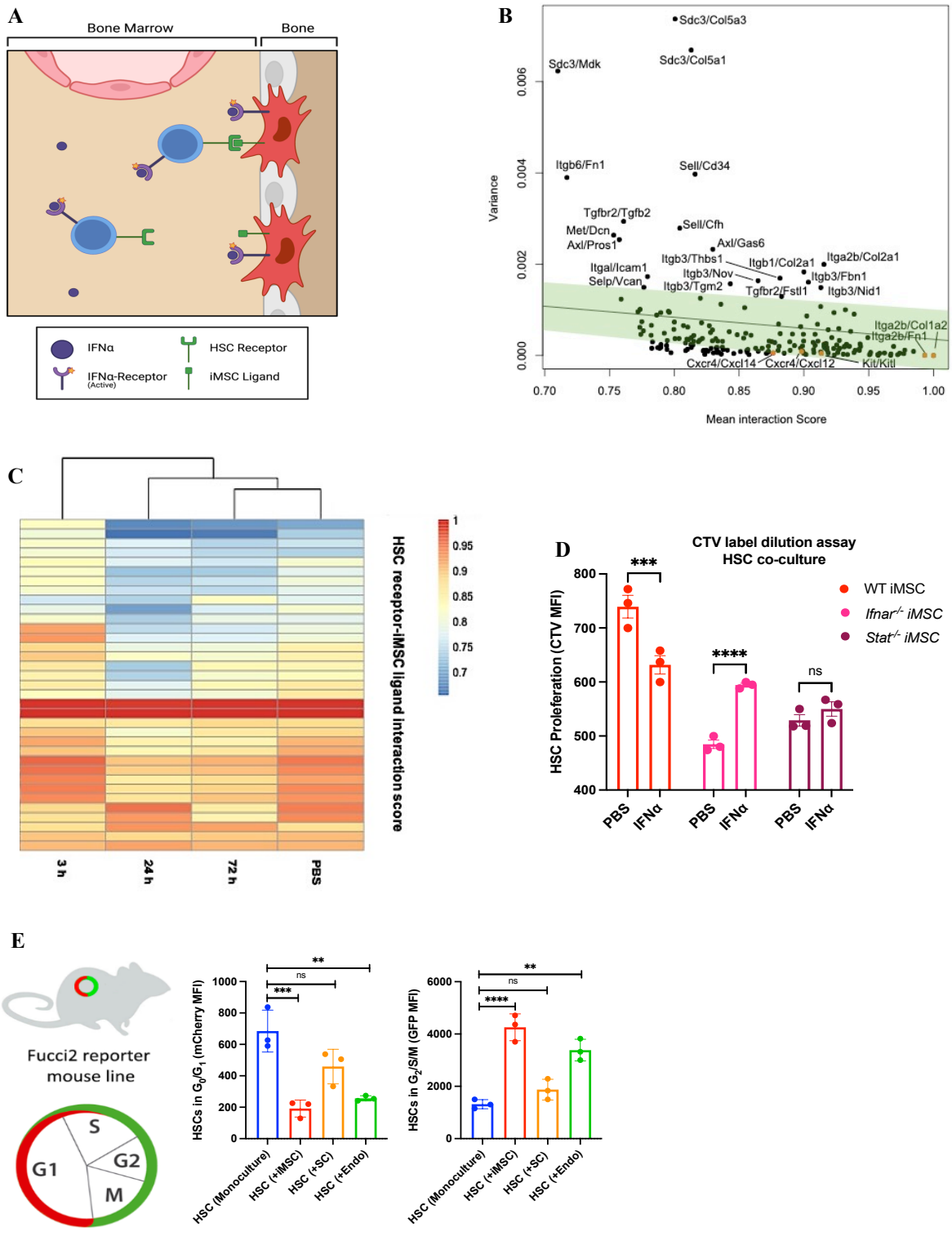

Figure 13. Dynamic interactions between iMSCs and HSCs during the acute inflammation response in the bone marrow

(A) Graphical representation of direct receptor-ligand interaction of HSCs and iMSCs in an acute inflammation response of the bone marrow. (B) The plot represents the interaction score of HSC-receptor and iMSC-ligand pairs on the x-axis vs. changes in the interaction over IFNα treatment time-course plotted as variance on the y-axis, based on the RNA-sequencing data set. (n = 3/4) (C) Heatmap

following the kinetics of HSC-receptor and iMSC-ligand interaction pairs upon IFNα stimulation. (n = 3/4) (D) Cell trace violet (CTV) label dilution assay comparing the proliferation response of HSCs co-cultured with WT, *Ifnar*$^{-/-}$ or *Stat1*$^{-/-}$ iMSCs upon IFNα treatment (1000IU/ml) *in vitro*. (Mean ± SEM, n ≥ 3, unpaired two-tailed student's t-test performed between PBS and IFNα treated HSCs within the specific co-culture setups: * p ≤ 0.05, ** p ≤ 0.01, *** p ≤ 0.001, **** p ≤ 0.0001, ns: non-significant). (E) Cell cycle analysis of FUCCI-expressing HSCs either in monoculture or co-cultured with iMSC, SCs or ECs for 48 h *in vitro*. (Mean ± SEM, n ≥ 3, unpaired two-tailed student's t-test performed between HSC monoculture and individual HSC co-culture setups: * p ≤ 0.05, ** p ≤ 0.01, *** p ≤ 0.001, **** p ≤ 0.0001, ns: non-significant).

To understand the functional implications of iMSCs in the HSC stress response, we co-cultured long-term HSCs (LT-HSC: Lin^{-} Kit^{+} Sca1^{+} CD48^{-} CD150^{+} CD34^{-}) with WT, *Ifnar*$^{-/-}$ or *Stat*$^{-/-}$ iMSCs in a CTV label dilution assay to assess proliferation. Upon IFNα treatment *in vitro*, the HSCs co-cultured with WT iMSCs showed significant cell proliferation response, consistent with our *in vivo* findings (Figure 13D). In contrast, the HSCs co-cultured with *Ifnar*$^{-/-}$ iMSCs and stimulated with IFNα exhibited decreased proliferation compared to its PBS control. Of note, HSCs co-cultured with *Ifnar*$^{-/-}$ iMSCs compared to WT iMSCs showed much higher proliferation at baseline in the PBS control, which suggested that the response is linked to the loss of the IFNAR. Co-culturing HSCs with *Stat*$^{-/-}$ iMSCs had no effect on the proliferative capacity of HSCs suggesting that the iMSC-driven IFNα response of the HSCs *in vitro* was signaled, at least in part, through the canonical JAK-STAT pathway. In addition, we fluorescently-sorted HSPCs (Lin^{-} Kit^{+} Sca1^{+} CD150^{+} CD48^{-}) from the ISRE-eGFP reporter mice and performed an *in vitro* IFNα time-course either in monoculture or co-culture with iMSCs (Figure 15A). The HSPCs showed no difference in ISRE induction upon IFNα stimulation when comparing HSPC monoculture *vs.* iMSC coculture (Figure 15B). These results are concurrent with the fact that HSCs can themselves sense IFNα via their surface receptor IFNAR. Interestingly, the HSPCs in co-culture, in contrast to monoculture, showed heightened Sca1 protein levels 24 h and 48 h post stimulation. As Sca1 is an ISG, its

upregulation in this experiment implies that the functional response of HSPCs to inflammation was modulated through the presence of iMSCs *in vitro* (Figure 15C).

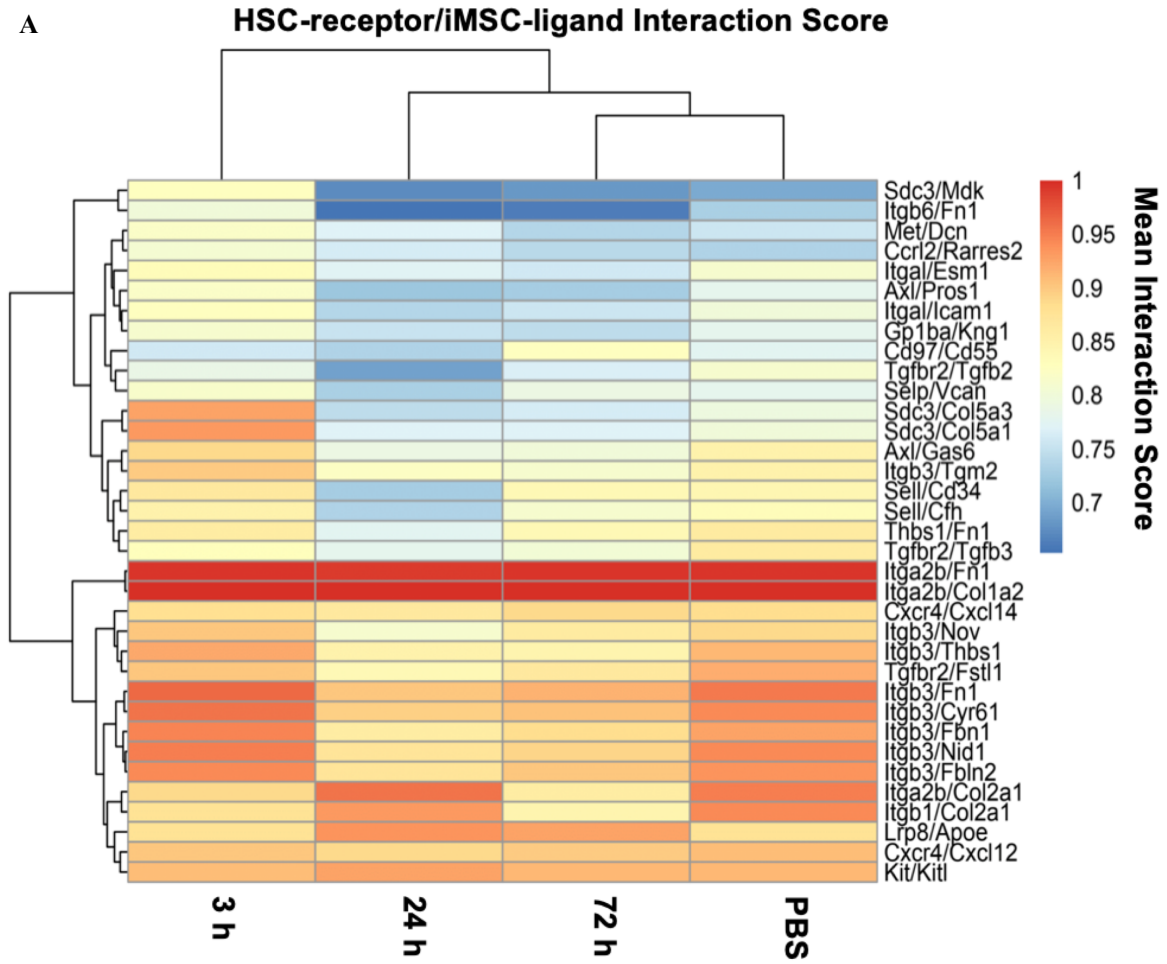

Figure 14. Unique changes in receptor-ligand interaction pairs between HSCs and iMSCs upon acute inflammatory response

(A) Heatmap following the kinetics of HSC-receptor and iMSC-ligand interaction pairs upon IFNα stimulation. (n = 3/4)

Next, we studied the direct effect of iMSCs on the cell cycle status of the HSCs upon IFNα stimulation. For this, we isolated HSCs from florescent ubiquitination-based cell cycle indication (FUCCI) reporter mice and co-cultured them with the iMSCs from WT, *Ifnar*$^{-/-}$ or *Stat*$^{-/-}$ mice (Figure 15D). In brief, the FUCCI reporter mouse model is based on two fluorescent proteins mCherry and eGFP being fused to cell-cycle-depended degradation motifs. Thus, FUCCI-expressing cells emit florescence of different wavelengths at distinct phases providing a robust tool for monitoring cell cycle progression. The FUCCI-expressing HSCs when co-

cultured with WT iMSCs showed a significant increase in the proportion of cells in the G_2M phase upon IFNα induction. This enhanced cycling effects on the HSCs were lost upon co-culturing with *Ifnar*$^{-/-}$ and *Stat*$^{-/-}$ iMSCs highlighting that the iMSCs directly lead to HSC cycling upon IFNα stress in culture. When co-culturing HSCs with BL-iMSCs, BM-SCs or endothelial cells though, we found that FUCCI-expressing HSCs showed the highest significant increase in the G_2/S/M proportions specifically in an iMSC cell-type dependent manner (Figure 13E).

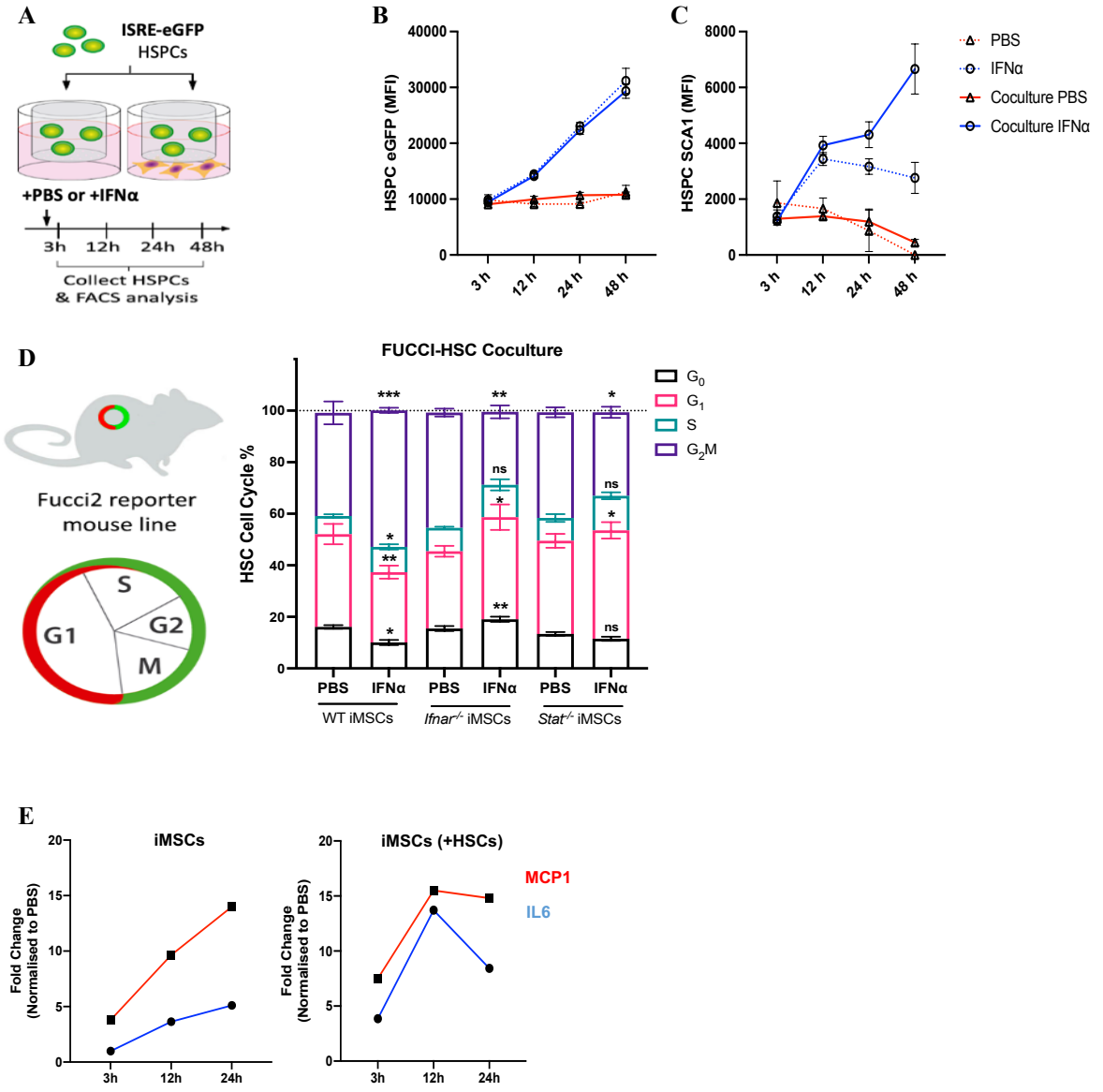

Figure 15. Functional response of HSCs to inflammatory stress is modulated by the presence of iMSCs

(A) Schematics of a trans-well experimental setup in which HSPCs isolated from ISRE-eGFP reporter mice were co-cultured with WT iMSCs over an IFNα (1000 IU/ml) treatment time course. (B) Changes in ISG expression in HSPCs (Lineage$^-$ cKIT$^+$ Sca1$^+$ CD48$^-$ CD150$^+$), visualized through eGFP

expression, upon IFNα treatment time course *in vitro* either as monoculture or co-cultured in a trans-well with WT iMSCs. (Mean ± SEM, n ≥ 3). (C) Kinetics of Sca1 protein expression in WT HSPCs over the IFNα treatment time course *in vitro* either as monoculture or co-cultured in a trans-well with WT iMSCs. (Mean ± SEM, n ≥ 3). (D) Cell cycle phase analysis of FUCCI-expressing HSCs 48 h post IFNα treatment *in vitro* when co-cultured with WT, *Ifnar*$^{-/-}$ or *Stat1*$^{-/-}$ iMSCs. (Mean ± SEM, n ≥ 3, unpaired two-tailed student's t-test performed between cell cycle phase matched PBS and IFNα treatment within their respective co-culture setup: * $p \leq 0.05$, ** $p \leq 0.01$, *** $p \leq 0.001$, **** $p \leq 0.0001$, ns: non-significant). (E) Kinetics of MCP1 and IL6 protein levels in supernatant, 3, 12 and 24 h post IFNα (1000 IU/ml) stimulation *in vitro* either as iMSC monoculture or in co-culture with WT HSCs. (n = 1)

Hypothesizing that the variance in receptor-ligand interaction and the profound functional changes observed in the HSCs affect the iMSCs, we next studied the role of the HSC IFNα response on the iMSC pro-inflammatory function. Using an *in vitro* protein immune-assay, we compared the supernatant from the iMSCs co-cultured with HSCs post IFNα treatment (Figure 16A). Our data uncovered distinct protein level changes in cytokine expression between monocultured and co-cultured iMSCs including a decrease of IL-19, IL-15 and IL-1b and an upregulation of CXCL5, CCL2 and CCL5 (Figure 16B). More specifically, we resolved the temporal dynamics for two pro-inflammatory cytokines for the *in vitro* co-culture of HSCs with iMSCs *vs.* the monoculture of iMSCs. Herein, MCP-1 protein concentration showed a trend towards reaching a plateau at 12 h post IFNα stimulation and IL-6 seemed to decrease in concentration at 24 h (Figure 15E). Taken together, this data infers a cellular cross-talk between iMSCs and HSCs upon acute inflammation.

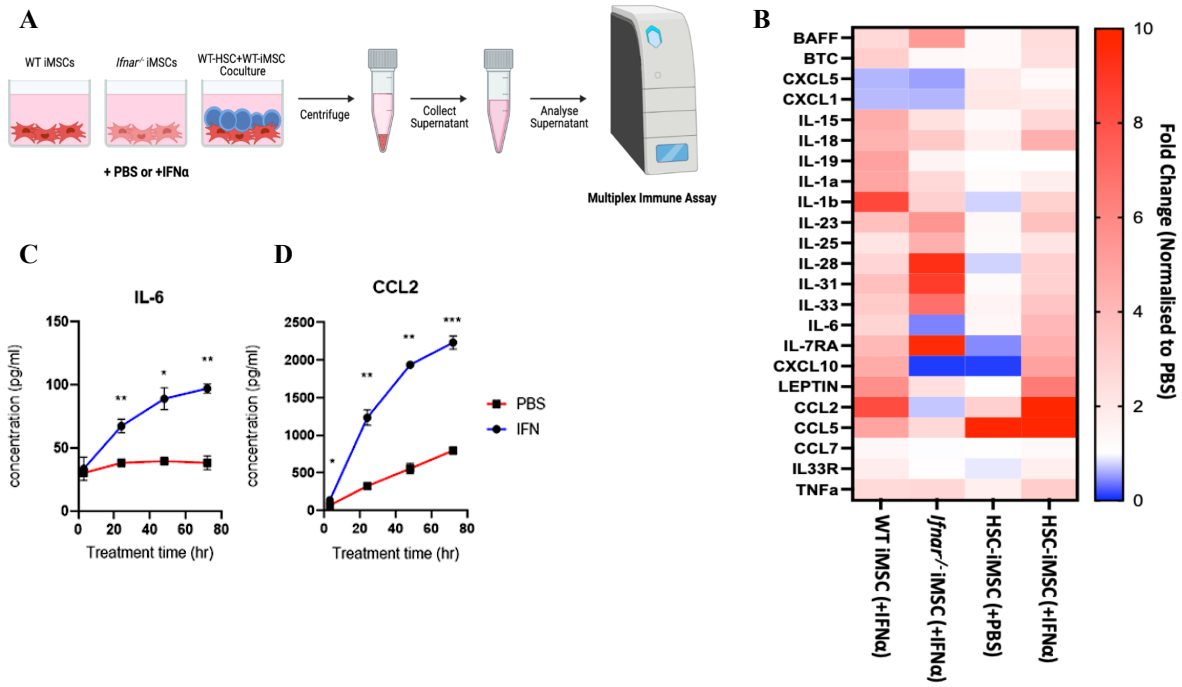

Figure 16. Changes in the pro-inflammatory cytokine profile of the iMSCs at the protein level upon IFNα stimulation

(A) Experimental setup of *in vitro* protein multiplex assay of WT and *Ifnar*$^{-/-}$ iMSC monoculture, and co-culture with HSCs (for 24 h) upon IFNα (1000 IU/ml) treatment. (B) Heatmap representing fold changes in cytokine protein levels in supernatant of WT and *Ifnar*$^{-/-}$ iMSC monocultures, and HSC cocultures (for 24 h) with WT iMSC *in vitro* upon IFNα (1000 IU/ml) treatment. Represented data is normalized to WT iMSC PBS monoculture control expression levels. (Mean of n = 3). (C) Temporal dynamics of IL-6 and CCL2 protein expression upon IFNα (1000 IU/ml) stimulation over time of WT iMSCs *in vitro*. (Mean ± SEM, n ≥ 3, unpaired two-tailed student's t-test performed between PBS and IFNα treatment at each individual time-point: * $p \leq 0.05$, ** $p \leq 0.01$, *** $p \leq 0.001$, **** $p \leq 0.0001$, ns: non-significant).

3.1.6 A disease-relevant transcriptional iMSC signature identified by single-cell RNA sequencing

Until here we have identified the cellular compartments of the BM by their cell surface marker expression, which neglects the intra-cell type heterogeneity. We hypothesized that an unbiased single-cell transcriptome screening could dissect subsets of iMSCs with functional differences in acute inflammation. Thus, we performed droplet-based single-cell RNA-seq on

the total digested bone lining fraction from WT mice over a time after a single injection of IFNα (Figure 17A). We characterized the BM stroma and analyzed temporal changes upon inflammation stress in collaboration with Brigitte J. Bouman and Laleh Haghverdi. Unsupervised clustering of the dataset merging all time-points identified 15 distinct sub-clusters (Figure 17C). We attributed cell types to clusters by comparing top differentially expressed genes (DEGs) and uniquely expressed genes (UEGs) across clusters (Figure 18A). Broadly the 15 clusters where grouped into 5 major cell populations: hematopoietic cell types predominately expressing *Cd34, Ly6a* and *Car1*, mesenchymal cells with high expression of *Cxcl12, Pdgfrα* and *Vcam1,* muscle cells expressing *Myl9, Acta2* and *Mustn1*, fibroblast-like cells expressing *Col11a1, Hapnln1* and *Col1a1,* and Schwann cells expressing *Sox10, S100* and *Gap43* (Figure 17B). Further, we validated transcriptional fingerprints of our single-cell clusters by performing label transfer using datasets from *Baccin et al, 2019* and *Tikhonova et al.,2019* (Figure 18B & C) (40,134). Overall, these validations indicate the robustness of the identified transcriptional single-cell clusters.

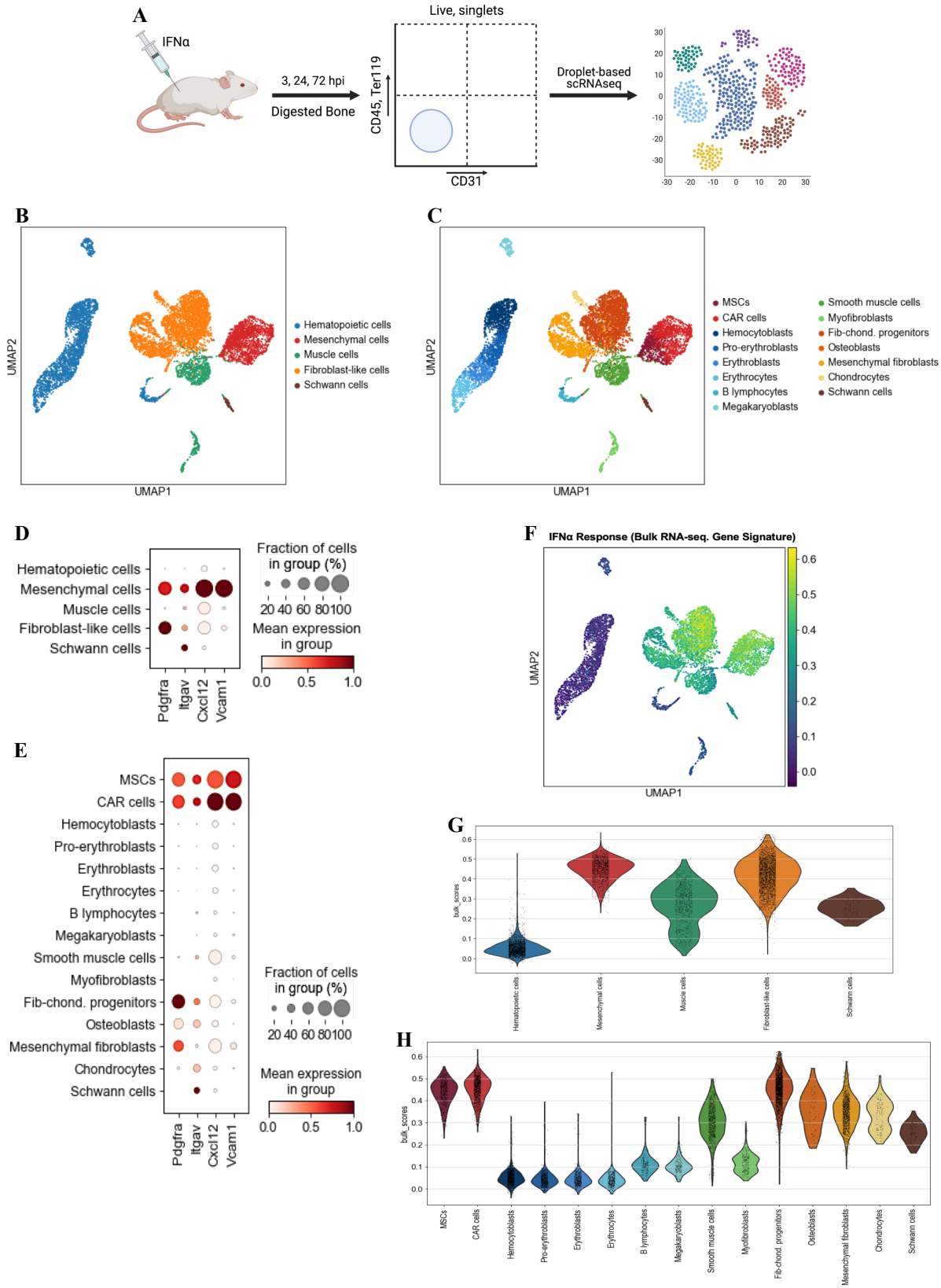

Figure 17. Dissecting the iMSC heterogeneity at the single cell-transcriptomic level

(A) Experimental setup displaying IFNα injections ($5x10^6$ units/kg) at three different time points (3 h, 24 h or 72 h) followed by FACS sorting of the digested bone for droplet-based single-cell RNA sequencing. (B) UMAP visualization (n = 9000 cells) of the five major SC-cell types in the digest bone

lining fraction with color-coded clustering (Merged UMAP representing PBS, 3 h, 24 h and 72 h datasets with n = 4 mice pooled per timepoint). (C) UMAP visualization (n = 9000 cells) of the fifteen SC-cellular clusters in the digest bone lining fraction with color-coded clustering (Merged UMAP representing PBS, 3 h, 24 h and 72 h datasets with n = 4 mice pooled per timepoint). (D) Expression levels of genes associated with Mesenchymal cells used for bulk iMSC identification for each of the five major SC-cell types (size of circle represents fraction of cells in group and color of the circle indicated the mean expression levels). (E) Expression levels of genes associated with Mesenchymal cells used for bulk iMSC identification for each of the fifteen SC-cellular clusters (size of circle represents fraction of cells in group and color of the circle indicated the mean expression levels). (F) Bulk-RNA-seq gene signature of the iMSC population overlaid onto the UMAP representing (n= 9000 cells) merged SC-RNA-seq data. (scale: bulk gene signature score). (G) Expression levels of the iMSC bulk-RNA-seq gene signature by each of the five major SC-cell types (scale: bulk gene signature score). (H) Expression levels of the iMSC bulk-RNA-seq gene signature by each of the fifteen SC-cellular clusters (scale: bulk gene signature score)

In order to understand the heterogeneity within the iMSC population, we used the gene markers and cell surface markers that we identified in the bulk iMSC sequencing and verified the expression of those in a single-cell niche dataset of a bone-lining stromal fraction that was obtained by using a less stringent sorting approach. Our data showed that the marker *Pdgfr* and *Itgav*, which were used as cell surface markers for sorting of the bulk iMSCs, were expressed by multiple mesenchymal (MSCs, CAR cells) and fibroblast (fib-chond. progenitors, osteoblasts, mesenchymal fibroblasts) single cell clusters (Figure 17D & E). With regard to iMSC-specific genes, *Cxcl12* and *Vcam1* were expressed by subsets of both MSCs and CAR cells (Figure 17E). Therefore, our data confirmed that the structural markers *Pdgfr*, *Itgv*, *Cxcl12* and *Vcam1* were heterogeneously expressed by differing subsets of niche cells.

To assess the heterogeneity in the IFNα response of iMSCs, we next used the iMSC IFN response gene expression signature and verified its expression in the single-cell niche dataset. Here, we observed that there was an overlap of the bulk gene signature with multiple cellular clusters (Figure 17F). In more detail, we found that multiple clusters of mesenchymal (MSCs, CAR cells) and fibroblast-like cells (fib-chond. progenitors, osteoblasts, mesenchymal fibroblasts) correlated with the bulk gene signature (Figure 17G & H). Thus, both analyses

confirmed that the iMSC markers and response were mediated by a heterogenous set of mesenchymal and fibroblast-like cells.

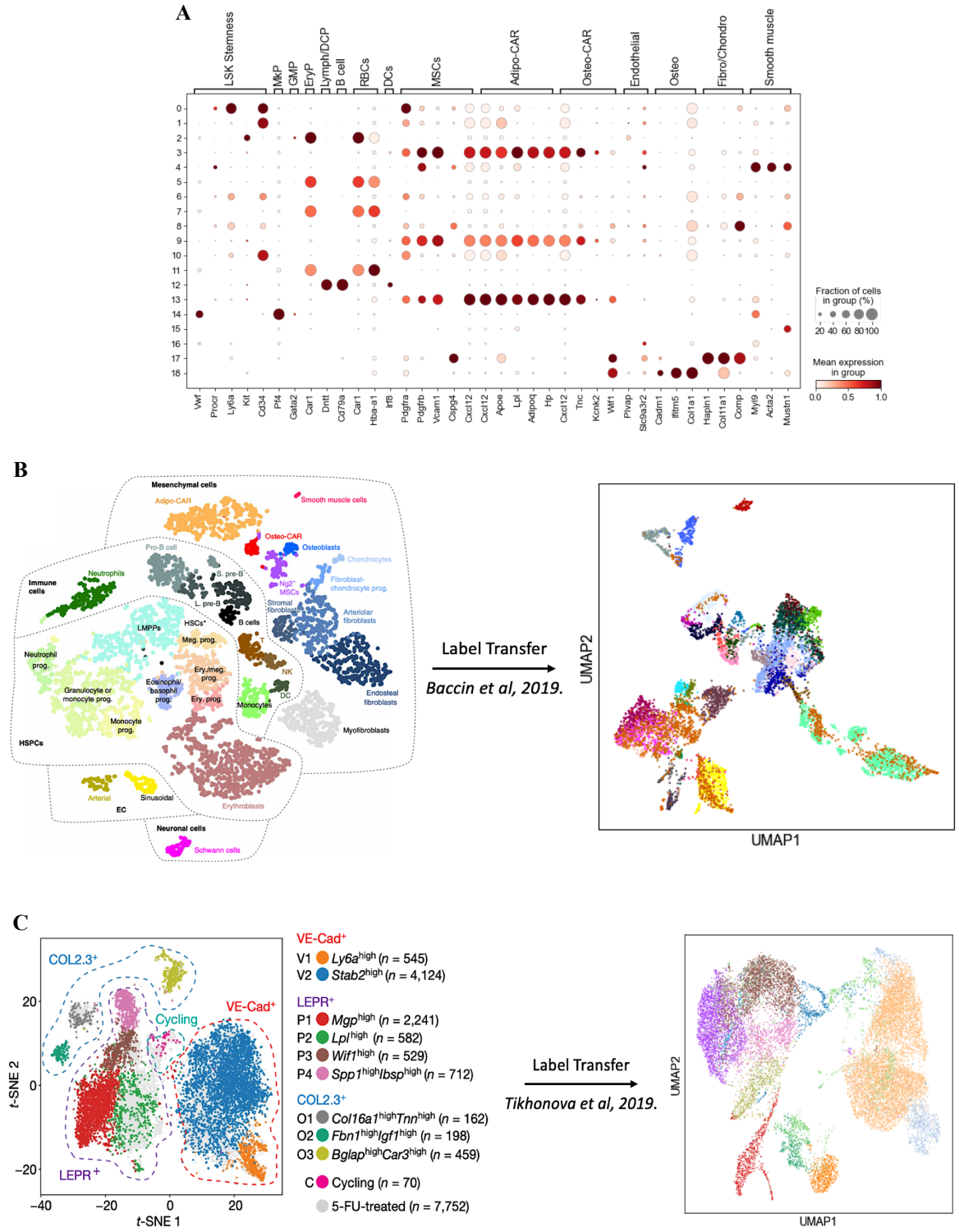

Figure 18. Identification of bone marrow stromal cell types by SC-RNA-seq

(A) Dot-plot representing the marker gene expression levels (x-axis) of the SC-cellular clusters (y-axis), size of circle represents fraction of cells in group and color of the circle indicated the mean expression levels. (B) Label transfer from *Baccin et al.,2019* dataset, UMAP represents color-coded clustering

based on pairwise correspondences between individual cells from the two SC-datasets. (C) Label transfer from *Tikhonova et al.,2019* dataset, UMAP represents color-coded clustering based on pairwise correspondences between individual cells from the two SC-datasets.

To identify the cellular source of the inflammation response, we next analyzed the bone marrow stroma upon IFNα treatment at the single-cell level. In line with our functional proliferation time-course and bulk RNA-seq data, the bone-lining stromal fraction cluster exhibited similar temporal kinetics at the single-cell level (Figure 19A). Using the top 100 DEGs from a combined dataset (merged PBS, 3 h, 24 h & 72 h dataset), we traced the major response upon stimulation down to a sub-population of mesenchymal cells (MSCs & CAR cells) (Figure 19B to D). Further, we made use of a publicly available ISG dataset to identify the direct IFNα-responding population in our single-cell dataset (Figure 19F) (227–229). Interestingly, the same sub-population of mesenchymal cells (comprising of MSCS & CAR cells) stood out as the main ISG inducing cell-type within the bone marrow upon IFNα stimulation. Therefore, the conventional single-cell clustering cannot resolve the inflammation responding sub-pollution from the mesenchymal cell cluster. We thus decided to use a cell type independent SC analysis strategy to resolve the temporal gene expression changes of the IFNα response (Figure 19E). There were marked transcriptional changes at 3 h post stimulation which progressively leveled out over the time course suggesting that the inflammation responding cell fraction is functionally unique within the murine mesenchymal cell compartment.

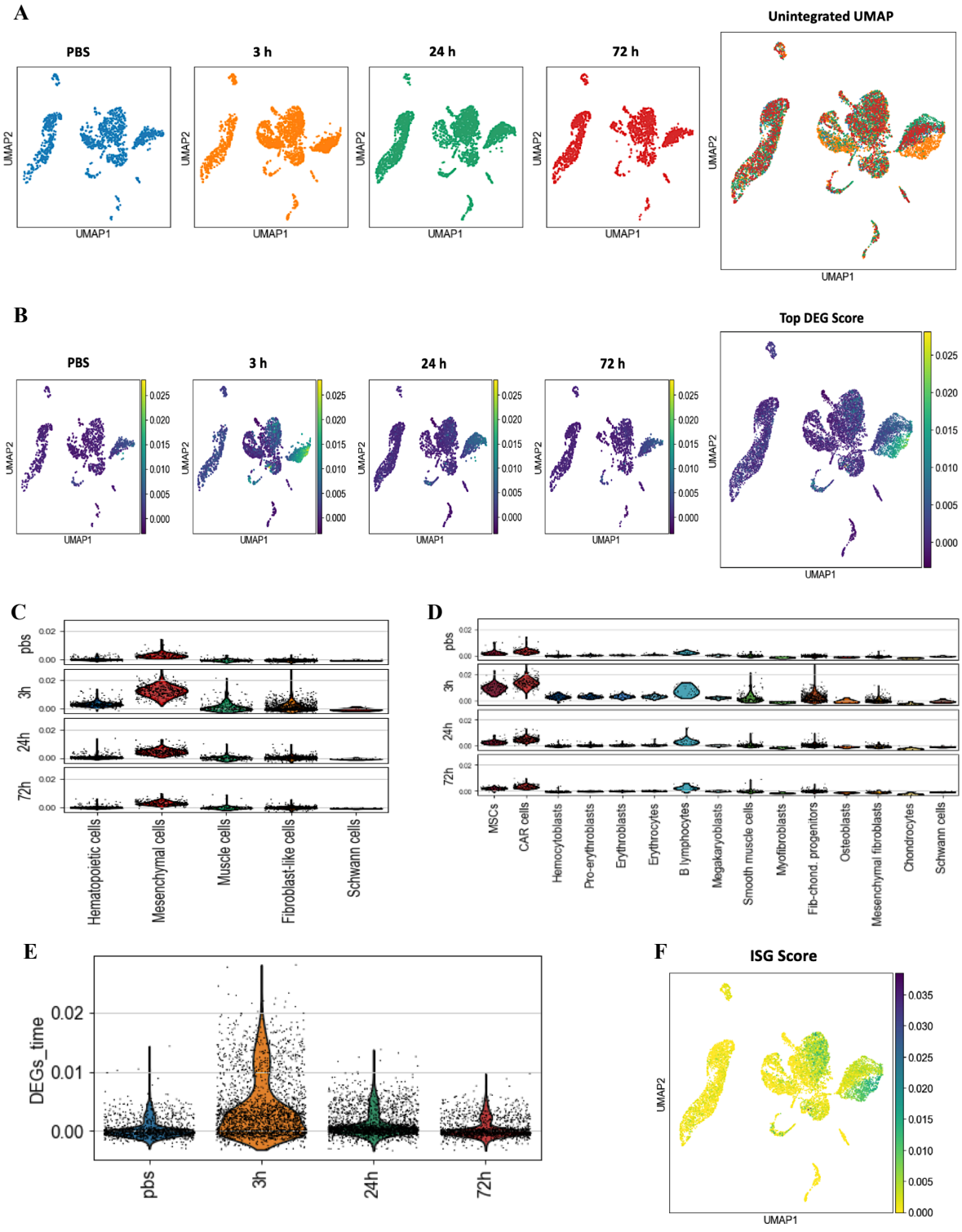

Figure 19. Characterization of the bone marrow stromal inflammatory response by SC-RNA-seq

(A) Unintegrated UMAP visualization of the SC-data for PBS (n = 3000 cells), 3 h (n = 2000 cells), 24 h (n = 2000 cells), 72 h (n = 2000 cells) and merged (n = 9000 cells). Color-coded based on time-point. (B) Top 100 differentially expressed genes (DEGs) represented on using UMAP for PBS (n = 3000 cells), 3 h (n = 2000 cells), 24 h (n = 2000 cells), 72 h (n = 2000 cells) and merged (n = 9000 cells) datasets. (Scale: DEG Score)**.** (C) Expression levels of top 100 DEGs for each of the five major SC-cell types over-time (Scale: DEG Score). (D) Expression levels of top 100 DEGs for each of the fifteen SC-

cellular clusters over-time (Scale: DEG Score). (E) Violin plot representing the top 100 DEGs kinetics (PBS, 3 h, 24 h & 72 h) at the SC-transcriptomic level (Scale: DEG Score)**.** (F) UMAP visualization of ISG gene signature overlaid on the fifteen SC-cellular clusters in the digest bone lining fraction (Merged UMAP representing PBS, 3 h, 24 h and 72 h datasets with n = 4 mice pooled per timepoint, Scale: ISG Score.)

To finally define the inflammation-responding sub-fraction of mesenchymal cells, we extracted a transcriptional signature which combined the conventional MSC single cell fingerprint with the inflammation-response genes and unique metabolic processes. Herewith, we propose a novel iMSC signature comprising of 100 genes to specifically identify the stress-responding population within the bone marrow stroma at the single cell level (Figure 20A; top 20 signature genes shown in Figure 20C). Further, we validated the iMSC signature by transferring the signature onto the time-course merged complete bone marrow stroma dataset. Interestingly, the mesenchymal cells specifically expressed the iMSC signature and recapitulated the temporal dynamics of the single cell data (Figure 20B).

Given that the iMSCs accounted for the majority of the BM stromal response to acute stress, we questioned the role of iMSCs in the disease setting. To study this, we collaborated with Nils B. Leimkühler and Rebekka K. Schneider and made use of their recently published myeloproliferative neoplasms (MPN) murine model dataset; *Leimkühler et al.,2021* (231). In brief, progressive BM fibrosis was induced in the MPN model using thrombopoietin (ThPO) cDNA and the murine non-hematopoietic BM stroma was profiled using single-cell RNA-seq. We overlaid our transcriptional iMSC gene signature onto their disease dataset (Figure 20D). Interestingly, our iMSC signature marked and identified the IFN^{high} MSCs within the MPN dataset that were shown to be strongly primed by a response to type I and type II interferons, confirming that the iMSC signature can potentially be a crucial tool to understand pathogenesis in a disease bone marrow.

Taken together, we propose a novel iMSC signature to unravel inflammation dynamics of the BM microenvironment and improve our understanding of diseases originating in the BM (Figure 20E).

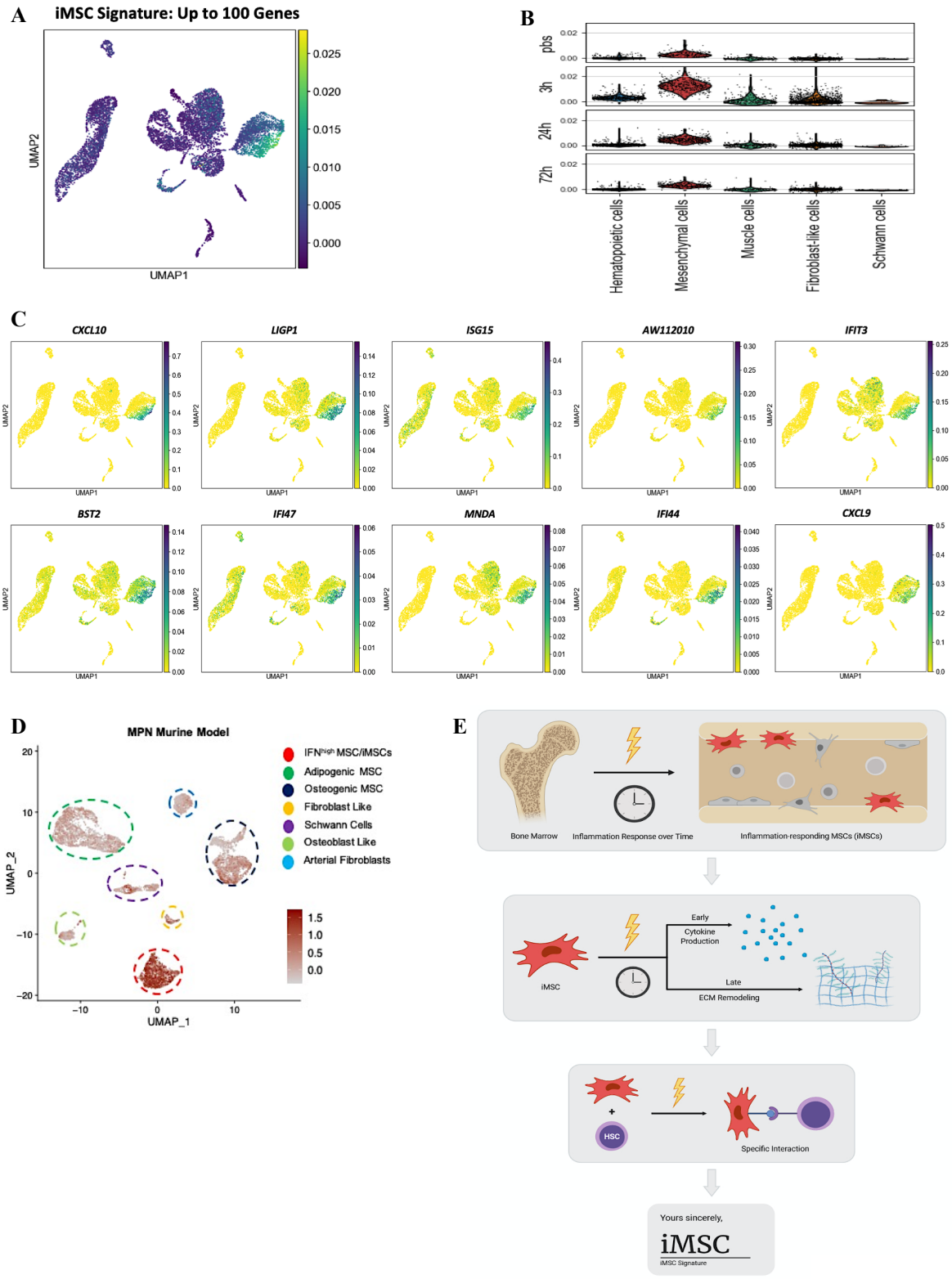

Figure 20. See legend on following page

Figure 20. Inference of a unique transcriptional iMSC signature with application in a disease model

(A) UMAP (n = 9000 cells) representing the iMSC transcriptional gene signature comprising of MSC marker genes, interferon response genes and metabolic genes (100 iMSC signature genes plotted, Scale: Gene Score). (B) iMSC gene signature represented for each of the five SC-cell types over-time (PBS, 3 h, 24 h & 72 h, Scale: Gene Score). (C) Top 10 iMSC signature genes visualized using UMAP (n = 9000 cells) of the fifteen SC-cellular clusters (Scale: Gene Score). (D) iMSC signature (100 signature genes) overlaid onto the *Leimkühler et al.,2021* MPN SC-dataset represented using UMAP (n = 2294 cells). (E) Graphical summery highlighting the bone-lining origin of the iMSCs, with distinct stress response states, inflammation specific interactions with HSCs and a unique SC-transcriptional iMSC signature that identified the disease prorogating IFN^{high} MSCs within the MPN dataset.

3.2 *Ex vivo* Hematopoietic Stem Cell (HSC) expansion using reinvigorating Mesenchymal Stem Cells (rMSCs) for personalized medicine

In the first part of my thesis, we identified a fraction of MSCs as the major responders to IFNα-mediated inflammation in an *in vivo* mouse model. In this second part of the thesis, we aimed at isolating a functional murine MSC population for *in vitro* culture and *ex vivo* expansion of HSCs, and ultimately, applied this protocol for human MSC isolation in order to obtain sufficient numbers of HSCs for clinical application.

3.2.1 Bone lining-derived rMSCs facilitate phenotypic and functional *ex vivo* HSC expansion

To optimize HSC culture, we studied the native bone marrow cellular components based on their ability to support phenotypic and functional *ex vivo* HSC expansion. Murine bone marrow-derived plastic adherent stromal cells (PASCs), known for their HSC-supportive function and *in vitro* expansion potential, were isolated by flushing the bones of the femur, tibia or hip and selecting for stromal cells based on their characteristic ability to adhere to plastic upon serial media change in culture (Figure 21A). In contrast, bone lining-derived reinvigorating Mesenchymal Stem Cells (rMSCs) were isolated from digested bones using fluorescence-activated cell sorting (FACS) by negatively selecting for surface marker expression of CD31 (endothelial cell marker), CD45 (pan hematopoietic marker) and Ter119 (mature erythrocyte marker), and positively selecting for stromal cell markers CD51 and PDGFRα. We established a robust pipeline for mouse-matched rMSC isolation and *ex vivo* culture. Herewith, we reproducibly isolated a homogenous population of about 3,000 rMSCs per mouse (Figure 21B). In contrast, PASCs had a very high inter-mouse variability in stromal cell numbers ranging from 15,000 to 55,000 PASCs. Next, we dissected the differences between

the two stromal cell types PASCs and rMSCs at the transcriptional level assessing the most prominent murine mesenchymal stem cell (MSC) genes *Leptin* and *Nestin*. Both of which have been shown to play a direct role in HSC maintenance, homing and transplantation (26,67,124,226). Strikingly, the bone marrow-derived PASCs expressed significantly lower mRNA levels of *Leptin* (about 2-fold lower) and *Nestin* (about 1.5-fold lower) in comparison to the bone lining-derived rMSCs (Figure 21C & D). Furthermore, the rMSCs showed significantly higher stem cell frequency (1 in 4.31 cells) in contrast to PASCs (1 in 48.8 cells) after 7d *ex vivo* expansion followed by extreme limiting dilution analysis (ELDA) (Figure 21E). Finally, to test whether rMSCs serve as an active HSC attractant in the culture, we performed *ex vivo* co-culture of the two cell types. Our immunofluorescent microscopy data demonstrated that the bone-lining rMSCs, unlike their bone marrow counterpart PASCs, specifically attract HSCs to anchor on the rMSC surface after 24 h of co-culture (Figure 21F).

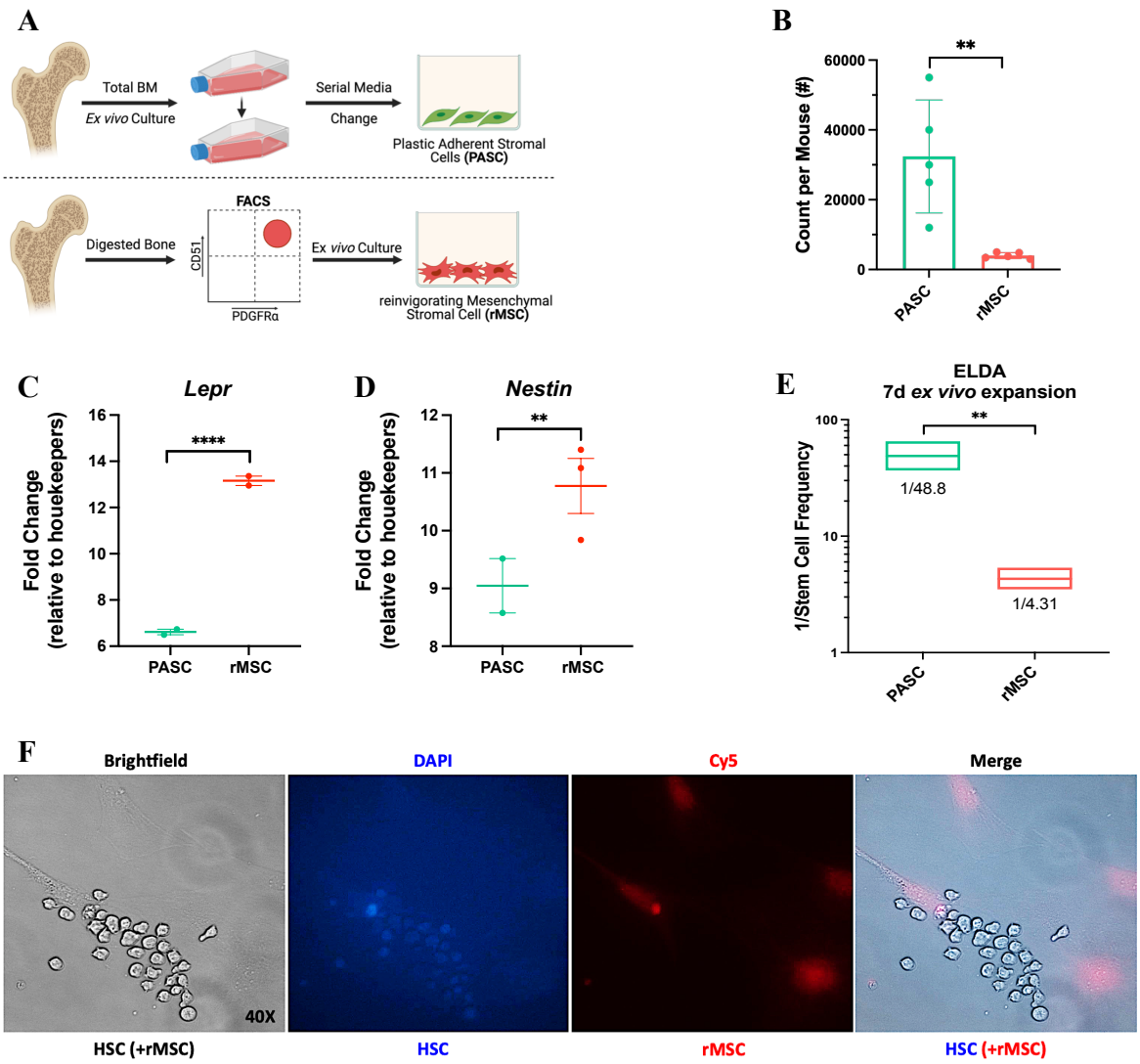

Figure 21. Isolation and identification of the murine bone lining-derived reinvigorating Mesenchymal Stem Cells (rMSCs)

(A) Schematics of bone marrow-derived PASCs isolation by flushing the bones of the femur, tibia or hip and selecting for stromal cells based on their characteristic ability to adhere to plastic upon serial media change in culture. While, bone lining-derived rMSCs were isolated from digested bones using fluorescence-sorting by surface marker expression for $CD45^-$, $Ter119^-$, $CD31^-$, $CD51^+$ & $PDGFR\alpha^+$. (B) Bar graph representing the absolute cell counts of PASCs or rMSCs isolated per mouse. (Mean ± SEM, n = 6, unpaired two-tailed student's t-test performed between marked groups: * $p \leq 0.05$, ** $p \leq 0.01$, *** $p \leq 0.001$, **** $p \leq 0.0001$, ns: non-significant). (C) & (D) Transcriptional levels of crucial murine stromal genes *Lepr* and *Nestin* plotted as fold change relative to housekeepers (*Beta-Actin* & *Gapdh*) for PASCs and rMSCs. (Mean ± SEM, $n \geq 3$, unpaired two-tailed student's t-test performed between marked groups: * $p \leq 0.05$, ** $p \leq 0.01$, *** $p \leq 0.001$, **** $p \leq 0.0001$, ns: non-significant). (E) Limiting dilution analysis of PASCs and rMSCs (Box plots denotes mean with upper and lower limits calculated using the ELDA software, n = 32). (F) Brightfield and immunofluorescence imaging

of HSCs and rMSCs either in monoculture or co-culture stained with label dilution dye cell trace violent (DAPI) and cell trace far-red (Cy5), respectively. (Magnification: 40X)

Given that rMSCs are a homogenous *ex vivo* cultured stromal population with significantly higher stem cell frequency than the convectional PASCs, we hypothesized that they might also outperform the PASCs in their HSC expansion potential. To test this hypothesis, we fluorescently sorted 100 long-term HSCs (LT-HSCs; defined using the cell surface markers: Lineage$^-$ cKIT$^+$ Sca1$^+$ CD48$^-$ CD150$^+$ & CD34$^-$) from the bone marrow of three pooled mice and cultured them *ex vivo* in F12-based serum-free medium supplemented with cytokines (100 ng ml^{-1}TPO and 10 ng ml^{-1} SCF) and 0.1% PVA either in monoculture or in co-culture with the same number of PASCs or rMSCs for 10 days (Figure 22A). Using immunofluorescent imaging and label dilution dyes, we visualized that the actively dividing rMSCs served as the focal point of attachment and cell division for the LT-HSCs in culture (Figure 22B). Further, upon examining the HSC stemness marker expression at the protein level 10 days post *ex vivo* expansion, we observed that the HSCs co-cultured with rMSCs maintained notably higher Sca1 and CD150 levels in comparison to HSC monoculture or co-culture with PASCs (Figure 22C). We quantified the frequency of phenotypic HSCs 10 days post culture by flow cytometric analysis using the cell surface markers: Lineage$^-$ Sca1$^+$ cKit$^+$ CD150$^+$ and plotted them as the proportion of viable cells. There was a significantly higher frequency of phenotypic HSCs when co-culturing HSCs with rMSCs than with PASCs or in monoculture (around 62%, 25%, and 40% of viable cells for rMSC coculture, PASC co-culture, and monoculture, respectively) (Figure 22D). Next, we wanted to assess the fold expansion of HSCs. However, as we had observed big differences in the fraction of HSCs with the original HSC phenotype described above in the different co-cultures (Figure 22C & D), instead of quantifying the absolute number of HSCs in the culture, we assessed the fold change in cell numbers having the HSC marker expression. The rMSC co-culture setting resulted in a 44-fold expansion of the initial 100 LT-HSCs (Figure 22E). In comparison, the rMSC co-culture led to a 11-times higher expansion of

phenotypic HSCs than the PASC co-culture, and a 4.9-times higher expansion than the HSC monoculture. In addition, we compared the stem cell frequency in the expanded HSCs derived from the three culture systems using ELDA. Interestingly, LT-HSCs co-cultured with rMSCs showed the highest stem cell frequency of 1 in 2.33 cells in comparison to HSC monoculture with 1 in 4.96 cells followed by PASC co-culture with 1 in 6.61 cells (Figure 22F). In line with these observations, HSCs co-cultured with rMSCs for a Colony-forming unit-granulocyte, erythroid, macrophage, megakaryocyte (CFU-GEMM) assay also generated significantly more colonies and exhibited higher confluency (~20,000, ~14,000, and ~16,000 colonies, or ~59%, ~50%, and ~46% confluency for rMSC co-culture, PASC co-culture, and HSC monoculture, respectively) (Figure 23A & B). Notably, HSCs in the rMSC co-culture showed the least loss in CFU potential when compared to freshly fluorescence-sorted HSCs used as a positive control for the CFU assay. In addition to the *in vitro* characterizations, we next assessed the function of expanded HSCs *in vivo*. In order to do so, we transplanted the HSCs from the rMSC co-culture expansion into lethally irritated recipient mice (Figure 22G). Interestingly, these HSCs showed stable bone marrow engraftment (~90% of LT-HSC engraftment) 16 weeks post-transplantation along with the reconstitution of peripheral blood components such as B cells, T cells and granulocyte lineage (Figure 22I & H, Figure 23F-H). For further validation, we assessed the transplantation potential of HSCs from rMSC co-culture in parallel with HSCs from monoculture and PASC co-culture (Figure 23C). The data confirmed the functional fitness of HSCs expanded in rMSC co-culture (Figure 23D & E).

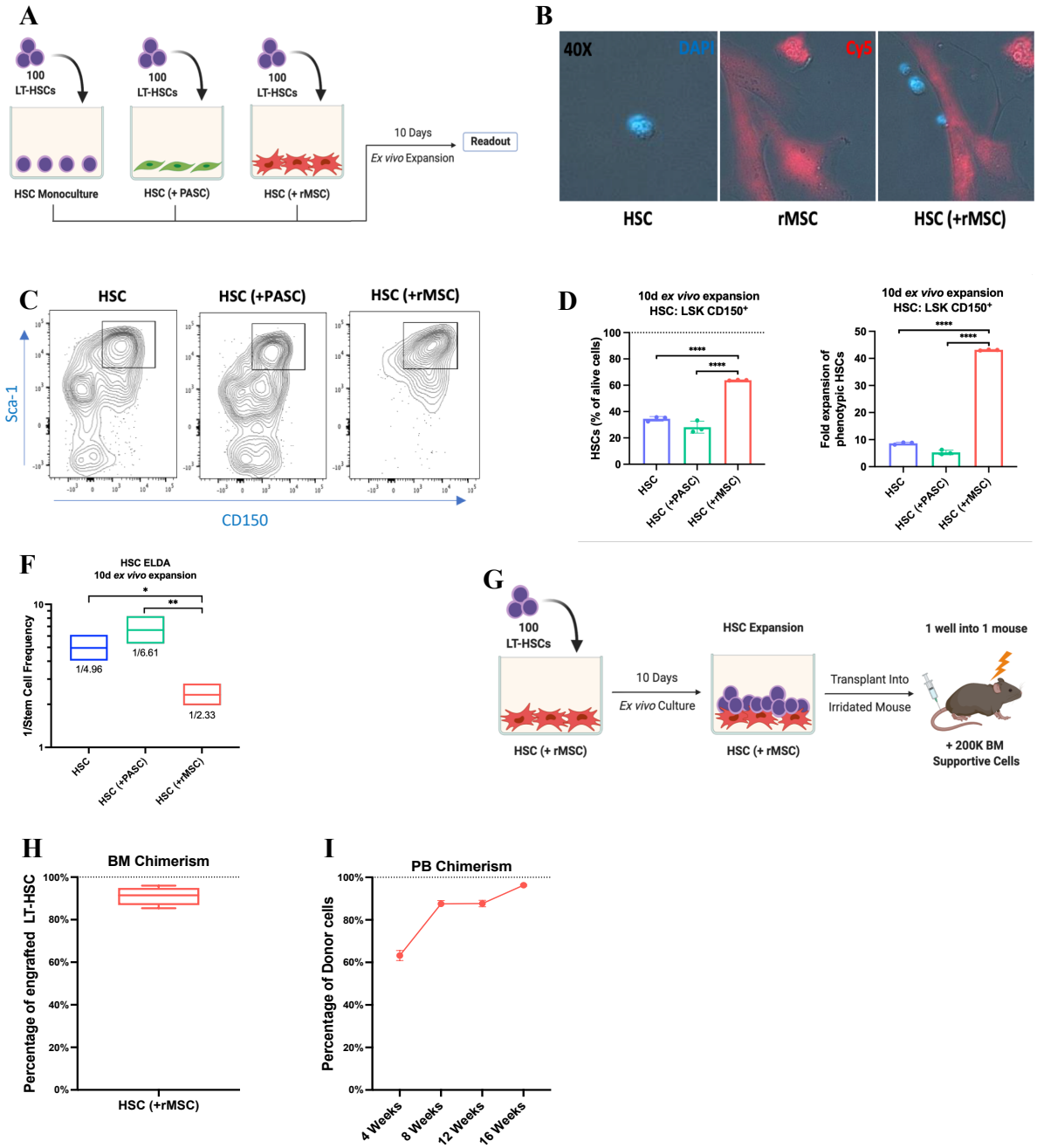

Figure 22. rMSCs promote phenotypic and functional *ex vivo* HSC expansion

(A) Experimental setup of 100 LT-HSCs (Lineage$^-$ cKIT$^+$ Sca1$^+$ CD48$^-$ CD150$^+$ & CD34$^-$) fluorescence-sorted from three pooled WT mice and cultured either in monoculture or in co-cultured 3000 PASCs or rMSCs for 10 days *ex vivo*. (B) Immunofluorescence imaging of HSCs and rMSCs either in monoculture or co-culture stained with label dilution dye cell trace violent (DAPI) and cell trace far-red (Cy5), respectively. (Magnification: 40X). (C) Flow cytometry plots representing Sca-1 and CD150 marker expression post 10 day *ex vivo* expansion of HSCs in monoculture or in co-culture with PASCs or rMSCs. (D) Frequency of LSK CD150$^+$ HSCs post 10 day culture plotted as proportion of viable cells for the three culture systems. (Mean ± SEM, n ≥ 3, unpaired two-tailed student's t-test performed between marked groups: * $p \leq 0.05$, ** $p \leq 0.01$, *** $p \leq 0.001$, **** $p \leq 0.0001$, ns: non-significant).

(E) Fold expansion of the phenotypic HSC pool (Fold Exp. X Freq. of HSCs) calculated for the three culture systems. (Mean ± SEM, n ≥ 3, unpaired two-tailed student's t-test performed between marked groups: * p ≤ 0.05, ** p ≤ 0.01, *** p ≤ 0.001, **** p ≤ 0.0001, ns: non-significant). (F) Stem cell frequency assessment of HSCs post 10 day *ex vivo* expansion using the three culture systems. (Box plots denote mean with upper and lower limits calculated using the ELDA software, n = 32). (G) Schematic of the 100 LT-HSCs co-cultured with rMSCs transplanted into C57BL/6-CD45.1 lethally irradiated mouse post 10-days *ex vivo* expansion, along with 200K supportive total bone marrow cells from C57BL/6-CD45.1/CD45.2 mouse. (H) BM engraftment 16 weeks post-transplantation of HSCs *ex vivo* expanded using rMSCs (Mean ± SEM, n = 6). (I) Peripheral blood reconstitution at 4, 8, 12 and 16 weeks post-transplantation of HSCs *ex vivo* expanded using rMSCs (Mean ± SEM, n = 6).

Having elucidated the strong *ex vivo* expansion potential for phenotypic and functional HSCs using bone-lining rMSCs, we next wanted to perform a comprehensive comparison study including all currently established cellular and non-cellular HSC expansion systems (21,23,212,222). First, we *ex vivo* co-cultured 100 LT-HSCs for 10-days with the mouse bone marrow stromal cell line OP9 or with rMSCs. Here, HSCs co-cultured with rMSCs showed a 2.5-fold higher proportion of phenotypic HSCs, 3.3-fold higher absolute HSC count, and a 7-fold expansion of the phenotypic HSC pool than HSCs from OP9 coculture (Figure 24A to C). For the comparison of rMSC co-culture with established non-cellular compound-based expansion protocols, 100 fluorescence-sorted LT-HSCs were plated into cell culture plates pre-coated with fibronectin, retronectin, Matrigel, gelatin or P-lysin. Impressively, HSCs co-cultured with rMSCs exhibited a minimum loss in the frequency of phenotypic HSCs, a maximum increase in the absolute HSC number, and the highest fold change in expansion of phenotypic HSCs in comparison to all the other non-cellular coatings (Figure 24D to F). Finally, to test how our rMSC-based HSC expansion performs in comparison to alternative media compositions, we performed ELDA after culturing 100 LT-HSC in Walter's cytokine optimized serum-containing medium, Yamazaki's cytokine optimized medium with PVA and fibronectin coating, or the rMSC cytokine-supplemented PVA-containing co-culture system. Here, the HSCs co-cultured with rMSCs exhibited the highest frequency of stem cells with 1 in 2.27 cells

followed by HSCs expanded in Yamazaki's medium with 1 in 4.75 cells and HSCs from the Walter's media with 1 in 13.5 cells (Figure 24G).

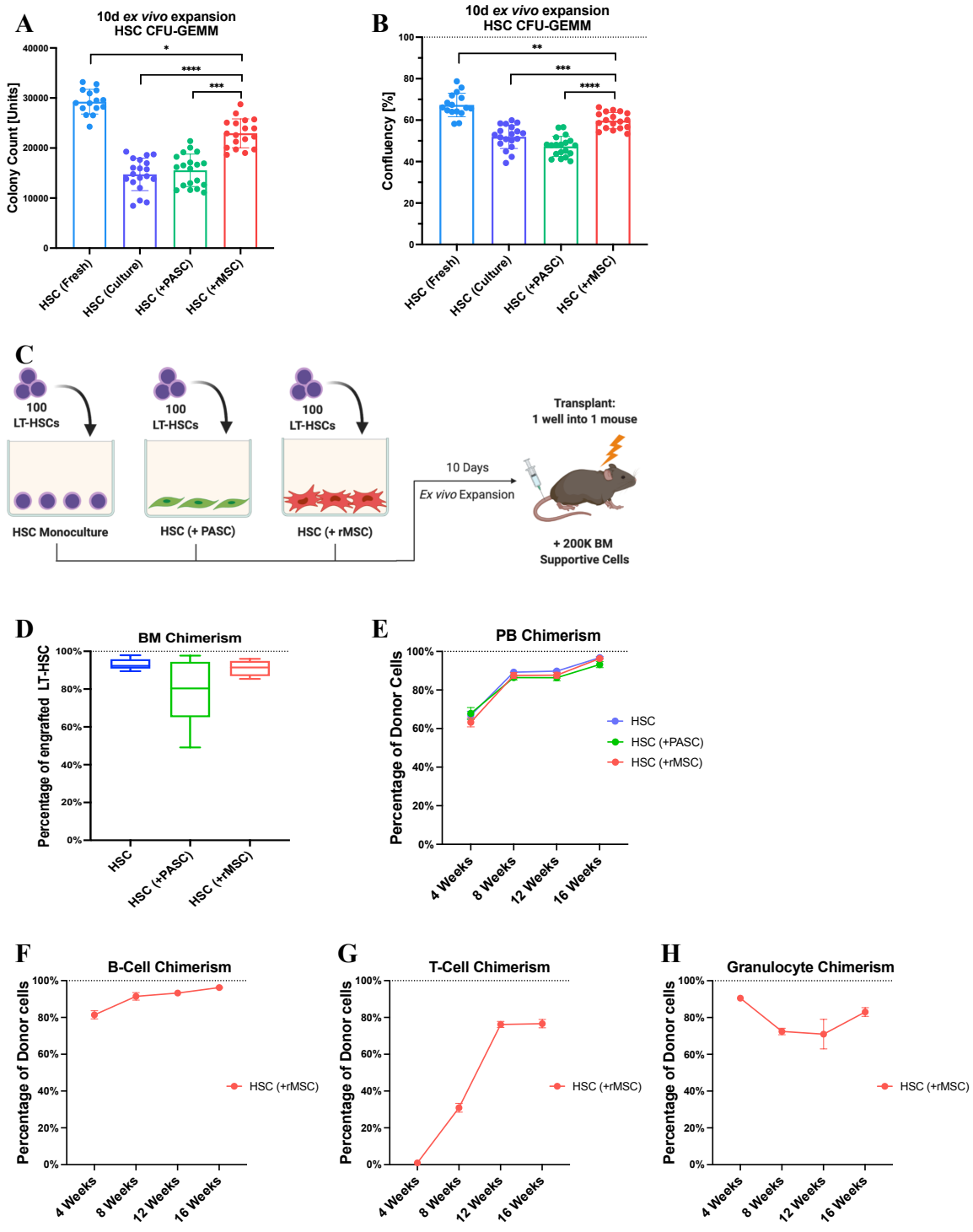

Figure 23. Functional characterization of the HSCs expanded *ex vivo* with rMSCs

(A) Colony count per 100 fresh florescence-sorted HSCs or culture expanded HSCs in monoculture or culture with PASCs and rMSCs from 100 starting cells. (Mean ± SEM, n = 20, CFU with 100 cells per well, unpaired two-tailed student's t-test performed between marked groups: * $p \leq 0.05$, ** $p \leq 0.01$, *** $p \leq 0.001$, **** $p \leq 0.0001$, ns: non-significant). (B) Confluency per well of 100 fresh florescence-

sorted HSCs or culture expanded HSCs in monoculture or culture with PASCs and rMSCs from 100 starting cells. (Mean ± SEM, n = 20, CFU with 100 cells per well, unpaired two-tailed student's t-test performed between marked groups: * $p \leq 0.05$, ** $p \leq 0.01$, *** $p \leq 0.001$, **** $p \leq 0.0001$, ns: non-significant). (C) Schematic of the 100 LT-HSCs cultured in monoculture or co-culture with PASCs or rMSCs transplanted into C57BL/6-CD45.1 lethally irradiated mouse post 10 days *ex vivo* expansion, along with 200K supportive total bone marrow cells from C57BL/6-CD45.1/CD45.2 mouse. (D) BM engraftment 16 weeks post-transplantation of HSCs *ex vivo* expanded using the three culture systems (Mean ± SEM, n = 6). (E) Peripheral blood reconstitution 4, 8, 12 and 16 weeks post-transplantation of HSCs *ex vivo* expanded using the three culture systems (Mean ± SEM, n = 6). (F) B-cell chimerism 4, 8, 12 and 16 weeks post-transplantation of HSCs *ex vivo* expanded using rMSCs (Mean ± SEM, n = 6). (G) T-cell chimerism 4, 8, 12 and 16 weeks post-transplantation of HSCs *ex vivo* expanded using rMSCs (Mean ± SEM, n = 6). (H) Granulocyte chimerism 4, 8, 12 and 16 weeks post-transplantation of HSCs *ex vivo* expanded using rMSCs (Mean ± SEM, n = 6).

Taken together, our data revealed the capability of the bone lining-derived rMSCs to promote *ex vivo* expansion of LT-HSCs that maintain their phenotypic characteristics, their stemness, and their function to reconstitute the bone marrow upon transplantation. Notably, our rMSC co-culture system outperforms all existing alternatives for HSC expansion including systems using stromal cells, non-cellular coating factors, or different medium compositions.

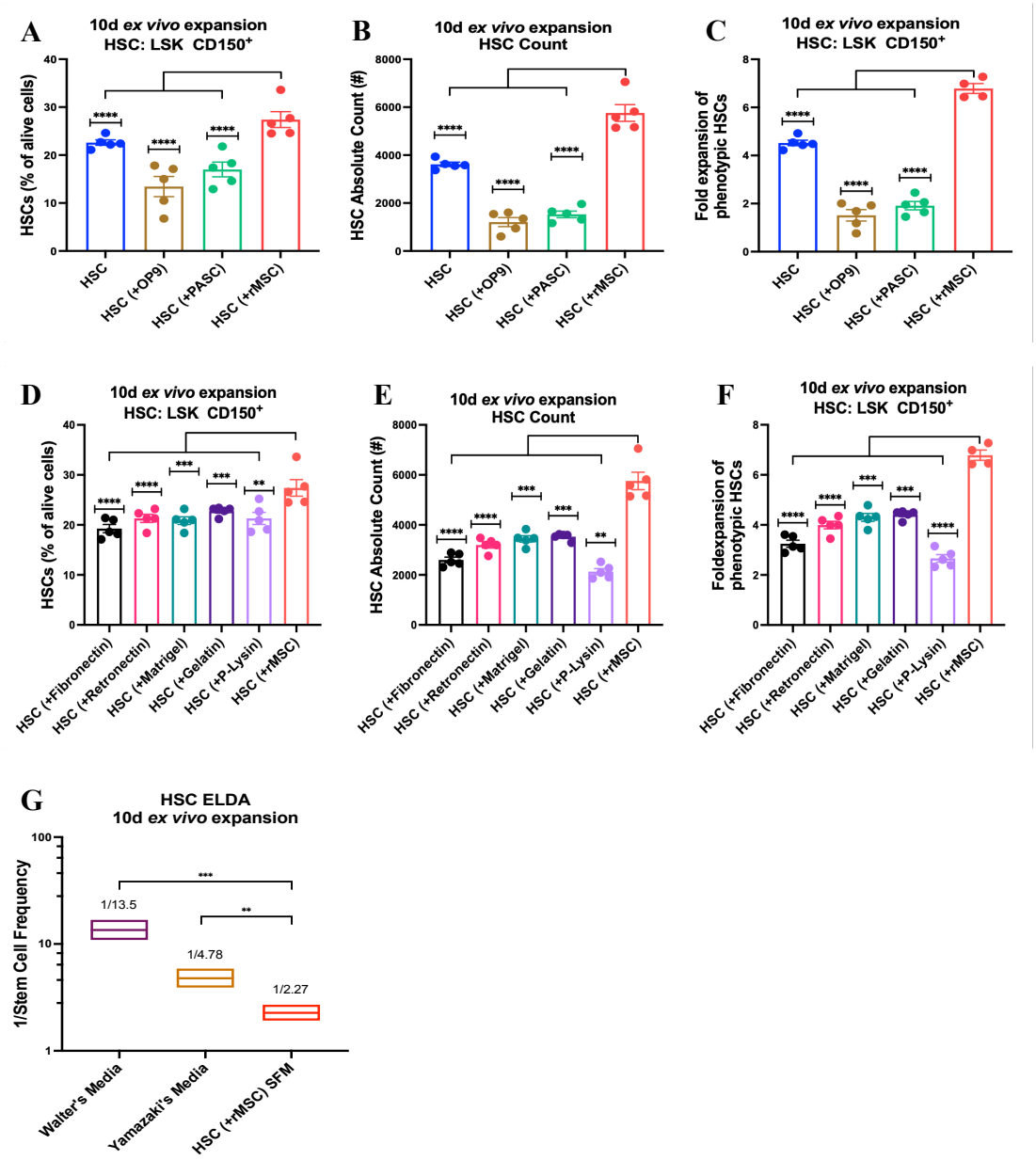

Figure 24. Comparing rMSC-based HSC expansion with alternative HSC *ex vivo* expansion systems

(A) Frequency of phenotypic HSCs (Lineage$^-$ Sca1$^+$ cKit$^+$ CD150$^+$) expanded in monoculture or in co-culture with the same number of OP9 cells, PASCs or rMSCs for 10 days *ex vivo*. (Mean ± SEM, n = 5, unpaired two-tailed student's t-test comparing data points against HSC(+rMSC) co-culture: * $p \leq 0.05$, ** $p \leq 0.01$, *** $p \leq 0.001$, **** $p \leq 0.0001$, ns: non-significant). (B) Absolute HSC counts post 10 day expansion in monoculture or in co-culture with the same number of OP9 cells, PASCs or rMSCs. (Mean ± SEM, n = 5, unpaired two-tailed student's t-test comparing data points against HSC(+rMSC) co-culture: * $p \leq 0.05$, ** $p \leq 0.01$, *** $p \leq 0.001$, **** $p \leq 0.0001$, ns: non-significant). (C) Fold expansion of the phenotypic HSC pool (Fold Exp. X Freq. of HSCs) calculated for the four culture systems. (Mean ± SEM, n = 5, unpaired two-tailed student's t-test comparing data points against HSC(+rMSC) co-culture: * $p \leq 0.05$, ** $p \leq 0.01$, *** $p \leq 0.001$, **** $p \leq 0.0001$, ns: non-significant). (D) Frequency of

phenotypic HSCs (Lineage$^-$ Sca1$^+$ cKit$^+$ CD150$^+$) plated into cell culture plates pre-coated with Fibronectin, Retronectin, Matrigel, Gelatin, P-Lysin or in co-culture with rMSCs for 10 days *ex vivo*. (Mean ± SEM, n = 5, unpaired two-tailed student's t-test comparing data points against HSC(+rMSC) co-culture: * $p \leq 0.05$, ** $p \leq 0.01$, *** $p \leq 0.001$, **** $p \leq 0.0001$, ns: non-significant). (E) Absolute HSC counts post 10 day expansion in cell culture plates pre-coated with Fibronectin, Retronectin, Matrigel, Gelatin, P-Lysin or in co-culture with rMSCs. (Mean ± SEM, n = 5, unpaired two-tailed student's t-test comparing data points against HSC(+rMSC) co-culture: * $p \leq 0.05$, ** $p \leq 0.01$, *** $p \leq 0.001$, **** $p \leq 0.0001$, ns: non-significant). (F) Fold expansion of the phenotypic HSC pool (Fold Exp. X Freq. of HSCs) calculated for the six culture systems. (Mean ± SEM, n = 5, unpaired two-tailed student's t-test comparing data points against HSC(+rMSC) co-culture: * $p \leq 0.05$, ** $p \leq 0.01$, *** $p \leq 0.001$, **** $p \leq 0.0001$, ns: non-significant). (G) Stem cell frequency assessment of HSCs post 10 day *ex vivo* expansion in Walter's cytokine optimized serum-containing medium, Yamazaki's cytokine optimized medium with PVA and fibronectin coating, or the rMSC cytokine-supplemented PVA-containing co-culture system. (Box plots denotes mean with upper and lower limits calculated using the ELDA software, n = 32).

3.2.2 The rMSCs enable long term *ex vivo* HSC expansion

Time lapse microscopy revealed the striking accumulation of proliferating HSCs on the rMSC surface over time (Figure 25) leading to the question, how would HSCs behave in a long-term expansion setup with regard to their proliferation, stemness and function. Thus, we performed similar experiments as described above but this time extending the 100 LT-HSC co-cultures to 7, 14, and 21 days (Figure 26A). As expected, the frequency of phenotypic HSCs reduced with the increase in *ex vivo* expansion days across the three culture systems (Figure 26B). However, the HSCs co-cultured with rMSCs exhibited a significantly higher proportion of phenotypic HSCs in comparison to HSCs in monoculture and PASCs co-culture at every time point. This superiority of the rMSC co-culture on the HSCs became even more pronounced when comparing their fold expansion of the phenotypic HSC pool over the 21-day expansion time-course (Figure 26C). Interestingly, the HSCs co-cultured with rMSCs already outperformed the other two HSC expansion systems 7 days post culture with this difference in fold expansion of phenotypic HSCs being ~100, and ~10,000-fold higher than for HSCs in

monoculture and PASC co-culture, respectively at the 21-day time-point. In accordance with these observations, HSCs in co-culture with rMSCs upon functional CFU-GEMM assay also generated significantly more colonies and contributed to higher confluency at all times (Figure 27A & B). Notably, the rMSC-HSC co-culture, unlike the HSCs from the other two culture systems, maintained robust fold expansion of HSC colonies even after 21 days *ex vivo* expansion (Figure 26D).

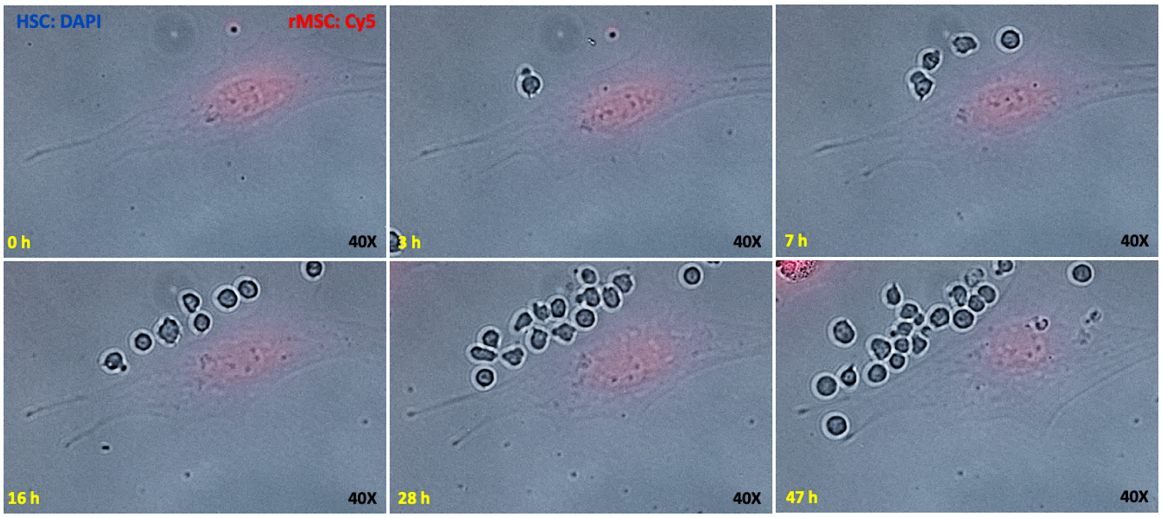

Figure 25. rMSCs serve as a focal point of attachment and active proliferation for the *ex vivo* cultured HSCs

Time laps microscopy (0 h to 47 h) of HSCs and rMSCs co-cultured and stained with label dilution dye cell trace violent (DAPI) and cell trace far-red (Cy5), respectively. (Magnification: 40X)

Next, we examined the expression of HSC maintenance and function genes at the transcriptional level in HSCs over a 28-day long-term expansion time course in order to verify any changes in these HSCs after long-term culture. The HSCs co-cultured with rMSCs showed marked upregulation in the mRNA level of most HSC maintenance and function genes tested in direct comparison to HSCs in monoculture and PASC co-culture, with the highest expression at 28 days followed by the second highest expression at 14 days (Figure 26E). This noticeable increase in the levels of HSC maintenance and function genes specifically by the HSCs in rMSC co-culture suggest the maintenance of LT-HSC potential in the co-culture and might in part explain the prominent *ex vivo* expansion potential of the rMSCs, especially at the later time

points were the rMSC co-culture effect was most dramatic compared to HSCs in monoculture or PASC co-culture. In order to quantify individual transcriptional changes, we assessed the temporal expression of the four most crucial HSC genes as per literature: *Slam1*, *Cxcr4*, *Notch1* and *SCF (42,85,121,124,136)*. The HSCs co-cultured with rMSCs showed maximum expression of *Slam1* and *Notch1* at the 28-day timepoint, expressing ~5-fold, and ~30-fold higher *Slam1* and *Notch1*, respectively, compared to that of HSCs in monoculture (Figure 26F & H*)*. On the other hand, *Cxcr4* and *SCF* expression reached their peak at the 14-day timepoint for the HSCs co-cultured with rMSC, expressing ~25-fold, and ~27-fold higher *Cxcr4* and *SCF*, respectively, in comparison with that of HSCs in monoculture (Figure 26G & I).

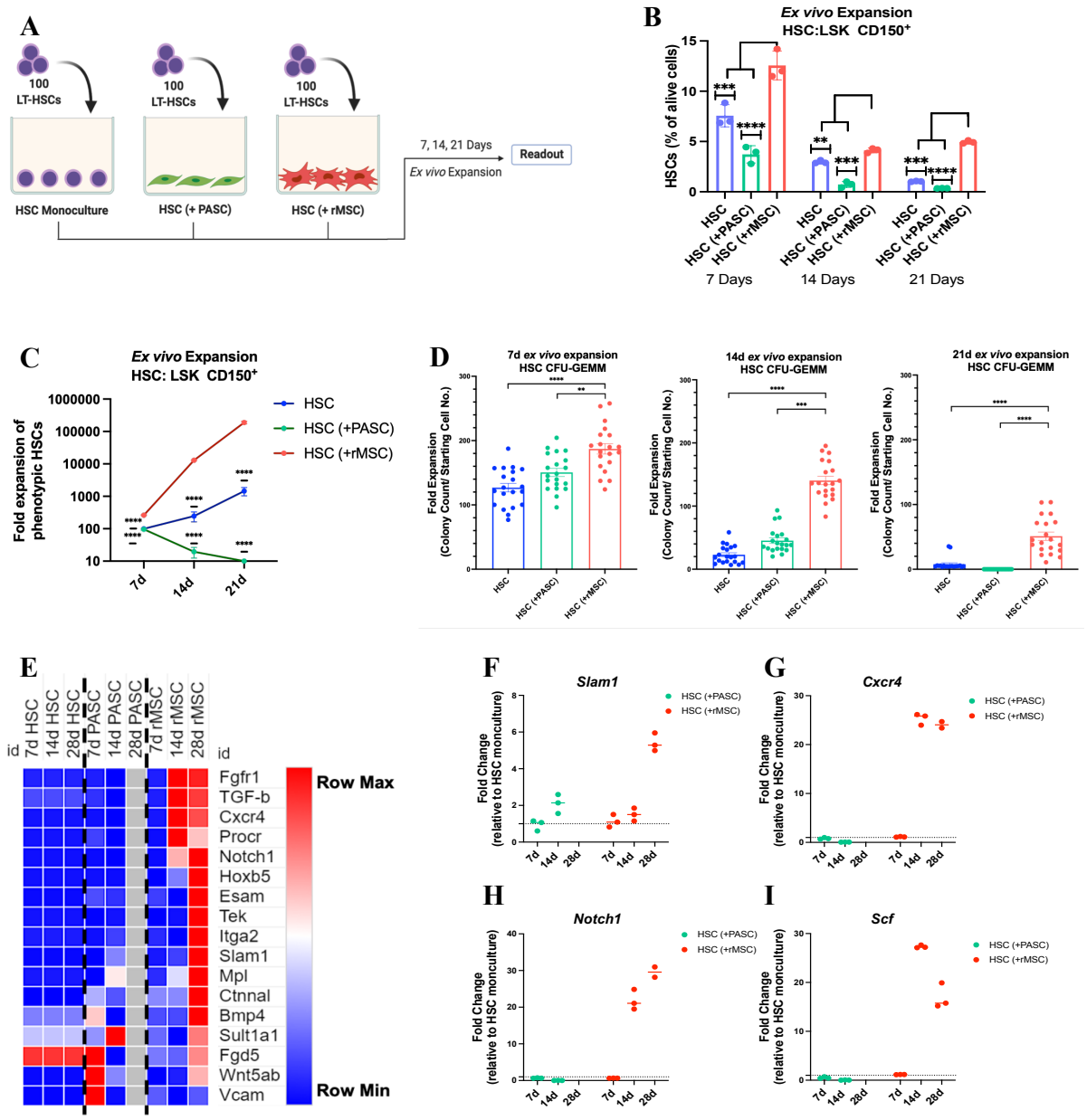

Figure 26. rMSCs enable long term ex vivo HSC expansion

(A) Experimental setup of 100 LT-HSCs (Lineage$^-$ cKIT$^+$ Sca1$^+$ CD48$^-$ CD150$^+$ & CD34$^-$) fluorescence-sorted from three pooled WT mice and cultured either in monoculture or in co-cultured with 3000 PASCs or rMSCs for 7, 14 or 21 days *ex vivo*. (B) Frequency of phenotypic HSCs (Lineage$^-$ Sca1$^+$ cKit$^+$ CD150$^+$) expanded in monoculture or in co-culture with 3000 PASCs and rMSCs for 7, 14 or 21 days *ex vivo*. (Mean ± SEM, n ≥ 3, unpaired two-tailed student's t-test comparing data points against HSC(+rMSC) co-culture per time-point: * $p \leq 0.05$, ** $p \leq 0.01$, *** $p \leq 0.001$, **** $p \leq 0.0001$, ns: non-significant). (C) Fold expansion of the phenotypic HSC pool (Fold Exp. X Freq. of HSCs) calculated for HSCs from the three culture systems post 7, 14 or 21 day expansion. (Mean ± SEM, n ≥ 3, unpaired two-tailed student's t-test comparing data points against HSC(+rMSC) co-culture per time-point: * $p \leq 0.05$, ** $p \leq 0.01$, *** $p \leq 0.001$, **** $p \leq 0.0001$, ns: non-significant). (D) Fold expansion of HSC colonies over the three time points assessed by Colony-forming unit− granulocyte, erythroid,

macrophage, megakaryocyte (CFU-GEMM) assay of the HSCs from the three culture systems. (Mean ± SEM, n = 20, unpaired two-tailed student's t-test performed between the indicated two data sets: * $p \leq 0.05$, ** $p \leq 0.01$, *** $p \leq 0.001$, **** $p \leq 0.0001$, ns: non-significant). (E) Heatmap of HSC maintenance and function genes expressed at the transcriptional level in HSCs expanded as monoculture or as co-culture with PASCs and rMSCs after a 7, 14 or 28 day long-term expansion. (Scale: row normalized units, mean from n = 5). (F) & (G) Temporal transcriptional expression dynamics of crucial HSC genes *Slam1* and *Notch1* in HSCs expanded as monoculture or as co-culture with PASCs and rMSCs for 7, 14 or 28 days. (Mean ± SEM, $n \geq 3$, scale: fold change normalized to the gene expression in HSC-monoculture). (H) & (I) Temporal transcriptional expression dynamics of crucial HSC genes *Cxcr4* and *SCF* in HSCs expanded as monoculture or as co-culture with PASCs and rMSCs for 7, 14 or 28 days. (Mean ± SEM, $n \geq 3$, scale: fold change normalized to the gene expression in HSC-monoculture).

To sum it up, our data showed that the rMSC co-culture system maintained the highest frequency of phenotypic HSCs, which means that in the presence of rMSCs the HSCs do not differentiate as quickly. The transcriptional data confirmed that instead of losing maintenance and function genes, the expanded HSC population had a marked increase in these genes after long-term expansion up to 4 weeks indicating that the rMSC co-culture enhanced the stability and maintenance of even the expanded HSCs. Consequently, the rMSC-based HSC expansion protocol exceeded all expectations and provided a reproducible and robust approach to expand phenotypic and functional HSCs to absolute numbers that were ~100 times higher than any other described method could produce. Of note, our rMSC co-culture system demonstrated the feasibility of a sufficiently long HSC culture and expansion, which would allow for genetic manipulation, selection, amplification and usage of genetically engineered HSC for therapeutic purpose.

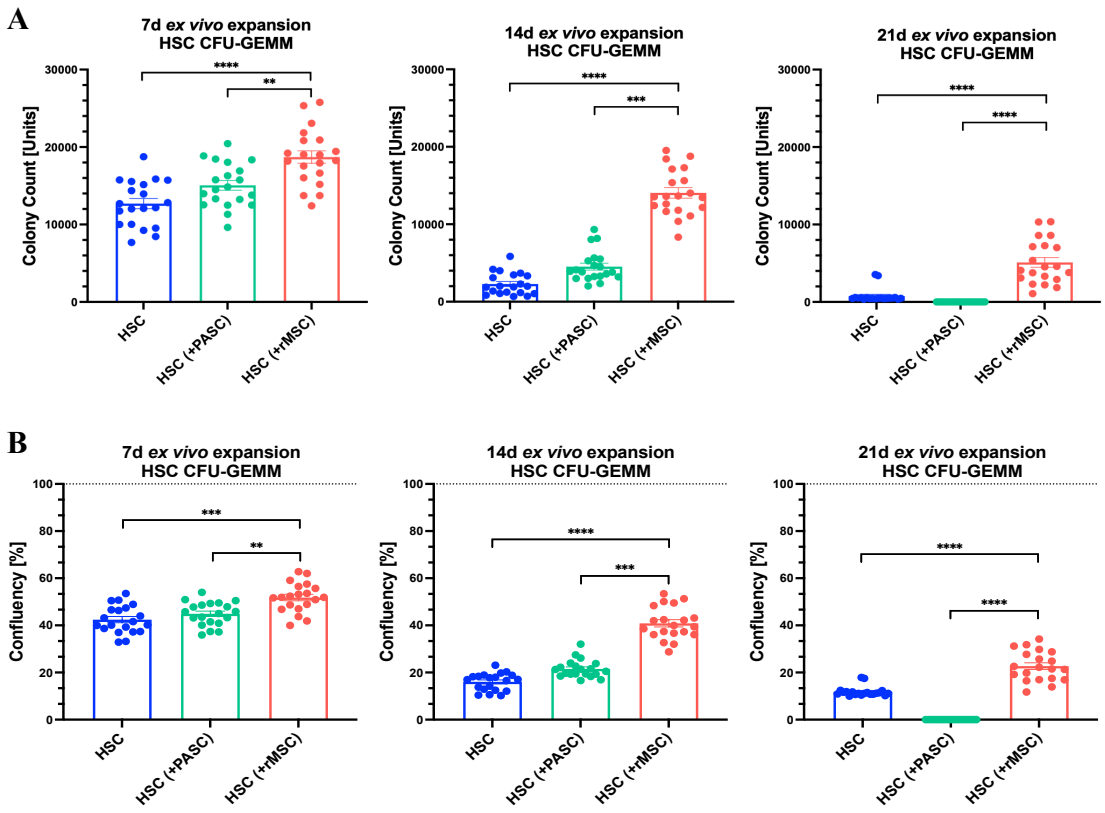

Figure 27. HSCs expanded long-term by rMSCs maintain their functional potential

(A) Colony counts of 100 starting HSCs *ex vivo* in monoculture or in co-culture with PASCs and rMSCs post 7, 14 and 21 days expansion. (Mean ± SEM, n = 20, CFU with 100 cells per well, unpaired two-tailed student's t-test performed between marked groups: * $p \leq 0.05$, ** $p \leq 0.01$, *** $p \leq 0.001$, **** $p \leq 0.0001$, ns: non-significant). (B) Confluency per well of HSCs in monoculture or in co-culture with PASCs or rMSCS post 7, 14 and 21 days expansion. (Mean ± SEM, n = 20, CFU with 100 cells per well, unpaired two-tailed student's t-test performed between marked groups: * $p \leq 0.05$, ** $p \leq 0.01$, *** $p \leq 0.001$, **** $p \leq 0.0001$, ns: non-significant).

3.2.3 Single HSC *ex vivo* expansion is facilitated by co-culture with rMSCs

As we know that a phenotypically homogenous HSC population can be functionally heterogenous, we next wanted to assess the single cell expansion potential of our HSCs similar to what has been show by Wilkinson et al. (213). So, we florescence-sorted single LT-HSCs and *ex vivo* expanded them either in monoculture or co-culture with rMSCs for 10, 20 and 30 days (Figure 28A). We observed considerable variability between the two culture systems in their ability to long-term expand a single HSC, with ~20% HSCs in monoculture giving rise to

a colony, in contrast to ~80% HSCs forming colonies when in co-culture with rMSCs (Figure 28B). Further, the rMSC co-culture maintained a significantly higher proportion of phenotypic HSCs at all times (Figure 28C). Notably, the rMSC co-culture promoted a more homogenous expansion of the single HSC clones with almost 5-times more clones above the 5% mark in frequency of phenotypic HSC after 30 days *ex vivo* expansion. The single HSC-rMSC co-culture also showed a marked exponential fold expansion of the phenotypic HSC pool with a ~80, ~120, and ~200-fold difference in comparison to HSCs expanded as monoculture at 10-day, 20-day, and 30-day timepoint, respectively (Figure 28D).

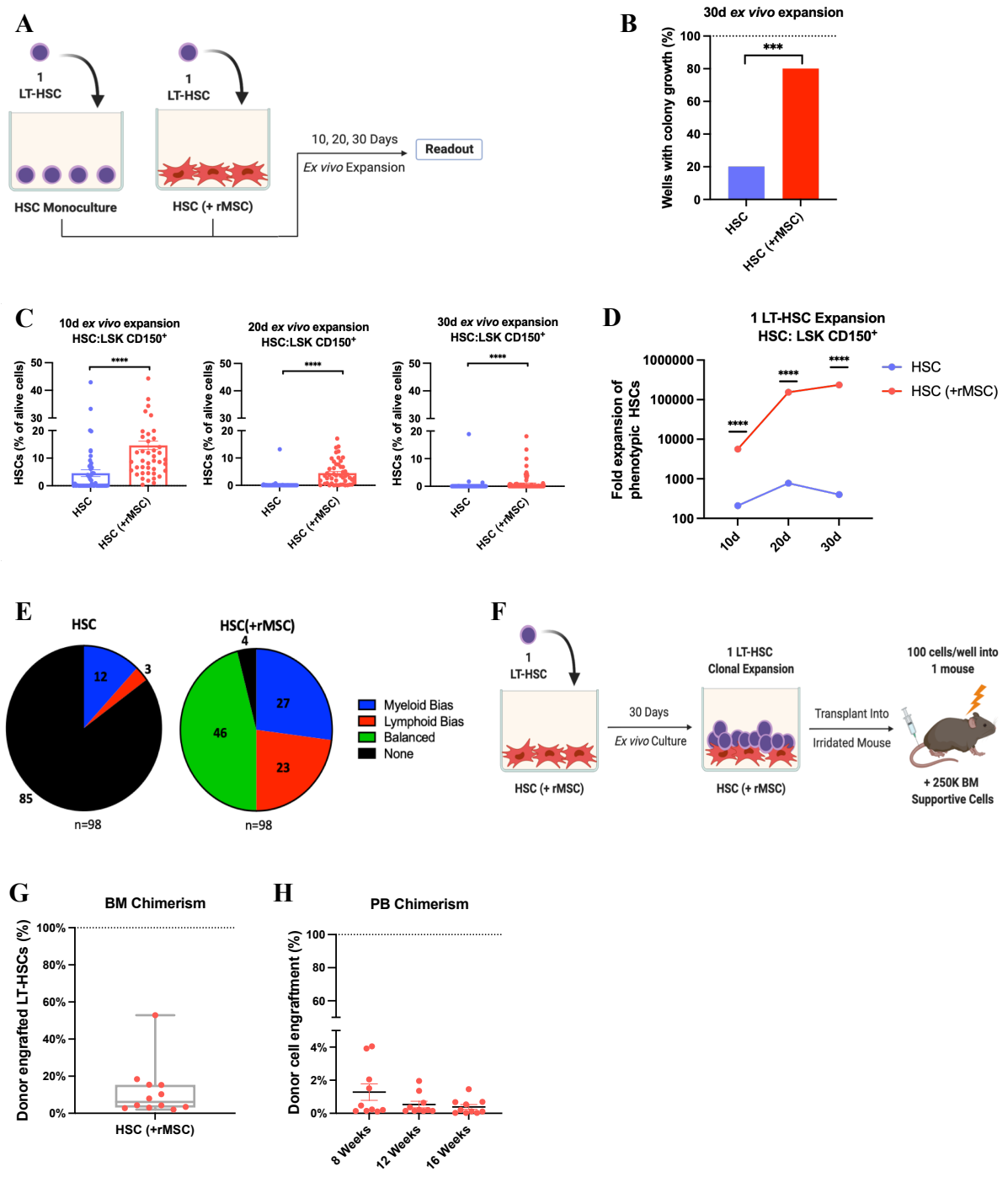

Figure 28. Single HSC *ex vivo* expansion is facilitated by co-culture with rMSCs

(A) Experimental setup of 1 LT-HSCs (Lineage$^-$ cKIT$^+$ Sca1$^+$ CD48$^-$ CD150$^+$ & CD34$^-$) fluorescence-sorted from three pooled WT mice and cultured either in monoculture or in co-cultured with 3000 rMSCs for 10, 20 or 30 days *ex vivo*. (B) Proportion of wells with colony out-growth post 30 days *ex vivo* expansion of a single LT-HSC either in monoculture or in co-culture with rMSCs. (n = 98, with two independent experiments, unpaired two-tailed student's t-test performed between the indicated data sets: * $p \leq 0.05$, ** $p \leq 0.01$, *** $p \leq 0.001$, **** $p \leq 0.0001$, ns: non-significant). (C) Frequency of phenotypic HSCs (Lineage$^-$ Sca1$^+$ cKit$^+$ CD150$^+$) expanded either in monoculture or in co-culture with rMSCs for 10, 20 or 30 days *ex vivo*. (Mean ± SEM, $n \geq 3$, unpaired two-tailed student's t-test performed

between the indicated data sets: * $p \leq 0.05$, ** $p \leq 0.01$, *** $p \leq 0.001$, **** $p \leq 0.0001$, ns: non-significant). (D) Fold expansion of the phenotypic HSC pool (Fold Exp. X Freq. of HSCs) calculated for HSCs from the two culture systems post 10, 20 or 30 days expansion of the starting single LT-HSC. (Mean ± SEM, $n \geq 3$, unpaired two-tailed student's t-test performed between the indicated data sets: * $p \leq 0.05$, ** $p \leq 0.01$, *** $p \leq 0.001$, **** $p \leq 0.0001$, ns: non-significant). (E) Differentiation skewing analysis via flow-cytometry post 30 days *ex vivo* expansion of a single LT-HSC either in monoculture or in co-culture with rMSCs. Pie-chart represents proportion of HSC clones with myeloid bias (≥65% of viable cells per clone expressing myeloid markers: $CD41^+$, $CD34^+$, $CD71^+$, $CD11b^+$ & $GR1^+$), lymphoid bias (≥65% of viable cells per clone lymphoid markers: $CD127^+$, $CD34^-$, $CD4^+$, $CD8^+$ & $B220^+$), balanced output (at least 45% of viable cells per clone expressing both myeloid & lymphoid markers) or no viable colony out-growth (classified as none). (n = 98). (F) Schematic of 100 clonally expanded HSCs using the rMSC culture system transplanted into C57BL/6-CD45.1 lethally irradiated mouse post 30 days *ex vivo* expansion of the starting single LT-HSC, along with 250K supportive total bone marrow cells from C57BL/6-CD45.1/CD45.2 mouse. (G) BM engraftment 16 weeks post-transplantation of clonally expanded HSCs using rMSCs *ex vivo* (Mean ± SEM, n = 12). (H) Peripheral blood reconstitution at 8, 12 and 16 weeks post-transplantation of clonally expanded HSCs using rMSCs *ex vivo* (Mean ± SEM, n = 12).

Since one of the fundamental challenges of *ex vivo* single HSC expansion is to maintain the HSC-characteristic functional multilineage differentiation potential, we assessed the differentiation skewing post 30-day clonal expansion of a single HSCs in our rMSC co-culture. Out of the 98 HSC clones assed via flow cytometry, 27% and 24% showed myeloid and lymphoid bias, respectively, whereas the majority of 46% clones possessed a balanced multilineage differentiation potential (Figure 28E). On the other hand, the 85% of HSCs expanded in monoculture did not give rise to any colonies with the remaining 12% and 3% differentiating into myeloid and lymphoid lineages, respectively. Furthermore, we dissected the differentiation potential of the single HSC clones expanded *ex vivo* in rMSC co-culture into three myeloid primed and two lymphoid primed linages. The clonally expanded HSC generated 75% granulocyte-macrophage cells, 22% erythroid-megakaryocytes and 3% myeloid progenitors within the myeloid-primed fraction, whereas, in the lymphoid-primed fraction there were 86% mature-lymphocytes and 14% lymphoid progenitors (Figure 29A).

In addition to the *in vitro* characterizations of the single HSC expansion in the rMSC co-culture system, we next assessed the function of these clones HSCs *in vivo*. In order to do so, we expanded single LT-HSCs for 30 days in *ex vivo* culture with rMSCs and transplanted 100 HSC clones into lethally irradiated recipient mice (Figure 28F). Noteworthily, these clones showed stable bone marrow engraftment of ≥ 2% in all 12 recipient mice (mean: ~13.5% LT-HSC engraftment) 16 weeks post-transplantation (Figure 28G). We also detected robust peripheral-blood chimerism (mean: ~0.5% 16-week post-transplantation) along with the reconstitution of peripheral blood components such as B cells, T cells and granulocyte lineage (Figure 28H, Figure 29B to D). These experiments confirmed bona fide HSC self-renewal potential of the rMSC co-culture system.

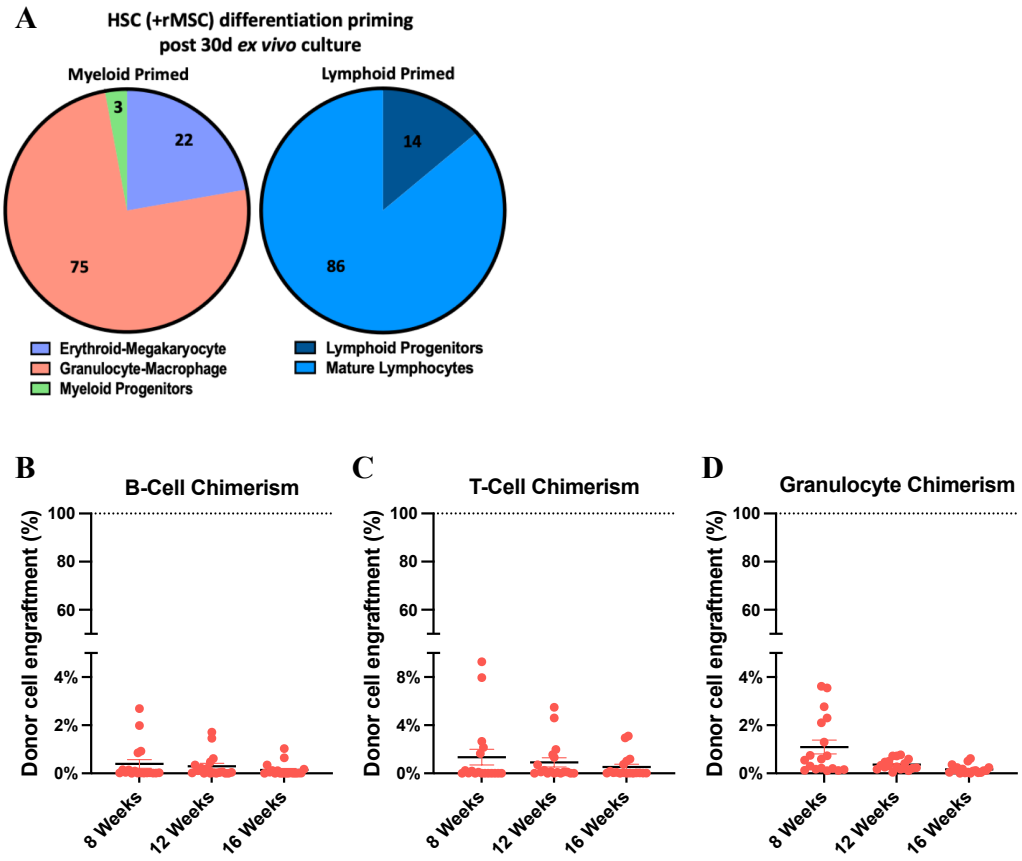

Figure 29. *In vitro* and *in vivo* function of single LT-HSC expanded *ex vivo* using rMSCs

(A) Differentiation priming analysis via flow-cytometry post 30 days *ex vivo* expansion of a single LT-HSC in co-culture with rMSCs. Pie-chart represents proportion of rMSC expanded HSC clones which are myeloid primed with ≥65% of viable cells per clone expressing erythroid-megakaryocyte ($CD71^+$ & $Ter119^+$), granulocyte-macrophage ($CD11b^+$ & $Gr1^+$) or myeloid progenitor ($CD41^+$ & $CD34^+$) markers

or lymphoid primed with ≥65% of viable cells per clone expressing either lymphoid progenitor ($CD34^-$ & $CD127^+$) or mature lymphocyte ($CD4^+$, $CD8^+$ & $B220^+$) markers. (n = 98). (B) B-cell chimerism at 8, 12 and 16 weeks post-transplantation of clonally expanded HSCs using rMSCs (Mean ± SEM, n = 12). (C) T-cell chimerism 8, 12 and 16 weeks post-transplantation of clonally expanded HSCs using rMSCs (Mean ± SEM, n = 12). (D) Granulocyte chimerism 8, 12 and 16 weeks post-transplantation of clonally expanded HSCs using rMSCs (Mean ± SEM, n = 12).

3.2.4 Donor-matched rMSCs express human HSC support and maintenance genes

A substantial goal of stem cell research is to provide human HSCs for different clinical applications including bone marrow transplantations. However, the major roadblock in bone marrow transplants is the limited availability of human HSCs, which could not be addressed with currently existing *ex vivo* expansion protocols. As we have shown the successful long-term *ex vivo* expansion of murine HSCs using murine rMSCs, we now focused on the translation of this approach from the murine to the human system. In doing so, we designed a donor-individualized experimental strategy that allowed for the isolation of both HSCs and rMSCs from the same patient sample (Figure 30A). First, to identify a human bone lining-derived stromal analogue to murine rMSCs, we created a robust pipeline for human femur-head serial digestion followed by fluorescence-sorting of human rMSCs using the cell surface markers: $Lineage^-$ $CD31^-$ $CD51^+$ and $PDGFR\alpha^+$ (Figure 30B). We characterized these human rMSCs by flow cytometry using established human mesenchymal stromal markers: CD271, CD90, CD105 and CD73 (Figure 30C). Further, we demonstrated that the human rMSCs isolated from individual donors using our pipeline can be *ex vivo* cultured and expanded while maintaining their characteristic fibroblast-like architecture and plastic adherent property (Figure 30D). Next, we assessed the transcriptional levels of crucial human HSC support and maintenance genes, *Col1a* (stromal matrisomal gene involved in HSC maintenance) and *G-CSF* (known to stimulate the survival and proliferation of HSCs). The human rMSCs exhibited ~1.4 and ~1.2-fold higher expression of *Col1a* and *G-CSF* genes, respectively, in comparison to donor-matched PASCs

(Figure 30E & F). This data suggests that the human rMSCs might be superior to conventional human PASCs for *ex vivo* HSC expansion in a donor-individualized system.

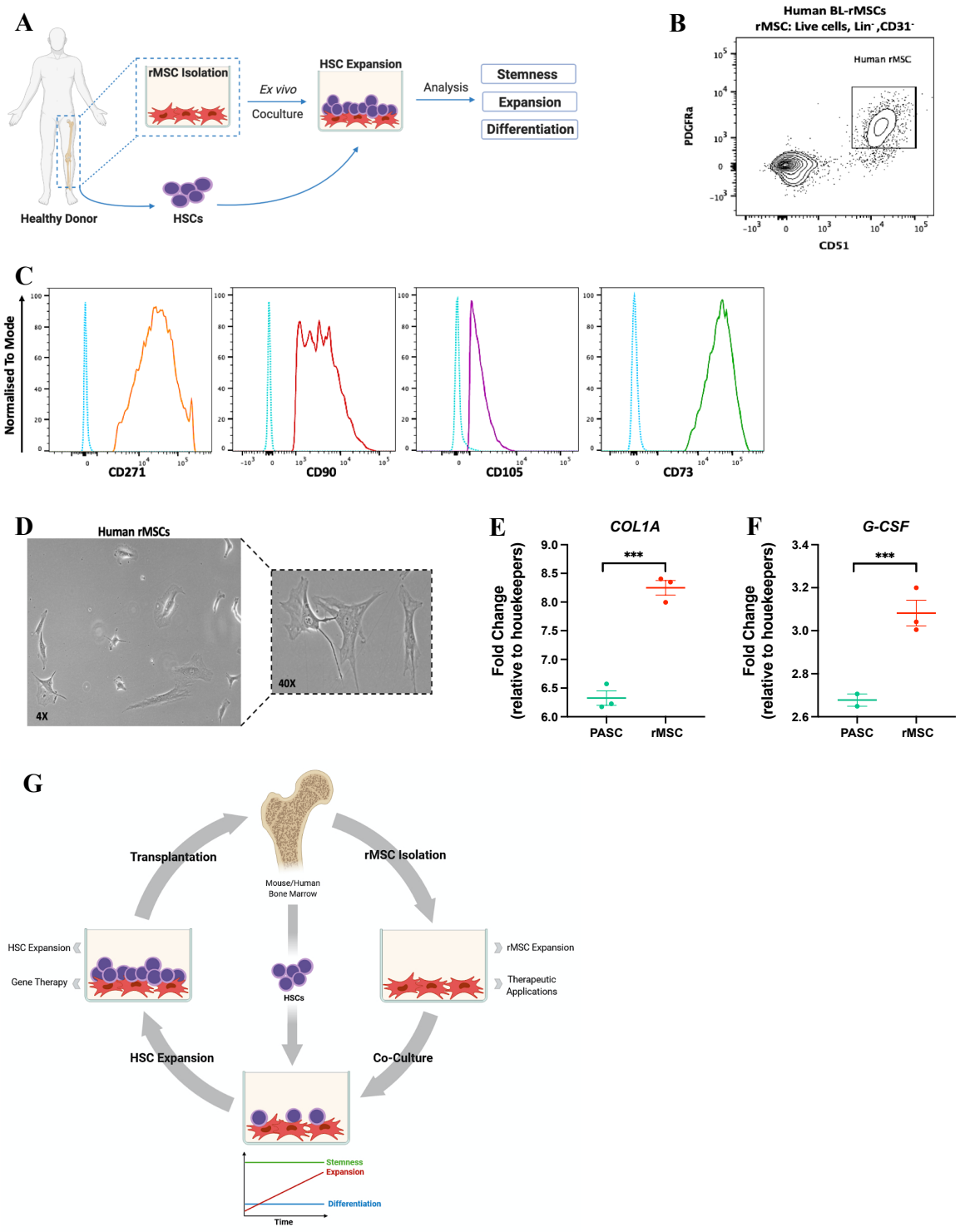

Figure 30. Characterization of human rMSCs for ex vivo HSC expansion in a donor-individualized system

(A) Pipeline for donor individualized florescence-sorting based isolation of both HSCs ($CD45RA^-$, $CD38^-$, $CD90^+$, $CD34^+$) and rMSCs ($Lineage^-$, $CD31^-$, $CD51^+$ & $PDGFR\alpha^+$) from the same digested

femur-head followed by *ex vivo* HSC expansion using donor-matched rMSCs. (B) Fluorescence-sorting plot representing the gating strategy (Lineage$^-$, CD31$^-$, CD51$^+$ & PDGFRα$^+$) and population distribution (within CD51$^+$ & PDGFRα$^+$) of the human bone-lining derived rMSCs. (n = 4, experiment performed on 4 individual donor samples). (C) Flow-cytometry characterization of human rMSCs using established human mesenchymal stromal markers CD271, CD90, CD105 and CD73. (Scale: mode normalized expression values, Unstained rMSC control as blue dotted-line, n = 4, experiment performed on 4 individual donor samples). (D) Brightfield images of florescence-sorted human rMSCs in culture at 4X and 40X magnification. (rMSCs in passage: 3, n = 4, experiment performed on 4 individual donor samples). (E) & (F) Transcriptional levels of crucial human HSC support and maintains genes *Col1a* and *G-CSF* plotted as fold change relative to housekeepers (*Beta-Actin* & *Gapdh*) for human PASCs and human rMSCs. (Mean ± SEM, n ≥ 3, unpaired two-tailed student's t-test performed between marked groups: * $p \leq 0.05$, ** $p \leq 0.01$, *** $p \leq 0.001$, **** $p \leq 0.0001$, ns: non-significant). (G) Graphical summary of the potent murine and human *ex vivo* LT-HSC expansion system based on donor-matched bone lining-derived rMSCs with the potential for broad application in HSC research and personalized curative therapy.

In conclusion, we have developed a very potent *ex vivo* LT-HSC expansion system based on bone lining-derived rMSCs (Figure 30G). The long-term expanded HSCs using rMSCs maintained phenotypic stemness, showed marked reduction in differentiation, and possessed functional bone marrow reconstitution capabilities upon transplant. Thus, our rMSC-based system for HSC expansion could play a pivotal role in research to reduce the number of mice used for *ex vivo* experiments. Moreover, our donor individualized rMSC-based human HSC expansion system could potentially be used for curative therapy for numerous diseases including immunodeficiencies and leukemia.

4 DISCUSSION

4.1 Inflammation-responding Mesenchymal Stem Cells (iMSCs) dynamically modulate the bone marrow microenvironment response to stress

Inflammation is a key component in a complex biological response of the body to harmful stimuli. In the context of the bone marrow, inflammation is an overarching process central to most, if not all, forms of stress challenges and disease settings including leukemia and immunodeficiencies. Current research in the field is focused on understanding inflammation in the context of the HSC and its niche response (23,41,85,136). While such research provides descriptive understanding of the niche and its interplay, it falls short in translating it to functional applications confounded in part by a single marker approach of classifying the niche cell diversity (26,66,67,125). In this study, we aimed at functionally characterizing an unbiased bone marrow niche response to inflammation over time. We utilized the power of sequencing coupled with functional proliferation readout to identify iMSCs as the major responders to IFNα-mediated inflammatory stress. Our data revealed distinct transcriptional states of the iMSCs over the inflammation response time course with functional consequences on the bone marrow. Using ligand-receptor mapping, we further identified pivotal inflammation-specific interactions between iMSCs and HSCs within the bone marrow. Finally, we dissected the heterogeneity within the iMSC population based on inflammation response at the single-cell level to propose a transcriptional iMSC-signature with potential translational applications in disease settings, like leukemia and immunodeficiencies.

4.1.1 Temporal kinetics of the bone-lining iMSCs upon inflammation stress

We studied the unbiased bone marrow response to inflammation in the context of temporal kinetics at the early 3 h (IFNα sensing), mid 24 h (IFNα response) and late 72 h (recovery of the system) time-points. Our data revealed the IFNα triggered dynamics of the major cell types within the bone marrow at a functional level. Though studies have previously described HSC and endothelial cell kinetics upon various stressors in isolation (45,50,159,175), our data for the first time enabled the direct functional comparison of IFNα response across the different bone marrow cell types in a systematic manner. Notably, the iMSCs stood out as the major responders to IFNα-mediated stress with distinct temporal phases demonstrating their multi-facet role in both inflammation response and recovery. The early (3 h) pro-inflammatory response of the iMSCs confirms a large number of studies that defined the MSCs/CAR cells as the master chemokine and cytokine producers in the bone marrow while further sub-segregating the MSCs/CAR cells into functionally defined sub-populations of iMSCs (84,124,183,195). Our 72 h IFNα recovery data suggested molecular compartmentalization of the ECM factors between cellular subsets, with the iMSCs uniquely down-regulating ECM genes, including different collagens, to potentially restore homeostasis in the bone marrow after stress insult. Since a hallmark of aged BM stroma and chronic infection is the generalized reduction of ECM gene expression, it is tempting to speculate the involvement of iMSCs in these pathophysiological processes (154,156,232–234). Our single-cell RNA sequencing data captured the known heterogeneity within the BM stroma (REF known heterogeneity of the BM stroma) and also temporally resolves this heterogeneity in the course of the inflammation response. Thus, our temporal kinetic analysis of the IFNα stimulation postulated a central role for the bone-lining iMSCs in directly and dynamically orchestrating the inflammation response within the bone marrow, a finding that might have been under-represented using the conventional single-end point readout strategy. To place the iMSC-mediated temporal response

in the bigger picture of the bone marrow niche and unravel the mechanisms that regulate the multi-facet iMSC function, it will be necessary to systematically image the iMSC changes over the response time course and to conditionally delete the crucial iMSC factors to functionally understand their role in inflammation response and recovery.

4.1.2 Comparing the iMSCs to other bone marrow cell types

Multiple recent studies have classified the homeostatic bone marrow stromal population into defined cellular sub-types using advanced single-cell sequencing and improved imaging techniques (40,134,143,235). While such studies add to our understanding of the homeostatic BM stroma, it falls short in characterizing the niche upon perturbation. To address this, we functionally studied the unbiased BM microenvironment at the bulk and single-cell level upon inflammation stress, utilizing a top-down approach to define and characterize a functional IFNα-responding iMSC population in contrast to the conventional bottom-up approach of identifying new population at homeostasis and then attributing it a function. The iMSCs differed from the other bone marrow cell types in their spatial localization. This is an important factor as more than a few studies using genetic tools and imaging techniques have shown a correlation between the location of a stromal cell type and its function in the context of an HSC niche (39,39,125,136). Of note, since the isolation of both the bone-marrow and bone-lining stromal populations involved multiple rounds of mechanical and enzymatic digestion, we were bound to lose certain fractions of fragile cells, as it has been demonstrated in literature for the CAR-fraction (144,230). This technical shortcoming applies to all stromal cell studies to date which should be acknowledged while interpreting the results. Nonetheless, our bulk analysis of iMSCs, SCs and endothelial cells revealed previously unappreciated cell-type specific functions and molecular signatures upon inflammation challenge highlighting that the cell types differ not only in their surface marker expression and BM localization but also in their role in stress

response. For instance, while both stromal sub-sets respond to IFNα at 3 h, the iMSCs expressed functionally different cytokines and chemokines than their BM stromal counterparts suggesting defined tasks for the two stromal cell types in acute stress response. Further, the inverse trends in matrisomal transcriptional levels at the 72 h timepoint between the iMSC and the two BM cell types (SCs & endothelial cells) suggested an iMSC-mediated ECM re-modulatory mechanism with compensating feedback signaling from the two BM cell types. Furthermore, our single-cell sequencing dataset revealed that the bulk-defined iMSC population can be further sub-segregated into transcriptionally distinct stromal and fibroblast-like cell types. Interestingly, the inflammation response at the single-cell level could not be resolved using the well-studied stromal markers including *Cxcl12, Vcam1* & *Pdgfrα* (46,125,226) emphasizing the advantage of a cell-type specific transcriptional response signature over a skewed single marker approach for characterizing the perturbed BM niche. Whilst we have shown that the iMSC were defined based on their distinctive functional response to IFNα, we haven't methodically compared their overlap with known murine MSC sub-types. One can address this question bioinformatically by correlating our iMSC single cell signature with that of mice lacking one or more of the defined MSC populations including Lep$^{-/-}$, Nestin$^{-/-}$ and Col2.3$^{-/-}$ mice or functionally by conditional deletion of IFNAR in different MSC cre-mouse lines including *Lepr*-Cre, *Nes*-Cre & *Prxx1*-Cre (26,46,236,237).

4.1.3 The iMSCs modulate HSC response to acute inflammation

Elegant studies have demonstrated that HSCs can not only sense but also respond to inflammatory cytokines, in particular the HSCs can directly respond to IFNα treatment via the IFNAR receptor and enter active cell cycle. Our data reveals the compounding effect that the iMSCs have on the HSC response to inflammation. Even though the concept of stromal cells modulating the HSC stress response is not novel, with several studies showing that MSC sub-

types can alter niche and HSC response (26,42,45,46,125,138), our data supplements the literature by describing crucial iMSC and HSC interactions upon inflammation. Interestingly, our dynamic ligand-receptor analysis revealed no change in well-established HSC-specific interaction pairs including *Cxcr4-Cxcl14, Cxcr4-Cxcl12,* and *Kit-Kitl (42,198,238)* suggesting that these interactions are crucial at steady state for HSC maintenance but do not regulate HSC response to acute-stress. In contrast, previously unknown interaction pairs composed of iMSC ligands *Col5a3, Col5a1* and *Mdk* with the HSC receptor *Sdc3* seemed to be key for the modulation of the iMSC-mediated HSC inflammation response. Further, co-culture of HSCs with iMSCs indicated that the HSCs lose their proliferation and cell cycle capabilities when the iMSC response to IFNα was compromised suggesting a direct role of iMSCs in HSC stress response *in vitro*. Mechanistically, our data showed that the HSCs in monoculture can still sense IFNα, as demonstrated by the increased ISG expression. But HSCs only respond phenotypically when in co-culture with iMSCs indicating a potential functional codependence of HSCs on the iMSCs for stress response. Furthermore, we observed that the HSCs also effect the iMSCs pro-inflammatory function inferring a cellular cross-talk between iMSCs and HSCs upon acute inflammation. To test whether the variance in receptor-ligand interaction and the profound iMSC-mediated functional changes observed in the HSCs hold true *in vivo*, we need to study the functional HSC and iMSC response in a conditional deletion murine-model of IFNAR and STAT in *Vav1*-Cre (hematopoietic cell-specific) and *Lepr/Nes/Il7*-Cre (stromal cell specific) (74,136,239). Once the iMSC inflammation-modulatory effect on HSCs is established, it will be interesting to identify the mechanisms by which they promote and regulate the hematopoietic stress response.

4.1.4 The effect of iMSCs on its broader bone marrow microenvironment

Within the bone marrow, iMSCs typically make up about 0.01% of total cells and 0.1% of stromal cells, not accounting for the variability due to digestion. Thus, it is important to put iMSCs in perspective when interpreting the broader consequences of their inflammation response on the bone marrow as a whole. In addition to iMSCs, the bone marrow is also home to immune cells, which account for a proportionally larger fraction of the total bone marrow and function as professional inflammation responders (153,240,241). Our data showed that the iMSCs upregulated the antigen-processing and presenting gene sets at the 3 h time point suggesting a potential role of the iMSCs in the modulation of the immune cells in the bone marrow. Further, the iMSCs, upon IFNα treatment, directly interacted with macrophages in co-culture resulting in a skewing towards pro-inflammatory macrophages with marked decrease in the anti-inflammatory and tissue repair macrophage fraction, suggesting that the iMSCs play a broader pro-inflammatory role in orchestrating the immune cell response within the bone marrow. In contrast, the iMSCs exhibits an *in vitro* immunosuppressive effect on the T-cells upon inflammation stress. The concept of stromal cell-mediated immunomodulation of T-cells has already been postulated (242–244), but to the best of our knowledge it's here for the first time that we could dissect the functional T-cell response and link it to a specific stromal sub-type. Recent literature has used the revolutionary single-cell technology to show that the immune cells depend on multiple cues provided by tissue-resident stromal cells for their development and survival (245–248). Hence, it is of great interest to understand the cellular interactions and their mediators that are responsible for the immunomodulatory effect of the iMSCs on bone marrow immune cells. Whilst our complex transcriptional and functional dataset served as a foundation in understanding the broader bone marrow response to inflammation, it also raised important questions: How much cross-regulation is there among cell types in the bone marrow and what might this mean for crosstalk with various niche

components? The conditional deletion of specific niche factors including stromal cells and immune cells would make it possible to determine whether they have non-cell-autonomous effects on other cells in the bone marrow.

4.1.5 The role of iMSCs in disease setting

Given that inflammation is a hallmark of infection and most diseases, it is important to unravel the role of inflammation-responding iMSCs in these settings. In our attempt of doing so, we overlaid our single-cell transcriptional iMSC gene signature onto a Myeloproliferative Neoplasms (MPN) stromal dataset. Interestingly, our iMSC signature marked and identified the disease propagating IFN^{high} MSCs within the MPN bone marrow stromal data set suggesting that iMSCs might be directly involved in the pathogenesis of MPN. Further, our data also confirmed the widely studied stromal genese *Cxcl12* and *Vcam1* as potent iMSC markers at homeostasis but in contrast to literature both these marker genes do not exhibit major changes upon inflammation (42,46,249,250). These finding suggested that the iMSC inflammation response was independent of *Cxcl12* and *Vcam1* expression, and this in turn is very different from our current understanding where MSC/CAR-cell responses in a diseased stromal microenvironment are defined by changes in either of the two markers. To overcome the skewing due to the reliance on a single-marker approach for studying the disease bone marrow stroma, we proposed a comprehensive iMSC transcriptional signature (~100 genes) defined by the unbiased functional bone marrow response to inflammation. The iMSC-signature has potential application in characterizing the bone marrow stroma in diseases like myelodysplastic syndrome (MDS), myelofibrosis and other leukemias. In the immune context, the iMSC-signature might also be instrumental in our understanding of immunopathology resulting in autoinflammatory disease and tissue fibrosis as studies, including ours, have highlighted the importance of the communication channels between the immune cells and the stromal

environment (149,243,245,246). It will be necessary to systematically examine the expression of bone marrow stroma genes including iMSC-factors in hematopoietic tissues after injury or during the course of disease progression, and to conditionally delete these factors from candidate niche cells to functionally identify their key sources during bone marrow regeneration/recovery.

4.2 *Ex vivo* Hematopoietic Stem Cell (HSC) expansion for personalized medicine using reinvigorating Mesenchymal Stem Cells (rMSCs)

Bone Marrow Transplants (BMTs) have highlighted the Hematopoietic Stem Cells (HSCs) potential to restore a new functional hematopoietic system in diseased recipients. However, a major roadblock for this scientific breakthrough is our limited potential for *ex vivo* HSC expansion. In this study, we try to address this shortcoming by proposing a potent *ex vivo* HSC expansion system based on bone lining-derived reinvigorating Mesenchymal Stem Cells (rMSCs). Using a functional approach, we created a robust pipeline for the fluorescence-sorting based isolation and *ex vivo* expansion of rMSCs from both murine and individual human samples. The bulk and single HSCs were expanded long-term using rMSCs to maintain phenotypic stemness over multiple cell differentiation cycles and functional bone marrow reconstitution capabilities upon transplant. Our rMSC-based system for HSC expansion can play a pivotal role in research to reduce the number of mice used for *ex vivo* experiments. Moreover, our individual donor rMSC-based human HSC expansion system could potentially be used for curative therapy for numerous diseases including immunodeficiencies and leukemia.

4.2.1 The rMSCs as a unique cellular substrate

The use of cellular substrate for *ex vivo* HSC expansion is not a novel concept, with earlier studies using fibroblast-like cells for this purpose which were later replaced in most parts by commercially available OP9-murine stromal cell line (23,97,214). Even in the clinic plastic adherent stromal cells (PASCs) are routinely used for human HSC expansion (23,251). These approaches offer only limited success with no advancement in clinical transplants, in part due to the intra-cellular heterogeneity and inadequate *ex vivo* HSC expansion potential of the

cellular substrates (96,252,253). In our study, we addressed this problem using a functional approach to identify and define a sub-stromal population of cultured rMSCs based on their *ex vivo* HSC maintenance and expansion capabilities. Our data showed that the bone lining-derived rMSCs, unlike the bone marrow-derived counterpart (PASCs), are a homogenous cellular population isolated by fluorescence-activated cell sorting (FACS) using a robust mouse-matched and donor-individualized pipeline. Further, the significantly higher expression of stromal genes *Leptin* and *Nestin* by the rMSCs in comparison to PASCs might contribute to their superiority in HSC expansion, as both *Leptin* and *Nestin* have been shown to play a direct role in HSC maintenance, homing and transplantation (26,67,125). Additionally, the dramatically higher stem cell frequency of rMSCs in contrast to PASCs highlights the homogeneity within the rMSC pool and hints towards a more stem cell like nature of the rMSCs which might contribute to their enhanced HSC expansion potential. To better understand the differences between the rMSCs and other cellular substrates, one should systematically compare their stromal marker expression and HSC expansion potential over multiple passages in culture. It is also of interest to unravel both the inter-cellular heterogeneity between rMSCs and other cellular substrates using bulk-sequencing approaches and intra-cellular heterogeneity within the rMSC pool using single-cell sequencing techniques.

4.2.2 The potent HSC expansion potential of the rMSC co-culture system

Our data shows that proliferating rMSCs serves as the focal point of attachment and cell division for the LT-HSCs in culture, suggesting the rMSCs actively contribute to HSC expansion, unlike the other established cellular substrates that serves as a passive support and feeder-layer for the HSCs/HSPCs in culture (99,254,255). Our 10-day *ex vivo* murine HSC culture dataset highlights the significant improvement in HSC culture, with a marked fold change in expansion, higher maintenance in stemness, and better bone marrow reconstitution

capabilities upon transplantation. Further, our long-term HSC culture data showed that the rMSC co-culture system maintained the highest frequency of phenotypic HSCs, which means that in the presence of rMSCs the HSCs do not differentiate as quickly. The transcriptional data confirmed that instead of losing maintenance and function genes, the expanded HSC population had a marked increase in these genes after long-term expansion up to 4 weeks indicating that rMSC co-culture enhanced the stability of the expanded HSCs. Consequently, the rMSC-based HSC expansion protocol exceeded all expectations and provided a reproducible and robust approach to expand phenotypic and functional HSCs to absolute numbers that were ~100 times higher than any other described method could produce. Furthermore, our assessment of single LT-HSC expansion data revealed the HSC in co-culture with rMSCs exhibited a more homogenous expansion of the single-HSC clones while maintaining their phenotypic characteristics, their stemness, and their function to reconstitute the bone marrow upon transplantation of 100 clonally expanded HSCs post 30-day *ex vivo* culture of the starting single LT-HSC with the rMSCs into lethally irritated recipient mice. These experiments confirmed bona fide HSC self -renewal potential of the rMSC co-culture system, with a potential to play pivotal role in research to reduce the number of mice used for *ex vivo* experiments. To further assess the potential of our rMSC co-culture expansion system, it would be interesting to perform transplant experiments in non-irradiated and non-conditioned recipient mice as radiation-based bone-marrow conditioning is the gold-standard prerequisite to make space for donor HSCs in bone-marrow transplantation (256,257). Donor engraftment in non-irradiated and non-conditioned recipient animals (including NOD/SCID mice and cKIT deficient mice) has shown to be possible but normally not feasible, in part, because of the large numbers of HSCs required for the transplant (213,258–260). Thus, such an experimental approach would push the functional HSC *ex vivo* expansion limits of our rMSC-based expansion system.

4.2.3 The superiority of the rMSC-based culture system

The concept of HSC expansion in itself is not new, with studies proposing innovative solutions and companies providing optimized media. Over the past decade a multitude of different cellular and non-cellular HSC expansion systems have been established (23,214,253,254).We performed a comprehensive study comparing these expansion systems with our rMSC-based HSC expansion technique. Our data revealed that not only is our rMSC-based expansion system superiors to the conventional OP9-murine stromal cell line (261–263), they also outperform all the tested non-cellular compound-based expansion systems (96–98,213,223,252) in their absolute HSC numbers and fold expansion of phenotypic HSCs. These findings demonstrated the advantage of the rMSC-based HSC expansion system over the other established expansion techniques and suggested a role for the bone marrow niche cellular component in HSC *ex vivo* maintenance and expansion. Further, our data comparing the rMSC-based HSC expansion to alternative media compositions (152,213) highlights the synergistic effect of our co-culture system by combining a serum-free cytokine optimized medium with functionally defined rMSCs on the HSC stem cell frequency. Though, our data shows significantly higher HSC expansion potential upon co-culture with rMSCs in comparison to HSC expansion in defined Walters and Yamazaki media (152,213), we are yet to determine the causative factors responsible for this characteristic effect of the rMSCs. In future work, the expansion potential of HSCs by the rMSCs should be studied comprehensively by RNA sequencing, mass spectrophotometry and electron-microscopy to identify potentially novel rMSC-specific HSC expansion factors, deduce rMSCs ECM components *in-vitro* and visualize the physical interaction dynamics between HSCs and rMSCs.

4.2.4 The human HSC expansion capabilities of the rMSCs

A substantial goal of stem cell research is to provide human HSCs for different clinical applications including bone marrow transplantations. However, the major roadblock in bone marrow transplants is the limited availability of human HSCs, which cannot be addressed with currently existing *ex vivo* expansion protocols (23,251). As we have shown the successful long-term *ex vivo* expansion of murine HSCs using murine rMSCs, our obvious next goal was the translation of this approach from the murine to the human system. As our first step, we identified a human bone lining-derived stromal analogue to murine rMSCs and created a robust pipeline for donor-individualized human rMSC isolation. Further, our characterization and comparison data for human rMSCs and human PASCs revealed significantly higher expression of crucial human HSC support and maintenance genes by the rMSCs, suggesting that the human rMSCs might be superior to the conventional human PASCs for *ex vivo* HSC expansion in a donor-individualized system. In future work, the human HSC expansion potential of the rMSCs will be studied comprehensively. This includes the analysis of the expansion potential, the maintenance of the stem-cell frequency and the function to reconstitute peripheral blood and bone marrow upon transplant into immunodeficient mice. Our eventual goal is to demonstrate that the rMSC co-culture system can be used to promote clinically meaningful *ex vivo* expansion of donor-specific HSCs.

4.2.5 Personalized medicine application of rMSC-expanded HSCs

The modern idea of personalized medicine is based on the concept of tailoring diagnostics and treatments to the need of an individual patient. This idea of individualized medicine for bone marrow transplants has been described as a paradigm shift in patient-treatment but has been limited by the lack of patient-specific HSC expansion that could be

genetically engineered for therapy. In this study, we propose a patient individualized experimental strategy that allowed for the isolation of both HSCs and rMSCs from the same patient sample, followed by patient-specific HSC *ex vivo* expansion. Our work demonstrated that the human rMSCs isolated from individual patients using our pipeline can be *ex vivo* cultured and expanded while maintaining their characteristic fibroblast-like architecture and plastic adherent property. Further, our data also suggests that the human rMSCs might outperform the existing clinically used PASCs in their HSC maintenance and expansion potential. Thus, we believe that our patient individualized rMSC-based human HSC expansion system could potentially be used for curative gene therapy of HSCs and re-transplantation back into the patient for numerous diseases including immunodeficiencies and leukemia.

4.3 General Discussion

The bone marrow microenvironment in itself has a complex biological makeup with numerous cell types interacting with each other through both juxtracrine and paracrine signaling. Thus, it is important to put both our studies of the *in vivo* inflammation-responding and *in vitro* reinvigorating MSCs in the perspective of the broader bone marrow niche. With our data shedding new light on the function, dynamics and clinical capabilities of the bone marrow, we are inclined to revisit our conceptual understanding of the bone marrow niche. In this section, I have addressed and discussed a few such conceptual ideas about the broader bone marrow niche.

4.3.1 A functionally characterized BM niche

Our current model of the BM niche is centered around the HSC microenvironment termed HSC-niche or HSC-instructive niche. The majority of recent studies focuses on defining the bone marrow components in the context of HSC maintenance, activation and proliferation (26,125,136). While such research supplements our understanding of HSC biology, it underrepresents the broader role of the cellular bone marrow microenvironment. In our studies, we addressed this shortfall by opting for a non-conventional functional approach of characterizing the cellular diversity of the bone marrow. Using this approach *in vivo*, we identified a sub-population of MSCs, termed iMSCs, that both specifically and dynamically responds to inflammation. Further, our *in vitro* datasets revealed a novel population of rMSCs with a potent function of *ex vivo* HSC expansion. Thus, our data highlight the importance of a functionally designed study for the unbiased bone marrow niche resulting in a practical and applicable model of the bone marrow. To further improve our understanding of a functionally characterized niche, it would be interesting to study changes in the cellular niche after

myeloablation and transplantation, using systematic whole-bone imaging and global sequencing approaches.

4.3.2 Static *vs.* dynamic BM niche concept

The advent of multiplex single-cell sequencing and advanced bone microscopy techniques have contributed to the recent surge in bone marrow niche research, with studies reporting novel cell types and an ever-so-intricate communication with their microenvironment at homeostasis (40,143,157,262). Given that most biological processes occur over-time, including the body's inflammation response to infection, injuries and toxins (148,149,245), we accounted for time as a variable in our study of the bone marrow niche upon inflammation stress. Our bulk data revealed characteristic proliferation kinetics of the different bone marrow cellular components and highlighted the distinct transcriptional dynamics of the iMSCs. These are findings that might have been underrepresented in previous single end-point analysis (26,86). Further, using our over-time single-cell RNA sequencing dataset, we could systematically correlate distinct stress response processes to individual bone marrow cell types and delineate the cellular sources of inflammation response within the stroma. Thus, our temporal kinetics study upon acute inflammation suggest a new dynamic niche model of the bone marrow demonstrating previously unappreciated functions and cross-talk among the cell types in the bone marrow.

4.3.3 From a structural to a functional definition of the BM niche

The current strategy in bone marrow research is increasingly focused on a few cell types and their function, sometimes taking them out of the context of the entire bone marrow niche. For example, multiple studies suggested a direct role of SCF and CXCL12-expressing stromal

cells in HSC function and stress response but did not account for the fact that *in vivo* there are 100 times fewer HSCs than stromal cells that express high levels of SCF and CXCL12 in the bone marrow (42,46,124,195). Moreover, our current convergent approach of studying the bone marrow also falls short in understanding the broader crosstalk with or co-regulation by various cellular niche components. In our study, we characterized an unbiased bone marrow niche with focus on the functional response without a selection for cell types rather than studying the response of structurally pre-defined cell-types. Our experimental approach unravels a previously unacknowledged cellular compartmentalization of the bone marrow response. Hence, our data underlines the importance of studying the bone marrow in its broader context, and further studies are needed to understand the proximity of niche cells to each other and what it might mean for the co-regulation and function of the bone marrow as a whole.

4.3.4 BM microenvironment or organ system

Taking a step back from the concept of the bone marrow 'niche', the bone marrow in itself also acts as a vital and complex organ with a unique balance between its mechanical structure and cellular composition (17,264,265). In this context, it will be of interest to decipher if the bone marrow as an organ system has different 'niches' that home specific stromal cell types and support independent hematopoietic processes. An innovative way to address this question would include using the cutting-edge spatial transcriptomic analysis techniques on the whole bone mount-sections at the single-cell level. Given that the majority of the studies on the bone marrow, including ours, are performed in isolation of the physiological changes in the body, it raises considerable interest in understanding the extent to which the bone marrow cellular components and their processes are regulated by long-range signals from the systemic physiological changes, such as pregnancy and nutrition.

4.3.5 Potential future of the BM niche

The model of the bone marrow niche has evolved over the course of history, pitted with controversial concepts and challenging ideas, along with the evolution in scientific technology. Our current model of the bone marrow microenvironment comprises a multitude of novel cell types with intricate interactions and a sophisticated nomenclature of cellular sub-types (41,266–268). Our work complements previous studies and underlines the efficacy of an alternative approach to study the bone marrow niche. In light of the upcoming research, the model of the bone marrow might shift away from an 'HSC instructive-niche' to a broader 'cellular bone marrow niche' as more studies unravel the crucial HSC-independent functions of the different cell types in the bone marrow. Further, the advancement of technologies, like single-cell spatial transcriptomics, Saturn capture microdissection technique, advanced whole-bone spectral deconvolution imaging and tailored genetic animal models, will greatly contribute to our understanding of the bone marrow and perhaps challenge our current conceptualization of it, in both the healthy and the disease setting.

5 MATERIAL & METHODS

5.1 Materials

If not listed in the 'materials' section, used materials are mentioned in the 'methods' sections.

5.1.1 List of antibodies- Murine

Antigen	Clone	Fluorochrome	Company
B220	RA36b2	AL700	eBiosciences
c-Kit	2B8	BV711	BioLegend
CD11b	M1/70	AL700	BD Horizon
CD140a (PDGFRA)	APA5	PE-Cy7	BioLegend
CD150	TC15-12F12.2	PE-Cy7	BioLegend
CD31	390	Pacific Blue	eBiosciences
CD34	RAM34	BV421	BD Horizon
CD4	RM4-5	AL700	eBiosciences
CD45	30-F111	AL700	eBioscience
CD48	HM48-1	FITC	BioLegend
CD51	RMV-7	BV711	BD Horizon
CD8a	53-6.7	AL700	BioLegend
GR1	Rb6-8c5	AL700	BioLegend
Ter119	Ter119	AL700	eBioscience
Yellow zombie	-	BV570	BioLegend
TotalSeq™ anti-mouse Antibody	A0301	Hashtag	BioLegend
TotalSeq™ anti-mouse Antibody	A0302	Hashtag	BioLegend

TotalSeq™ anti-mouse Antibody	A0303	Hashtag	BioLegend
TotalSeq™ anti-mouse Antibody	A0304	Hashtag	BioLegend
Sca-1	D7	APC-Cy7	BD Horizon
CD45.1	A20.1	FITC	eBioscience
CD45.2	104	Pacific Blue	BioLegend
CD45.2	104	Alexa Fluor 700	BD Pharmigen

5.1.2 List of antibodies- Human

Antigen	Clone	Fluorochrome	Company
CD105	MJ7/18	BV711	BD
CD140a	Alpha-R1	BV421	BD
CD271	ME20.4	APC	Thermo Scientific
CD31	WM-59	APC-eFluor 780	Thermo Scientific
CD51	13C2	PE	Thermo Scientific
CD73	AD2	PE-Cy™7	BD
CD90	5E10	Alexa Fluor 700	Thermo Scientific
Human Hematopoietic Lineage Antibody Cocktail	RPA-2.10, OKT3, 61D3, CB16, HIB19, TULY56, HIR2	FITC	Thermo Scientific

5.1.3 List of kits

Kit	Source	Identifier
APC BrdU Flow Kit	BD Pharmigen	552598
Arcturus® PicoPure® RNA Isolation Kit	Life Technologies	KIT0204
CellTrace™ Far Red Cell Proliferation Kit	ThermoFisher Scientific	C34564
CellTrace™ Violet Cell Proliferation Kit	ThermoFisher Scientific	C34557
Chromium Next GEM Chip G Single Cell Kit	10x Genomics	1000120
Chromium Next GEM Single Cell 3' GEM, Library & Gel Bead Kit v3.1	10x Genomics	1000121
Dynabeads® Untouched™ Mouse Kit	ThermoFischer Scientific	11415D
MesenCult™ Expansion Kit	Stem Cell Technologies	05513
Mouse IFN Alpha All Subtype ELISA Kit	PBL Assay Science	PBL42115-1
StemMACS™ MSC Expansion Kit XF, human	Miltenyi Biotec	130104182
StemPro™ Adipogenesis Differentiation Kit	Gibco	A1007001
StemPro™ Chondrogenesis Differentiation Kit	Gibco	A1007101
StemPro™ Osteogenesis Differentiation Kit	Gibco	A1007201
SuperScript® VILOTM cDNA Synthesis Kit	Life Technologies	11754250

5.1.4 List of reagents

Reagent	Source	Identifier
BioCoat™ Poly-D-Lysine	Corning	354210
CD45 MicroBeads, human	Miltenyi Biotec	130-045-801
CD45 MicroBeads, mouse	Miltenyi Biotec	130-052-301
Collagenase Type IV, Powder	ThermoFisher Scientific	17104-019
CryoStor™ CS10 cell cryopreservation media	Sigma-Aldrich	C2874
Dispase II, Powder	ThermoFisher Scientific	17105-041

Gibco™ DMEM (1X) + GlutaMAX™-I	ThermoFisher Scientific	21885-025
Gibco™ Fetal Bovine Serum, Qualified, Brazil	ThermoFisher Scientific	10270-106
Gibco™ Ham's F-12 Nutrient Mix	ThermoFisher Scientific	11765-054
Gibco™ Hank's Balanced Salt Solution (1X)	ThermoFisher Scientific	14175-053
Gibco™ IMDM (1X) – Iscove's Modified Dulbecco's Medium	ThermoFisher Scientific	21980-032
Gibco™ Insulin-Transferrin-Selen Ethanolamin (ITS- X) (100X)	ThermoFisher Scientific	51500-056
Gibco™ StemPro™-34 SFM (1X)	ThermoFisher Scientific	10640-019
Giemsa's azur eosin methylene blue solution	Merck	109204
HEPES solution	Sigma-Aldrich	H0887
L-Glutamine 200 mM (100X)	ThermoFisher Scientific	25030-024
Matrigel, Growth Factor Reduced (GFR)	Corning	356231
MesenCult™ 10X Supplement (Mouse)	StemCell™ Technologies	05515
MesenCult™ Basal Medium (Mouse)	StemCell™ Technologies	05514
MesenPure™ 1000X	StemCell™ Technologies	05500
MethoCult™ GF M3434	StemCell™ Technologies	03434
Penicillin-Streptomycin	Sigma-Aldrich	P4458
Poly-L-Ornithine Solution (0.01%)	Merck-Millipore	A-004-C
Poly(vinyl alcohol)	Sigma-Aldrich	P8136
Primocin™	InvivoGen	ant-pm-1
Recombinant Murine SCF	PeproTech™	250-03
Recombinant Murine TPO	PeproTech™	315-14
Retronectin	TAKARA Clontech.	T202
RPMI-1640 Medium	Sigma-Aldrich	R8758

StemPro™-34 SFM	Gibco™	10639011
Trypsin – EDTA Solution	Sigma-Aldrich	T3924
UltraPure™ Distilled Water DNase/RNase Free	ThermoFisher Scientific	10977-035

5.1.5 List of special material

Instrument/Material	Source	Identifier
Corning® HTS Transwell® 96 well	CORNING	CLS3380-1EA
LS Columns	Miltenyi Biotec	130-042-401
Primaria™ 75 cm^2 Rectangular Straight Neck Cell Culture Flask	Corning	353810
Primaria™ Tissue Culture Plate, 24 Well, Flat Bottom with Low Evaporation Lid	Corning	353847
Primaria™ Tissue Culture Plate, 6 Well, Flat Bottom with Low Evaporation Lid	Corning	353846
Primaria™ Tissue Culture Plate, 96 Well, Flat Bottom with Low Evaporation Lid	Corning	353872
µ-Plate 96 Well Black for Immunofluorescence	Ibidi	82626
µ-Slide 8 Well Glass Bottom for Immunofluorescence	Ibidi	80827

5.1.6 List of instruments

Instrument/Material	Source	Identifier
10X Chromium Controller	10x Genomics	1000202
BD LSRFortessa™ Flow Cytometer	BD	BD Fortessa
BD™ LSR II	BD	BD LSR
Cell Observer	ZEISS	Zeiss Axio
CytoSMART™ Lux2	CytoSMART	JAB-1004
CytoSMART™ Omni	CytoSMART	XAB-1002

FACSAria™ Fusion Cell Sorter	BD	BD FACSAria
FACSAria™ I Cell Sorter	BD	BD FACSAria
FACSAria™ II Cell Sorter	BD	BD FACSAria
NovaSeq Sequencing System	Illumina	NovaSeq
Primo Vert Inverted Routine Microscope	ZEISS	3842000827
QuadroMACS Separator	Miltenyi Biotec	130-090-976
Thermo Scientific™ Heracell™ 240i CO2 Incubator, Electropolished Stainless Steel	ThermoFisher Scientific	51026331
Thermo Scientific™ Heracell™ VIOS 160i CO2 Incubator, Electropolished Stainless Steel	ThermoFisher Scientific	50145515
ZEISS LSM 710 ConfoCor 3	ZEISS	LSM 710

5.2 Methods

5.2.1 Mouse strains

All animal experiments were approved by the Animal Care and Use Committees of the German Regierungspräsidium Karlsruhe für Tierschutz und Arzneimittelüberwachung. Mice were maintained in individually ventilated cages at the DKFZ animal facility. Experiment matched female and male mice were used, with a minimum weight of 20 g per mice and of age between ten to fourteen weeks. Wildtype (WT) mice (C57BL/6J or B6.SJL-Ptprca Pepcb/BoyJ) were purchased from Harlan Laboratories or Charles River Laboratories, respectively. *Ifnar*$^{-/-}$ (Muller et al., 1994), *Stat1*$^{-/-}$ (Durbin et al., 1996), Ifitm3eGFP (Lange et al., 2008), FUCCI-reporter (Miyoshi et al., 2002), ISRE_eGFP (Tovey et al., 2006) have been previously described.

5.2.2 *In vivo* mice treatments

To induce an inflammation, mice were injected intraperitoneal with a single dose of 5mg/kg pI:C (Invitrogen) or 5x10^6 units/kg IFNα (Miltenyi Biotec) at the time points indicated in the figure legend. For BrdU proliferation assay, mice were injected intraperitoneal with a single dose of 200 µL (100µg/g) of BrdU solution (BD Biosciences) 16 hours before sacrifice.

5.2.3 Mouse bone preparation & bone lining-MSC isolation

In generally unless otherwise indicated in figure legend, a minimum of six mice with the same genetic background were used for BL-MSC preparation. To isolate mouse BL-MSCs, the hips, the bone marrow of femur and tibiae were flushed out with RPMI 1640 +2% FCS and

resulting bones were digested with 2 ml Digestion Buffer (2mg/ml collagenase IV and 1 mg/ml dispase in HBSS buffer) for 10 minutes at 37 °C. Digestion was blocked with 2 ml of FACS buffer (PBS with 2% FCS). Bone digestion was repeated twice, and the digested medium was centrifuged. Pelleted cells were digested with 1 ml of ACK lysing buffer (Gibco, ref. A1049201) to discard red blood cells for 10 minutes at room temperature. Lysis was blocked by adding 2 ml of FACS buffer and centrifuged. Hematopoietic cell depletion was performed by incubating cells with the CD45 microbeads (Miltenyi Biotech, ref. 130-052-301) for 15 minutes on ice, followed by filtering through magnetic LS columns. The resulting cells were incubated with a staining mix contacting zombie yellow, CD31, CD45, Ter119, PDGFRα & CD51 antibodies (details as listed in the material section) and FACS sorted into collection tubes containing DMEM medium (Gibco, ref. 21885-025) supplemented with 15% FCS, 1% Penicillin-Streptomycin (P/S) (Thermo Fischer, ref. 15070063), 0.2% Primocin (InvivoGen, ref. ant-pm-1) and 1% L-glutamine (Gibco, ref. 25030-024).

5.2.4 Mouse bone marrow preparation & HSC isolation

Bone marrow was prepared from femur, tibia, humerus, ilium, and columna vertebralis by crushing bones in RPMI-1640 medium supplemented with 2% FCS. For cell sorting, cells expressing the lineage markers CD11b (M1/70), Gr-1 (RB6.8C5), CD4 (GK1.5), CD8a (53.6.7), Ter119 (Ter119) and B220 (RA3-6B2) were depleted by incubation with rat monoclonal antibodies. Subsequently, cells were washed and incubated with anti-rat IgG-coated Dynabeads for 15 min (4,5µm supermagnetic polystyrene beads (Invitrogen), 1mL of beads / 3x108 bone marrow cells). Cells expressing lineage markers were depleted using magnetic separation and the remaining lineage-negative cells were isolated. The resulting cells were incubated with a staining mix contacting zombie yellow, Lin, Kit, Sca1, CD48, CD150 & CD34 antibodies (details as listed in the material section) and FACS sorted into collection

tubes containing StemPro-34 SFM medium (Gibco, ref. 11580356) supplemented with 10 ng/ml mouse SCF and 100 ng/ml mouse TPO, 0.2% Primocin (InvivoGen, ref. ant-pm-1) and 1% L-glutamine (Gibco, ref. 25030-024).

5.2.5 Bone lining-MSC *in vitro* culture

Sorted primary BL-MSCs were plated and expanded in Primaria cell culture vessels (Corning) in DMEM supplemented with 15% FCS, 1% P/S, 1% L-glutamine. Cells were grown under hypoxia (5% O2, 5% CO2) at 37ºC. Cell passage was performed by using Trypsin-EDTA solution (Sigma, ref. T3924). Generally, cells in passage nº 3-6 were used for the experiments. For long-term conservation, primary MSCs were frozen in CS10 cell cryopreservation medium (Merck, ref. C2874).

5.2.6 BrdU proliferation assay

For BrdU incorporation assays, mice were injected i.p. with 200 µL (100µg/g) of BrdU solution 16 h prior to the experiment. BM and BL were isolated as described and stained for surface markers. Subsequently, cells were fixed and BrdU staining was performed according to instructions of the BrdU Flow kit (BD Biosciences).

5.2.7 Ki67 cell cycle analysis

For Ki67-Hoechst cell cycle analysis, surface staining was performed as described for iMSCs and HSCs. Subsequently, cells were fixed and permeabilized using cytofix-cytoperm buffer (BD Biosciences) and incubated with Ki67 antibody (BD Biosciences) overnight at 4°C. Cells were stained with 25µg/mL Hoechst 33342 (Invitrogen) and analyzed.

5.2.8 Bone lining-MSC differentiation assay

For osteocyte, chondrocyte and adipocyte differentiation respectively, 5*103 cells/cm2, 1.6*107 cells/mL and 1*104 cells/cm2 iMSCs were seeded in Primaria 24-well plates (500µL/well). The iMSCs were thereafter allowed to attach overnight at 37˚C and 5% O2. Subsequently, as per the manufactures protocol, the respective differentiation medium was added (StemPro® Osteocyte/Chondrocyte Differentiation Basal Medium + StemPro® Osteogenesis Supplement, StemPro® Osteocyte/Chondrocyte Differentiation Basal Medium + StemPro® Chondrogenesis Supplement or StemPro® Adipocyte Differentiation Basal Medium + StemPro® Adipocyte Supplement; ThermoFisher Scientific, MA, USA). The wells were supplemented with either PBS as negative control or 1,000 IU/mL IFNα according to the experimental conditions. Media were refreshed every two to three days and differentiation was monitored weekly by light microscopy. The experiment was terminated after 21 days, 24 days and 14 days for osteocyte, chondrocyte and adipocyte differentiation respectively, followed by staining, visualization and spectrophotometry quantification using 2% Alizarin Red S solution (pH 4.2; Sigma-Aldrich), 1% Alcian Blue (Sigma-Aldrich) or 2% Oil Red O (Sigma-Aldrich), correspondingly.

5.2.9 iMSC-HSC co-culture experiments

Generally, unless otherwise indicated, the co-cultures were performed in 96-well plates. 2000 MSCs were plated in each well 10-12 hours prior to HSC seeding. The BD FACS Cell Sorter was used to sort 2000 LT-HSCs (Lin^- Kit^+ $Sca1^+$ $CD48^-$ $CD150^+$ $CD34^-$) freshly isolated from the mouse bone marrow. Cell number matched HSCs were seeded into the wells containing MSC previously plated. The HSP-iMSC co-cultures were cultured in an albumin-free medium composed of StemPro-34 SFM medium (Gibco, ref. 11580356) supplemented

with 10 ng/ml mouse SCF and 100 ng/ml mouse TPO and 0.1% polyvinyl alcohol. The IFNα treatment was initiated 12 hours post-HSC seeding by adding mouse IFN-α subtype 4 (Miltenyi biotech, cat no. 130-093-131) or PBS (as a negative treatment control) into the respective wells. Unless otherwise indicated the working concentration for IFNα was 1000 IU/ml.

5.2.10 RNA isolation, reverse transcription & quantitative real-time PCR

The FACS sorted cells were spun down, and pelleted cells were resuspended in extraction buffer (Arcturus Therapeutics) and snap-frozen. RNA isolation was performed using the PicoPure RNA isolation kit (Arcturus Therapeutics) following the manufacturer's protocol. The isolated RNA was used to synthesize the cDNA using the SuperScript VILO cDNA Synthesis Kit (Invitrogen, ref. 11754-250) and a thermocycler. The RT-qPCR was performed by mixing the resulting cDNA with the primer pair amplifying the genes of interest and the Power SYBR Green PCR Master Mix (Applied Biosystems, ref. 4367659) in the QuantStudio 5 Real-Time PCR System (Applied Biosystems). If not indicated otherwise, gene expression values were normalized to GAPDH and β-actin housekeeping genes and calculated using the ΔΔ-CT-method.

5.2.11 Flow cytometry analysis of bone marrow cell-types

Bone lining and bone marrow mononuclear cells were used for flow cytometric analysis. For FACS-sorting BD FACSAria II/III or Fusion flow cytometers (BD Bioscience) equipped with 405nm, 488nm, 561nm and 633nm (Aria) / 642nm (Fusion) lasers were used. For flow cytometric analyses, LSRII and LSRFortessa flow cytometers (BD Biosciences) equipped with 350nm, 405nm, 488nm, 561nm, and 640nm lasers were used. To stain iMSC, HSC, Endo and SCs, cells were incubated for 15 minutes with zombie yellow at room temperature (as per

manufactures protocol), followed by 30 minutes at 4°C with the respective pre-conjugated surface antibodies (as detailed in the material and results section). Subsequently, cells were washed in PBS twice and sorted/analyzed. Post-acquisition data analysis was done using FlowJo 10 software.

5.2.12 *In vitro* proliferation assay

The iMSCs and HSCs were stained with the Cell Trace Far-Red and Cell Trace Violet Cell Proliferation kit, respectively, using the manufacturer's protocol. The cells were plated in 24 or 96-well plates either in monoculture or co-culture followed by the IFNα treatment *in vitro*. The Cell Trace stained cells were collected 48-72 hours after treatment, and stained with iMSC and HSC markers as indicated above followed by flow cytometric analyzed using the FACS Fortessa equipment (BD Biosciences).

5.2.13 Bulk RNA sequencing

Mouse matched bone marrow HSCs and bone lining iMSCs from four WT mice were isolated and surface stained as detailed above. Followed by, FACS sorting of HSCs and iMSCs populations from the four independent biological replicates directly into the RNase-free microfuge tubes (ThermoFisher) containing extraction buffer (Arcturus Therapeutics) at 4 C until 1500 cell to 5000 cells were collected for each cell type. RNA isolation was performed using the PicoPure RNA isolation kit (Arcturus Therapeutics) following the manufacturer's protocol. The quality of the isolated RNA was measured using a Bioanalyzer 2100 (Agilent, Waldbronn, Germany). Library preparation, cluster generation and sequencing were performed at the Genomics and Proteomics Core Facility, DKFZ. The libraries were prepared using the SMARTer Stranded Total RNA-Seq - Pico Input Mammalian - kit (Takara Bio, USA) following

the manufacturer's instructions. For each sample 600 pg of input total RNA were used. The TruSeq SR Cluster Kit v4-cBot-HS (Illumina, Inc, California, USA) was employed for cluster generation using 8 pM of pooled normalized libraries on the cBOT. Sequencing was performed on the Illumina HiSeq 4000 single end 125 bp using the TruSeq SBS Kit v4-HS (Illumina, Inc, California, USA).

5.2.14 Single-cell RNA sequencing

Mouse bone marrow stroma was isolated from four independent WT mice at the indicated time-points by sequentially digesting flushed bones using digestion buffer containing collagenase IV and dispase at 37 °C. Hematopoietic cell depletion was performed by incubating cells with the CD45 microbeads (Miltenyi Biotech, ref. 130-052-301), following manufactures protocol. Subsequently, each of the four biological replicates for a time-point were stained with a unique Hashtag (TotalSeq A, Biolegend), following manufactures guidelines. The resulting cells were pooled for each time-point before immune-stained with zombie yellow, CD31, CD45 & Ter119 surface antibodies (details as listed in the material section) and FACS sorted into a 96-well round-bottom plates for the 10x platform. Unstained cells were used as negative controls to define gating. The libraries were prepared using the Chromium Single Cell Reagent Kits (v3.1), Chromium Single Cell G Chip Kit v3.1 and i7 Multiplex Kit (10x Genomics), and following the Single Cell Reagent Kits (v3.1) User Guide. Finalized libraries were sequenced on a Novaseq-6000 platform (Illumina), aiming for a minimum of 50.000 reads/cell using the 10x Genomics recommended number of cycles (28-8-0-91 cycles). We used cellranger (version 2.1.1) to align reads to mouse genome mm10 and for detection of cells with default parameters. Next, we used Seurat (v3.1.0) for high level analysis of the scRNA-seq.

5.2.15 Mouse multiplex immune assay

Conditioned media were collected at the time points indicated in the figure legends. The Immune Monitoring 48-plex Mouse ProcartaPlex Panel (Invitrogen, ref. EPX480-20834-901) was used according to the manufacturer's recommendations with a Bio-Plex 200 system (Bio-Rad). The experiment included a single replicate per experimental condition. Due to the absence of biological and technical replicates, no significant analysis could be performed. Instead, experimental conditions were compared to a reference condition, WT iMSC (+PBS) conditioned media, and targets with a log FC > 2 were considered potential candidates differentially expressed. As validation, IL-6 and CCL2 concentrations were obtained using the Mouse Inflammation Cytometric Bead Array (CBA) kit (BD Biosciences, ref. 552364), according to manufacturer's instructions.

5.2.16 HSC *ex vivo* expansion

The murine 100 LT-HSCs or single LT-HSC (Lineage$^-$ cKIT$^+$ Sca1$^+$ CD48$^-$ CD150$^+$ & CD34$^-$) were fluorescence-sorted from three pooled WT mice and cultured either in monoculture or in co-cultured with the same number (3000 cells) of PASCs or rMSCs for the indicated number of days *ex vivo*. The HSCs were expanded using serum-free Han's F-12 media supplemented with 1% ITSX, 10 mM HEPES, 1% P/S/G, 100 ng/ml mouse TPO, 10 ng/ml mouse SCF and 0.1% polyvinyl alcohol. Media change was performed every three days for the HSC mono-culture, while the HSCs in co-culture were re-platted onto fresh PASCs and rMSC every five days. The expanded HSCs from the different culture systems were assesses at the indicated end-point by CFU assay, ELDA, viable cell count, flow cytometry and transplantation (were indicated).

5.2.17 Colony-forming unit (CFU) assay

The CFU assay for multipotent granulocyte, erythroid, macrophage and megakaryocyte progenitor cells (CFU-GEMM) for different HSC single- and co-culture systems was performed with the complete MethoCult GF M3434 media from StemCell Technologies. As per the protocol suggested by StemCell Technologies. For the fresh HSC condition, the cells were taken for the CFU assay immediately after FACS cell sorting. All other conditions were firstly cultured for 7-10 days in their respective culture conditions and only then taken for the CFU assay. The CFU assays were performed with 20 replicates in 24-well plates (Falcon). Starting cell numbers for each condition were 100 cells per well for the primary CFU and 1000 cells per well for the secondary CFU. The plates were incubated for 6-10 days at normoxia and afterwards scanned with a high-resolution scanner (CytoSMART). For the secondary CFU, PBS was added to all wells in order to dissolve the viscous CFU medium. The cells were then counted for the absolute cell count and re-plated for the secondary CFU. Colony Count and confluency were analyzed and evaluated with the software Fiji/ImageJ.

5.2.18 Extreme limiting dilution analysis (ELDA)

The ELDA experiments were performed in 96-well plates (Primaria for rMSCs and PASCs, Falcon for HSC culture systems) with 32 replicates per condition and 50 cells per well as a starting point for the serial dilutions. 200 µl of cell suspension were plated into the first column of the 96-well plate and two-fold serial dilutions were performed all along the corresponding rows with a multichannel pipette. After 7 days of incubation, cell growth was evaluated under a normal brightfield microscope as either positive or negative. The raw data was then inserted into the ELDA software application (Hu and Smyth 2009). The algorithm provided a lower, an upper and an estimate value for the stem cell frequency of the analyzed

stem cell population, as well as a p-value to calculate the statistically significant. rMSCs and PASCs were taken for the ELDA immediately from a culture flask, whereas the different HSC conditions were firstly cultured for 7-10 days in their respective culture conditions and subsequently taken for the ELDA experiment.

5.2.19 Immunofluorescence time-lapse imaging

One day prior, rMSCs were collected, stained with Cell Trace Far-Red and plated into multiple wells of a 96-well plate designed for imaging experiments (µ-Plate 96 Well Black from Ibidi) at a plating density of 2000 cells per well. On the experiment day, HSCs were freshly sorted, stained with Cell Trace Violet and subsequently added into the corresponding wells either as monoculture or co-culture at a plating density of 2000 cells per well. The time-lapse experiment was performed using the Cell Observer from Zeiss for the indicated time duration as per figure legends. The rMSCs were visualized using the Far-red channel, whereas HSCs in the DAPI channel.

5.2.20 Material testing & substrate coating

This experiment was conducted with 5 replicates per coating material in 96-well plates (Primaria). The rMSCs, PASCs and OP9 cells were plated one day prior to the experiment at a plating density of 2000 cells per well in order to give them enough time to attach to the surface. Non-cellular substrates included fibronectin, retronectin, gelatin, matrigel, poly-lysine and ornithin were used to the coat wells of the 96-well plate at a volume of 50 µl per substrate. Fresh isolated and FACS sorted, 2000 HSCs were added to each well and the plate was incubated for 10-14 days at hypoxic conditions. Cell counts were assessed via the trypan blue and Neubauer cell counting chamber technique, along with FACS analysis.

5.2.21 Transplantation experiments

For the bulk expanded HSC transplantation experiment, 100 LT-HSCs was co-cultured with rMSCs were transplanted into C57BL/6-CD45.1 lethally irradiated mouse (2x500 rad) post 10-days *ex vivo* expansion, along with 200K supportive total bone marrow cells from C57BL/6-CD45.1/CD45.2 mouse. For the single-HSC *ex vivo* expansion and transplant experiment, 100 clonally expanded HSCs using the rMSC culture system transplanted into C57BL/6-CD45.1 lethally irradiated mouse (2x500 rad) post 30-days *ex vivo* expansion of the starting single LT-HSC, along with 250K supportive total bone marrow cells from C57BL/6-CD45.1/CD45.2 mouse. Peripheral blood was collected at indicated time points and analyzed by flow cytometry. Bone marrow engraftment was analyzed 16 weeks post-transplantation by sacrificing the mice and preparing the bone marrow as detailed above.

5.2.22 Human rMSC isolation, expansion & characterization

We designed a patient individualized experimental strategy that allowed for the isolation of both HSCs and rMSCs from the same patient sample. To isolate human rMSCs, the patient femur-head were sawed into small cubes and serially digestion using collagenase IV and dispase at 37 °C. Hematopoietic cell depletion was performed by incubating cells with the human CD45 microbeads (Miltenyi Biotech), following manufactures protocol. Subsequently, the results cells were fluorescence-sorting for human rMSCs using the cell surface markers: Lineage- CD31- CD51+ and PDGFRα+ into RNase-free microfuge tubes (ThermoFisher) containing DMEM medium (Gibco, ref. 21885-025) supplemented with 15% FCS, 1% Penicillin-Streptomycin (P/S) (Thermo Fischer, ref. 15070063), 0.2% Primocin (InvivoGen, ref. ant-pm-1) and 1% L-glutamine (Gibco, ref. 25030-024). Sorted primary human rMSCs were plated and expanded in Primaria cell culture vessels (Corning) under hypoxia (5% O2, 5%

CO2) at 37ºC. Cell passage was performed by using Trypsin-EDTA solution (Sigma, ref. T3924). Generally, cells in passage nº 3-5 were used for the experiments. For long-term conservation, primary human rMSCs were frozen in CS10 cell cryopreservation medium (Merck, ref. C2874). The patient-individualized rMSCs were characterized by flow cytometry using established human mesenchymal stromal markers: CD271, CD90, CD105 and CD73 (as detailed in the materials section).

5.2.23 Statistics

If not indicated otherwise statistical analyses were performed using an unpaired, two-tailed student's t test or a Mann–Whitney–Wilcoxon test and results are presented as mean ± SEM with $n \geq 3$. For bulk and single-cell RNAseq analysis p-values were adjusted for multiple testing.

5.2.24 Data analysis & visualization

Flow cytometry data were analyzed using FlowJo 10 software. Gene expression data were analyzed and visualized using Prism and R packages. Heatmaps are based on FPKM expression values if not stated otherwise and were generated using the online tool Morpheus (Broad Institute). Gene set enrichment analyses (GSEA) were performed and visualized using broad GSEA-software. Gene ontology analysis was performed using the PANTHER Overrepresentation Test (GO database release: 2018-04-04). For each test a background list containing all detected genes in this study was provided and statistics evaluated using Fisher's Exact test with FDR multiple test correction. Principal Component Analysis (PCA) and Hierarchical Clustering were created using R (v3.4.1) and the *ggpubr* and *dendextend* packages over the normalized FPKM expression values. The Hierarchical Clustering used the *Euclidian*

distance and the *Ward.D2* algorithm as the clustering method. In PCA plots, individual dots represent different biological replicates.

6 CONTRIBUTIONS & ACKNOWLEDGEMENTS

6.1 Contributions

6.1.1 Inflammation-responding Mesenchymal Stem Cells (iMSCs) dynamically modulate the bone marrow microenvironment response to stress

Co-authors:

Shubhankar Sood[1, 2], Yasmin Demerdash[1, 2], Brigitte J. Bouman[3], Adrien S. Jolly[4], Ramon B. Mascaro[1, 2], Lukas S. Klein[1, 2], Luisa Bast [1, 2], Franziska Pilz[1, 2], Pit Albert[1, 2], Florian Grünschläger[5], Nils B. Leimkühler[6], Rebekka K. Schneider[6], Laleh Haghverdi[3], Marieke Essers[1, 2].

Affiliation:

[1] Inflammatory Stress in Stem Cells, DKFZ.

[2] HI-STEM gGmbH, Heidelberg.

[3] Berlin Institute for Medical Systems Biology (BIMSB-MDC), Berlin.

[4] DKFZ, Heidelberg, Germany.

[5] HI-STEM, DKFZ, Heidelberg, Germany.

[6] Erasmus Medical Center, Rotterdam.

This project was conceptualized with guidance from Dr. Marieke Essers. The experiments were carried out together with Franziska Pilz, Ramon B. Mascaro, Lukas S. Klein, Yasmin Demerdash and Luisa Bast from the Essers Lab, HI-STEM, DKFZ. The bulk RNA sequencing was analysed in collaboration with Dr. Adrien S. Jolly from the Höfer Lab, DKFZ, and Yasmin Demerdash. For the single-cell bioinformatic analysis, we had support from

Brigitte J. Bouman and Dr. Laleh Haghverdi from the Haghverdi Lab at the Max-Delbrück Center Berlin, Florian Grünschläger from the Haas Lab, HI-STEM, DKFZ, and Dr. Daniel Hübschmann from the Hübschmann Lab, HI-STEM, DKFZ. The MPN dataset was provided by and analysed in collaboration with Dr. Nils B. Leimkühler and Prof. Dr. med. Rebekka K. Schneider from the Schneider Lab, Erasmus medical Centre, Rotterdam. The experiments on the immunomodulatory functions of iMSCs were designed and analysed out with help from Pablo H. Malmierca from the Haas Lab, HI-STEM, DKFZ. The FUCCI mice were kindly provided by Vera Thiel and Markus Sohn from the METICS Lab and Trumpp Lab, HI-STEM, DKFZ, respectively. The illustrations were designed with help from Pit Albert from the Essers Lab, HI-STEM, DKFZ.

For their technical support, we would like to thank the DKFZ Core Facilities for Flow Cytometry, Genomics and Proteomics, Omics IT and Data Management, and the Single Cell Open Lab with special thanks to Dr. Jan-Philipp Mallm.

This first project of the thesis, is currently being compiled into a manuscript. We aim at submitting the same to *Cell Stem Cell* by July 2021.

6.1.2 *Ex vivo* Hematopoietic Stem Cell (HSC) expansion using reinvigorating Mesenchymal Stem Cells (rMSCs) for personalized medicine

Co-authors:

Shubhankar Sood[1, 2], Lukas S. Klein[1, 2], Pit Albert[1, 2], Franziska Pilz[1, 2], Jennifer Wischhusen[3], Ramon B. Mascaro[1, 2], Nanni S. Schmitt[4], Darja Karpova[3], Daniel Nowak[4], Marieke Essers[1, 2].

Affiliation:

[1] Inflammatory Stress in Stem Cells, DKFZ.

[2] HI-STEM gGmbH, Heidelberg.

[3] HI-STEM, DKFZ, Heidelberg, Germany.

[4] UMM-Universitätsmedizin Mannheim, Germany.

This project was conceptualized with guidance from Dr. Marieke Essers. The experiments were carried out together with, Lukas S. Klein, Pit Albert, Ramon B. Mascaro and Franziska Pilz from the Essers Lab, HI-STEM, DKFZ. The optimization of the media composition for HSC culture was done with input from Dr. Darja Karpova from the Trumpp Lab, HI-STEM, DKFZ. The Extreme-Limiting Dilution Assay was performed with guidance from Dr. Jennifer Wischhusen from the Trumpp Lab, HI-STEM, DKFZ. The human patient samples were kindly organized and provided by Nanni Sabine Schmitt from the Nowak Lab at the UMM-Universitätsmedizin Mannheim. The mice for transplantation experiments were kindly provided by Melanie Ball from the Milsom Lab, HI-STEM, DKFZ, Adriana Pryzbylla from the Trumpp Lab, HI-STEM, DKFZ and Franziska Pilz. The different coating substrates for rMSC-HSC co-culture were kindly provided by Marleen Büchler from the Milsom Lab, HI-STEM, DKFZ, Andrea Barnert from the Trumpp Lab, HI-STEM, DKFZ, Vera Thiel from the

METICS Lab, HI-STEM, DKFZ, and Nuria V. Siguero from the Jackstatt Lab, HI-STEM, DKFZ.

For their technical support, we would like to thank the DKFZ Core Facilities for Flow Cytometry, and Microscopy with special thanks to Dr. Damir Krunic.

This second project of the thesis, is currently being compiled into a manuscript. We aim at submitting the same to *Nature* by September 2021.

6.2 Acknowledgements

I am deeply grateful to **Dr. Marieke Essers** who gave me the opportunity to perform my doctoral thesis in her lab. I would like to thank you for believing in my (sometimes over-the-top) ideas and supporting me in my endeavor of working towards them. Moreover, I thank you for the invaluable advice and guidance, for keen discussions, for critical proofreading and for creating a rewarding work environment. I have learned so much from you, that has helped shape me into a more critical and curious researcher.

I want to thank my TAC members, **Prof. Dr. Ingrid Lohmann, Dr. Michael Milsom** and **Prof. Dr. Claudia Waskow** for patiently guiding me throughout my PhD journey. I truly appreciate the time and effort you put in.

A special thank you goes to **Franziska Pilz** who has been my companion throughout my PhD journey. I feel so blessed to be working with you. You challenge me every single day and I honestly don't believe I would be where I am if it wasn't for you.

I am very grateful to all the students that I got the privilege to mentor, **Anna Hartley, Cecilia B. Battioni, Jari Scheersta, Luisa Bast, Ramon B. Mascaro, Pit Albert** and **Lukas Klein**. I've really enjoyed the opportunity to get to work closely with each one of you. Thank you for giving me the opportunity to learn how to be a good supervisor and for making it such a pleasure to be at work each day.

I deeply appreciate the whole **Essers group** for your continued support and all of the invaluable help provided on the projects. I honestly couldn't have asked for better colleagues. In particular, I want to thank **Dr. Paula Werner, Yasmin Demerdash** and **Andrea Kuck** for your crucial contribution to the projects and my PhD.

I am very thankful to **Dr. Simon Haas** for the many fruitful scientific discussions, and for sharing great ideas on the project. Further, I want to thank the Haas group, **Pablo M.**

Hernández, Florian Grünschläger, Dominik Vonficht and **Dr. Raphael Lutz**, for being such awesome collogues and friends.

A special thank you to **Pablo M. Hernández** for being my family in Heidelberg. Thank you so much for being there for me. Not only are you an amazing collaborator, but also an incredible mentor and a true friend. Your contributions to my PhD journey are unsurpassable.

I want to acknowledge the incomparable support and the 'can-do' attitude towards my PhD of **Dr. Ana-Matea Mikecin, Melanie Ball, Jeyan Jayarajan, Foteini Fotopoulou** and **Julia Knoch** from the Milsom group. In particular, I want to thank **Dr. Ana-Matea Mikecin** for always having my back and **Melanie Ball** for making my life outside the lab a whole lot more fun.

I am very appreciative of the time and effort put in by the METICS group, with **Vera Thiel, Dr. Roberto Würth, Sarah-Jane Neuberth, Paul Schwerd-Kleine, Corinna Klein** and **Steffi Ornella Kossi**. Special thanks to **Vera Thiel** for your never-ending positivity and for always jumping in to help. I also want to thank you for making life outside work very happening and fun.

I am grateful to **Prof. Dr. Andreas Trumpp** for creating this scientifically conducive ecosystem of HI-STEM. Further, I want to thank you for your input and advice on my PhD projects.

I am grateful for the unparalleled scientific input and ceaseless support by the Trumpp group, **Dr. Darja Karpova, Aino-Maija Leppä, Dr. Jennifer Wischhusen, Adriana Przybylla, Andrea Barnert, Simon Renders** and **Dr. Elisa Donato**. In particular, I want to thank **Dr. Darja Karpova** for your continuous encouragement and support, and **Aino-Maija Leppä** for being not only a great coworker but also an amazing friend.

A special thanks to **Dr. Jennifer Wischhusen** for your indispensable contribution in maintaining my work-life harmony and for always pushing me outside of my comfort zone,

encouraging me to be the best version of myself. I also really appreciate you taking the time to proofread my thesis. I simply couldn't have done it without you.

I want to thank members of the Augustin group, **Moritz Jakab, Ki Hong Lee, Benjamin Schieb, Ashik Abdul Pari, Dr. Mahak Singhal, Dr. Donato Inverso** and **Paula Argos Vélez** for being both great floor-collogues and friends. The enthusiasm, energy and sense of humor we shared made coming to work a pleasure.

A special thanks to **Khwab Sanghvi** from the Platten Lab for pushing me to be the best version of myself every day. You really have a special gift to connect with and inspire people. Thank you for always supporting and motivating me.

I am deeply appreciative of the patience and guidance of the **Flow Cytometry** core facility. In particular, I want to thank **Dr. Steffen Schmitt** for all of your support and effort with the project.

I want to acknowledge the irreplaceable support and advice by **Dr. Jan-Philipp Mallm** from the **Single-cell Open Lab** for both my project and the collaboration experiments.

A big thank you to my fellow members of the PhD Council-2018/19, **Michael Bonadonna, Oguzhan Kaya, Sonja Krausert, Khwab Sanghvi** and **Samantha Zottnick**, for sharing my passion to contribute towards the PhD student life at DKFZ.

I feel fortunate to have led the **Social Events and Networking Team** along with Michael Bonadonna in 2018/19. I am very grateful to each and every member on the team for all your effort in flawlessly executing the events. The time and effort everyone put in was astounding and we couldn't have done it without you.

I want to thank the **Graduate Office** for their valued assistance and continued support throughout my PhD. In particular, I am truly appreciative of **Dr. Lindsay Murrells** for the time and effort you put in.

I am grateful for the unparalleled administrative and financial support by **Dagmar Wolf** and **Erika Krückel** at HI-STEM.

Last but not least, I want to wholeheartedly thank my family, **Col. P.C. Sood, Dr. Meena Sood** and **Sheena Sood,** for always believing in me, inspiring me to dream big and teaching me to work hard to achieve it. Thank you for always supporting me. You are my lifeline.

In loving memory of my dog **Demi** who asked for so little but gave so very much. Wishing you peace to bring comfort, courage to face the days ahead and loving memories to forever hold in your heart.

7 REFERENCES

1. Rieger MA, Schroeder T. Hematopoiesis. Cold Spring Harb Perspect Biol. 2012 Dec 1;4(12).

2. Cooper B. The origins of bone marrow as the seedbed of our blood: from antiquity to the time of Osler. Proc (Bayl Univ Med Cent). 2011 Apr;24(2):115–8.

3. Wintrobe MM, 1901-. Blood, pure and eloquent. McGraw-Hill; 1980.

4. Yapijakis C. Hippocrates of Kos, the father of clinical medicine, and Asclepiades of Bithynia, the father of molecular medicine. Review. In Vivo. 2009 Aug;23(4):507–14.

5. Nutton V. Galen | Biography, Achievements, & Facts [Internet]. Encyclopedia Britannica. 2021 [cited 2021 May 29]. Available from: https://www.britannica.com/biography/Galen

6. Dechambre A, Lereboullet L, Hahn L. Dictionnaire encyclopédique des sciences médicales. [Internet]. 1877 [cited 2021 May 29]. (Quatrième série, F-K.; vol. Tome quatrième: FRAC-FRAN). Available from: https://gallica.bnf.fr/ark:/12148/bpt6k31291h/texteBrut

7. Neumann E. Du rôle de la moelle des os dansla formations du sang. CR Acad Sci (Paris). 1869;68:1112–3.

8. Neumann E. Das Gesetz der Verbreitung des roten und gelben Knochenmarkes, Centralbl. f. med. Wissenschaften. 1882;30:321.

9. Neumann E. Über die Bedeutung des Knochenmarks für die Blutbildung. Zentralblatt für die medizinischen Wissenschaften. 1868;44:122.

10. Neumann E. Hämatologische Studien. Virchows Archiv für pathologische Anatomie und Physiologie und für klinische Medizin. 1912;207(3):379–412.

11. Bizzozero G. Sulla funzione ematopoetica del midollo delle ossa. Zentralbl Med Wissensch. 1868;6:885.

12. Bizzozero J. Ueber einen neuen Formbestandtheil des Blutes und dessen Rolle bei der Thrombose und der Blutgerinnung. Archiv für pathologische Anatomie und Physiologie und für klinische Medicin. 1882;90(2):261–332.

13. Osler W. VI. An account of certain organisms occurring in the liquor sanguinis. Proceedings of the Royal Society of London. 1874;22(148–155):391–8.

14. Osler SW. The third corpuscle of the blood. Dornan; 1893.

15. Osler W. The principles and practice of medicine. D. Appleton; 1916.

16. Simpson E, Dazzi F. Bone Marrow Transplantation 1957-2019. Front Immunol. 2019;10:1246.

17. Morgan EF, Unnikrisnan GU, Hussein AI. Bone Mechanical Properties in Healthy and Diseased States. Annu Rev Biomed Eng. 2018 Jun 4;20:119–43.

18. Hannah SS, McFadden S, McNeilly A, McClean C. "Take My Bone Away?" Hypoxia and bone: A narrative review. J Cell Physiol. 2021 Feb;236(2):721–40.

19. Parmar K, Mauch P, Vergilio J-A, Sackstein R, Down JD. Distribution of hematopoietic stem cells in the bone marrow according to regional hypoxia. PNAS. 2007 Mar 27;104(13):5431–6.

20. Smith JNP, Calvi LM. Concise Review: Current Concepts in Bone Marrow Microenvironmental Regulation of Hematopoietic Stem and Progenitor Cells. STEM CELLS. 2013;31(6):1044–50.

21. Morrison SJ, Scadden DT. The bone marrow niche for haematopoietic stem cells. Nature. 2014 Jan;505(7483):327–34.

22. Calvi LM, Link DC. Cellular Complexity of the Bone Marrow Hematopoietic Stem Cell Niche. Calcif Tissue Int. 2014 Jan 1;94(1):112–24.

23. Kumar S, Geiger H. HSC Niche Biology and HSC Expansion Ex Vivo. Trends in Molecular Medicine. 2017 Sep 1;23(9):799–819.

24. Wei Q, Frenette PS. Niches for Hematopoietic Stem Cells and Their Progeny. Immunity. 2018 Apr 17;48(4):632–48.

25. Calvi LM, Link DC. The hematopoietic stem cell niche in homeostasis and disease. Blood. 2015 Nov 26;126(22):2443–51.

26. Méndez-Ferrer S, Michurina TV, Ferraro F, Mazloom AR, MacArthur BD, Lira SA, et al. Mesenchymal and haematopoietic stem cells form a unique bone marrow niche. Nature. 2010 Aug;466(7308):829–34.

27. Lymperi S, Horwood N, Marley S, Gordon MY, Cope AP, Dazzi F. Strontium can increase some osteoblasts without increasing hematopoietic stem cells. Blood. 2008 Feb 1;111(3):1173–81.

28. Visnjic D, Kalajzic Z, Rowe DW, Katavic V, Lorenzo J, Aguila HL. Hematopoiesis is severely altered in mice with an induced osteoblast deficiency. Blood. 2004 May 1;103(9):3258–64.

29. Calvi LM, Bromberg O, Rhee Y, Weber JM, Smith JNP, Basil MJ, et al. Osteoblastic expansion induced by parathyroid hormone receptor signaling in murine osteocytes is not sufficient to increase hematopoietic stem cells. Blood. 2012 Mar 15;119(11):2489–99.

30. Calvi LM, Adams GB, Weibrecht KW, Weber JM, Olson DP, Knight MC, et al. Osteoblastic cells regulate the haematopoietic stem cell niche. Nature. 2003 Oct 23;425(6960):841–6.

31. Medvinsky A, Dzierzak E. Definitive hematopoiesis is autonomously initiated by the AGM region. Cell. 1996 Sep 20;86(6):897–906.

32. Dzierzak E, Speck NA. Of lineage and legacy: the development of mammalian hematopoietic stem cells. Nat Immunol. 2008 Feb;9(2):129–36.

33. Wright DE, Wagers AJ, Gulati AP, Johnson FL, Weissman IL. Physiological migration of hematopoietic stem and progenitor cells. Science. 2001 Nov 30;294(5548):1933–6.

34. Butler JM, Nolan DJ, Vertes EL, Varnum-Finney B, Kobayashi H, Hooper AT, et al. Endothelial cells are essential for the self-renewal and repopulation of Notch-dependent hematopoietic stem cells. Cell Stem Cell. 2010 Mar 5;6(3):251–64.

35. Hooper AT, Butler JM, Nolan DJ, Kranz A, Iida K, Kobayashi M, et al. Engraftment and reconstitution of hematopoiesis is dependent on VEGFR2-mediated regeneration of sinusoidal endothelial cells. Cell Stem Cell. 2009 Mar 6;4(3):263–74.

36. Winkler IG, Barbier V, Nowlan B, Jacobsen RN, Forristal CE, Patton JT, et al. Vascular niche E-selectin regulates hematopoietic stem cell dormancy, self renewal and chemoresistance. Nat Med. 2012 Nov;18(11):1651–7.

37. Gerber H-P, Malik AK, Solar GP, Sherman D, Liang XH, Meng G, et al. VEGF regulates haematopoietic stem cell survival by an internal autocrine loop mechanism. Nature. 2002 Jun 27;417(6892):954–8.

38. Sipkins DA, Wei X, Wu JW, Runnels JM, Côté D, Means TK, et al. In vivo imaging of specialized bone marrow endothelial microdomains for tumour engraftment. Nature. 2005 Jun 16;435(7044):969–73.

39. Nombela-Arrieta C, Pivarnik G, Winkel B, Canty KJ, Harley B, Mahoney JE, et al. Quantitative imaging of haematopoietic stem and progenitor cell localization and hypoxic status in the bone marrow microenvironment. Nat Cell Biol. 2013 May;15(5):533–43.

40. Tikhonova AN, Dolgalev I, Hu H, Sivaraj KK, Hoxha E, Cuesta-Domínguez Á, et al. The bone marrow microenvironment at single-cell resolution. Nature. 2019 May;569(7755):222–8.

41. Yu VWC, Scadden DT. Hematopoietic Stem Cell and Its Bone Marrow Niche. Curr Top Dev Biol. 2016;118:21–44.

42. Sugiyama T, Kohara H, Noda M, Nagasawa T. Maintenance of the hematopoietic stem cell pool by CXCL12-CXCR4 chemokine signaling in bone marrow stromal cell niches. Immunity. 2006 Dec;25(6):977–88.

43. Masuda S, Ageyama N, Shibata H, Obara Y, Ikeda T, Takeuchi K, et al. Cotransplantation with MSCs improves engraftment of HSCs after autologous intra-bone marrow transplantation in nonhuman primates. Exp Hematol. 2009 Oct;37(10):1250-1257.e1.

44. Ahn JY, Park G, Shim JS, Lee JW, Oh IH. Intramarrow injection of beta-catenin-activated, but not naive mesenchymal stromal cells stimulates self-renewal of hematopoietic stem cells in bone marrow. Exp Mol Med. 2010 Feb 28;42(2):122–31.

45. Ding L, Saunders TL, Enikolopov G, Morrison SJ. Endothelial and perivascular cells maintain haematopoietic stem cells. Nature. 2012 Jan 25;481(7382):457–62.

46. Greenbaum A, Hsu Y-MS, Day RB, Schuettpelz LG, Christopher MJ, Borgerding JN, et al. CXCL12 in early mesenchymal progenitors is required for haematopoietic stem-cell maintenance. Nature. 2013 Mar 14;495(7440):227–30.

47. Park D, Spencer JA, Koh BI, Kobayashi T, Fujisaki J, Clemens TL, et al. Endogenous bone marrow MSCs are dynamic, fate-restricted participants in bone maintenance and regeneration. Cell Stem Cell. 2012 Mar 2;10(3):259–72.

48. Zhang J, Niu C, Ye L, Huang H, He X, Tong W-G, et al. Identification of the haematopoietic stem cell niche and control of the niche size. Nature. 2003 Oct 23;425(6960):836–41.

49. Rafii S, Mohle R, Shapiro F, Frey BM, Moore MA. Regulation of hematopoiesis by microvascular endothelium. Leuk Lymphoma. 1997 Nov;27(5–6):375–86.

50. Kobayashi H, Butler JM, O'Donnell R, Kobayashi M, Ding B-S, Bonner B, et al. Angiocrine factors from Akt-activated endothelial cells balance self-renewal and differentiation of haematopoietic stem cells. Nat Cell Biol. 2010 Nov;12(11):1046–56.

51. Qian H, Buza-Vidas N, Hyland CD, Jensen CT, Antonchuk J, Månsson R, et al. Critical role of thrombopoietin in maintaining adult quiescent hematopoietic stem cells. Cell Stem Cell. 2007 Dec 13;1(6):671–84.

52. Yoshihara H, Arai F, Hosokawa K, Hagiwara T, Takubo K, Nakamura Y, et al. Thrombopoietin/MPL signaling regulates hematopoietic stem cell quiescence and interaction with the osteoblastic niche. Cell Stem Cell. 2007 Dec 13;1(6):685–97.

53. Zhou BO, Ding L, Morrison SJ. Hematopoietic stem and progenitor cells regulate the regeneration of their niche by secreting Angiopoietin-1. Elife. 2015 Mar 30;4:e05521.

54. Barker JE. Sl/Sld hematopoietic progenitors are deficient in situ. Exp Hematol. 1994 Feb;22(2):174–7.

55. Ogawa M, Matsuzaki Y, Nishikawa S, Hayashi S, Kunisada T, Sudo T, et al. Expression and function of c-kit in hemopoietic progenitor cells. J Exp Med. 1991 Jul 1;174(1):63–71.

56. Czechowicz A, Kraft D, Weissman IL, Bhattacharya D. Efficient transplantation via antibody-based clearance of hematopoietic stem cell niches. Science. 2007 Nov 23;318(5854):1296–9.

57. Nagasawa T, Hirota S, Tachibana K, Takakura N, Nishikawa S, Kitamura Y, et al. Defects of B-cell lymphopoiesis and bone-marrow myelopoiesis in mice lacking the CXC chemokine PBSF/SDF-1. Nature. 1996 Aug 15;382(6592):635–8.

58. Petit I, Szyper-Kravitz M, Nagler A, Lahav M, Peled A, Habler L, et al. G-CSF induces stem cell mobilization by decreasing bone marrow SDF-1 and up-regulating CXCR4. Nat Immunol. 2002 Jul;3(7):687–94.

59. Williams DE, Eisenman J, Baird A, Rauch C, Van Ness K, March CJ, et al. Identification of a ligand for the c-kit proto-oncogene. Cell. 1990 Oct 5;63(1):167–74.

60. Copeland NG, Gilbert DJ, Cho BC, Donovan PJ, Jenkins NA, Cosman D, et al. Mast cell growth factor maps near the steel locus on mouse chromosome 10 and is deleted in a number of steel alleles. Cell. 1990 Oct 5;63(1):175–83.

61. Flanagan JG, Leder P. The kit ligand: a cell surface molecule altered in steel mutant fibroblasts. Cell. 1990 Oct 5;63(1):185–94.

62. Martin FH, Suggs SV, Langley KE, Lu HS, Ting J, Okino KH, et al. Primary structure and functional expression of rat and human stem cell factor DNAs. Cell. 1990 Oct 5;63(1):203–11.

63. Zsebo KM, Williams DA, Geissler EN, Broudy VC, Martin FH, Atkins HL, et al. Stem cell factor is encoded at the Sl locus of the mouse and is the ligand for the c-kit tyrosine kinase receptor. Cell. 1990 Oct 5;63(1):213–24.

64. Huang E, Nocka K, Beier DR, Chu TY, Buck J, Lahm HW, et al. The hematopoietic growth factor KL is encoded by the Sl locus and is the ligand of the c-kit receptor, the gene product of the W locus. Cell. 1990 Oct 5;63(1):225–33.

65. Tzeng Y-S, Li H, Kang Y-L, Chen W-C, Cheng W-C, Lai D-M. Loss of Cxcl12/Sdf-1 in adult mice decreases the quiescent state of hematopoietic stem/progenitor cells and alters the pattern of hematopoietic regeneration after myelosuppression. Blood. 2011 Jan 13;117(2):429–39.

66. Omatsu Y, Sugiyama T, Kohara H, Kondoh G, Fujii N, Kohno K, et al. The essential functions of adipo-osteogenic progenitors as the hematopoietic stem and progenitor cell niche. Immunity. 2010 Sep 24;33(3):387–99.

67. Zhou BO, Yue R, Murphy MM, Peyer J, Morrison SJ. Leptin Receptor-expressing mesenchymal stromal cells represent the main source of bone formed by adult bone marrow. Cell Stem Cell. 2014 Aug 7;15(2):154–68.

68. Maes C, Goossens S, Bartunkova S, Drogat B, Coenegrachts L, Stockmans I, et al. Increased skeletal VEGF enhances beta-catenin activity and results in excessively ossified bones. EMBO J. 2010 Jan 20;29(2):424–41.

69. Koch U, Wilson A, Cobas M, Kemler R, Macdonald HR, Radtke F. Simultaneous loss of beta- and gamma-catenin does not perturb hematopoiesis or lymphopoiesis. Blood. 2008 Jan 1;111(1):160–4.

70. Hosokawa K, Arai F, Yoshihara H, Iwasaki H, Hembree M, Yin T, et al. Cadherin-based adhesion is a potential target for niche manipulation to protect hematopoietic stem cells in adult bone marrow. Cell Stem Cell. 2010 Mar 5;6(3):194–8.

71. de Sauvage FJ, Hass PE, Spencer SD, Malloy BE, Gurney AL, Spencer SA, et al. Stimulation of megakaryocytopoiesis and thrombopoiesis by the c-Mpl ligand. Nature. 1994 Jun 16;369(6481):533–8.

72. Nakada D, Oguro H, Levi BP, Ryan N, Kitano A, Saitoh Y, et al. Oestrogen increases haematopoietic stem-cell self-renewal in females and during pregnancy. Nature. 2014 Jan 23;505(7484):555–8.

73. Goncalves KA, Silberstein L, Li S, Severe N, Hu MG, Yang H, et al. Angiogenin Promotes Hematopoietic Regeneration by Dichotomously Regulating Quiescence of Stem and Progenitor Cells. Cell. 2016 Aug 11;166(4):894–906.

74. Omatsu Y, Seike M, Sugiyama T, Kume T, Nagasawa T. Foxc1 is a critical regulator of haematopoietic stem/progenitor cell niche formation. Nature. 2014 Apr 24;508(7497):536–40.

75. Schajnovitz A, Itkin T, D'Uva G, Kalinkovich A, Golan K, Ludin A, et al. CXCL12 secretion by bone marrow stromal cells is dependent on cell contact and mediated by connexin-43 and connexin-45 gap junctions. Nat Immunol. 2011 May;12(5):391–8.

76. Katayama Y, Battista M, Kao W-M, Hidalgo A, Peired AJ, Thomas SA, et al. Signals from the sympathetic nervous system regulate hematopoietic stem cell egress from bone marrow. Cell. 2006 Jan 27;124(2):407–21.

77. Yamazaki S, Ema H, Karlsson G, Yamaguchi T, Miyoshi H, Shioda S, et al. Nonmyelinating Schwann cells maintain hematopoietic stem cell hibernation in the bone marrow niche. Cell. 2011 Nov 23;147(5):1146–58.

78. Cheng C-W, Adams GB, Perin L, Wei M, Zhou X, Lam BS, et al. Prolonged fasting reduces IGF-1/PKA to promote hematopoietic-stem-cell-based regeneration and reverse immunosuppression. Cell Stem Cell. 2014 Jun 5;14(6):810–23.

79. Bowers E, Slaughter A, Frenette PS, Kuick R, Pello OM, Lucas D. Granulocyte-derived TNFα promotes vascular and hematopoietic regeneration in the bone marrow. Nat Med. 2018 Jan;24(1):95–102.

80. Arai F, Hirao A, Ohmura M, Sato H, Matsuoka S, Takubo K, et al. Tie2/angiopoietin-1 signaling regulates hematopoietic stem cell quiescence in the bone marrow niche. Cell. 2004;118(2):149–61.

81. Ceradini DJ, Kulkarni AR, Callaghan MJ, Tepper OM, Bastidas N, Kleinman ME, et al. Progenitor cell trafficking is regulated by hypoxic gradients through HIF-1 induction of SDF-1. Nat Med. 2004 Aug;10(8):858–64.

82. Sitnicka E, Lin N, Priestley GV, Fox N, Broudy VC, Wolf NS, et al. The effect of thrombopoietin on the proliferation and differentiation of murine hematopoietic stem cells. Blood. 1996 Jun 15;87(12):4998–5005.

83. Kimura S, Roberts AW, Metcalf D, Alexander WS. Hematopoietic stem cell deficiencies in mice lacking c-Mpl, the receptor for thrombopoietin. Proc Natl Acad Sci U S A. 1998 Feb 3;95(3):1195–200.

84. Yue R, Zhou BO, Shimada IS, Zhao Z, Morrison SJ. Leptin Receptor Promotes Adipogenesis and Reduces Osteogenesis by Regulating Mesenchymal Stromal Cells in Adult Bone Marrow. Cell Stem Cell. 2016 Jun 2;18(6):782–96.

85. Mendelson A, Frenette PS. Hematopoietic stem cell niche maintenance during homeostasis and regeneration. Nature Medicine. 2014 Aug;20(8):833–46.

86. Crippa S, Bernardo ME. Mesenchymal Stromal Cells: Role in the BM Niche and in the Support of Hematopoietic Stem Cell Transplantation. Hemasphere. 2018 Nov 16;2(6).

87. Schepers K, Campbell TB, Passegué E. Normal and Leukemic Stem Cell Niches: Insights and Therapeutic Opportunities. Cell Stem Cell. 2015 Mar 5;16(3):254–67.

88. Méndez-Ferrer S, Bonnet D, Steensma DP, Hasserjian RP, Ghobrial IM, Gribben JG, et al. Bone marrow niches in haematological malignancies. Nature Reviews Cancer. 2020 May;20(5):285–98.

89. Zanetti C, Krause DS. "Caught in the net": the extracellular matrix of the bone marrow in normal hematopoiesis and leukemia. Experimental Hematology. 2020 Sep 1;89:13–25.

90. Hynes RO. The Extracellular Matrix: Not Just Pretty Fibrils. Science. 2009 Nov 27;326(5957):1216–9.

91. Bissell MJ, Hall HG, Parry G. How does the extracellular matrix direct gene expression? Journal of Theoretical Biology. 1982 Nov 7;99(1):31–68.

92. Morgan MR, Humphries MJ, Bass MD. Synergistic control of cell adhesion by integrins and syndecans. Nature Reviews Molecular Cell Biology. 2007 Dec;8(12):957–69.

93. Meyaard L. The inhibitory collagen receptor LAIR-1 (CD305). Journal of Leukocyte Biology. 2008;83(4):799–803.

94. Leitinger B, Hohenester E. Mammalian collagen receptors. Matrix Biology. 2007 Apr 1;26(3):146–55.

95. Kechagia JZ, Ivaska J, Roca-Cusachs P. Integrins as biomechanical sensors of the microenvironment. Nature Reviews Molecular Cell Biology. 2019 Aug;20(8):457–73.

96. Leisten I, Kramann R, Ventura Ferreira MS, Bovi M, Neuss S, Ziegler P, et al. 3D co-culture of hematopoietic stem and progenitor cells and mesenchymal stem cells in collagen scaffolds as a model of the hematopoietic niche. Biomaterials. 2012 Feb;33(6):1736–47.

97. Schmal O, Seifert J, Schäffer TE, Walter CB, Aicher WK, Klein G. Hematopoietic Stem and Progenitor Cell Expansion in Contact with Mesenchymal Stromal Cells in a Hanging Drop Model Uncovers Disadvantages of 3D Culture. Stem Cells Int. 2016;2016:4148093.

98. Futrega K, Atkinson K, Lott WB, Doran MR. Spheroid Coculture of Hematopoietic Stem/Progenitor Cells and Monolayer Expanded Mesenchymal Stem/Stromal Cells in Polydimethylsiloxane Microwells Modestly Improves In Vitro Hematopoietic Stem/Progenitor Cell Expansion. Tissue Eng Part C Methods. 2017 Apr;23(4):200–18.

99. Mehrasa R, Vaziri H, Oodi A, Khorshidfar M, Nikogoftar M, Golpour M, et al. Mesenchymal stem cells as a feeder layer can prevent apoptosis of expanded hematopoietic stem cells derived from cord blood. Int J Mol Cell Med. 2014;3(1):1–10.

100. Parisuthiman D, Mochida Y, Duarte WR, Yamauchi M. Biglycan modulates osteoblast differentiation and matrix mineralization. J Bone Miner Res. 2005 Oct;20(10):1878–86.

101. Chen X-D, Fisher LW, Robey PG, Young MF. The small leucine-rich proteoglycan biglycan modulates BMP-4-induced osteoblast differentiation. FASEB J. 2004 Jun;18(9):948–58.

102. Bouvard D, Brakebusch C, Gustafsson E, Aszódi A, Bengtsson T, Berna A, et al. Functional Consequences of Integrin Gene Mutations in Mice. Circulation Research. 2001 Aug 3;89(3):211–23.

103. Adams GB, Chabner KT, Alley IR, Olson DP, Szczepiorkowski ZM, Poznansky MC, et al. Stem cell engraftment at the endosteal niche is specified by the calcium-sensing receptor. Nature. 2006 Feb;439(7076):599–603.

104. Silver IA, Murrills RJ, Etherington DJ. Microelectrode studies on the acid microenvironment beneath adherent macrophages and osteoclasts. Experimental Cell Research. 1988 Apr 1;175(2):266–76.

105. Misra S, Hascall VC, Markwald RR, Ghatak S. Interactions between Hyaluronan and Its Receptors (CD44, RHAMM) Regulate the Activities of Inflammation and Cancer. Front Immunol. 2015;6:201.

106. Lesley J, Hascall VC, Tammi M, Hyman R. Hyaluronan Binding by Cell Surface CD44. Journal of Biological Chemistry. 2000 Sep 1;275(35):26967–75.

107. Vincent T, Mechti N. Extracellular matrix in bone marrow can mediate drug resistance in myeloma. Leukemia & lymphoma. 2005;46(6):803–11.

108. Feng Y, Ofek G, Choi DS, Wen J, Hu J, Zhao H, et al. Unique biomechanical interactions between myeloma cells and bone marrow stroma cells. Progress in Biophysics and Molecular Biology. 2010 Sep 1;103(1):148–56.

109. Morikawa T, Takubo K. Hypoxia regulates the hematopoietic stem cell niche. Pflugers Arch. 2016 Jan;468(1):13–22.

110. Jež M, Rožman P, Ivanović Z, Bas T. Concise review: the role of oxygen in hematopoietic stem cell physiology. J Cell Physiol. 2015 Sep;230(9):1999–2005.

111. Takubo K, Goda N, Yamada W, Iriuchishima H, Ikeda E, Kubota Y, et al. Regulation of the HIF-1alpha level is essential for hematopoietic stem cells. Cell Stem Cell. 2010 Sep 3;7(3):391–402.

112. Ivanović Z, Dello Sbarba P, Trimoreau F, Faucher JL, Praloran V. Primitive human HPCs are better maintained and expanded in vitro at 1 percent oxygen than at 20 percent. Transfusion. 2000 Dec;40(12):1482–8.

113. Hermitte F, Brunet de la Grange P, Belloc F, Praloran V, Ivanovic Z. Very low O2 concentration (0.1%) favors G0 return of dividing CD34+ cells. Stem Cells. 2006 Jan;24(1):65–73.

114. Zhang CC, Sadek HA. Hypoxia and metabolic properties of hematopoietic stem cells. Antioxid Redox Signal. 2014 Apr 20;20(12):1891–901.

115. Cipolleschi MG, Dello Sbarba P, Olivotto M. The role of hypoxia in the maintenance of hematopoietic stem cells. Blood. 1993 Oct 1;82(7):2031–7.

116. Kubota Y, Takubo K, Suda T. Bone marrow long label-retaining cells reside in the sinusoidal hypoxic niche. Biochem Biophys Res Commun. 2008 Feb 8;366(2):335–9.

117. Godet I, Shin YJ, Ju JA, Ye IC, Wang G, Gilkes DM. Fate-mapping post-hypoxic tumor cells reveals a ROS-resistant phenotype that promotes metastasis. Nature Communications. 2019 Oct 24;10(1):4862.

118. Spencer JA, Ferraro F, Roussakis E, Klein A, Wu J, Runnels JM, et al. Direct measurement of local oxygen concentration in the bone marrow of live animals. Nature. 2014 Apr 10;508(7495):269–73.

119. Ma T, Grayson WL, Fröhlich M, Vunjak-Novakovic G. Hypoxia and Stem Cell-Based Engineering of Mesenchymal Tissues. Biotechnol Prog. 2009;25(1):32–42.

120. The Nobel Prize in Physiology or Medicine 2019 [Internet]. NobelPrize.org. [cited 2021 May 29]. Available from: https://www.nobelprize.org/prizes/medicine/2019/advanced-information/

121. Shiozawa Y, Havens AM, Pienta KJ, Taichman RS. The bone marrow niche: habitat to hematopoietic and mesenchymal stem cells, and unwitting host to molecular parasites. Leukemia. 2008 May;22(5):941–50.

122. Castro-Malaspina H, Gay R, Resnick G, Kapoor N, Meyers P, Chiarieri D, et al. Characterization of human bone marrow fibroblast colony-forming cells (CFU-F) and their progeny. Blood. 1980 Aug 1;56(2):289–301.

123. Mende N, Jolly A, Percin GI, Günther M, Rostovskaya M, Krishnan SM, et al. Prospective isolation of nonhematopoietic cells of the niche and their differential molecular interactions with HSCs. Blood. 2019 Oct 10;134(15):1214–26.

124. Comazzetto S, Murphy MM, Berto S, Jeffery E, Zhao Z, Morrison SJ. Restricted Hematopoietic Progenitors and Erythropoiesis Require SCF from Leptin Receptor+ Niche Cells in the Bone Marrow. Cell Stem Cell. 2019 Mar 7;24(3):477-486.e6.

125. Kunisaki Y, Bruns I, Scheiermann C, Ahmed J, Pinho S, Zhang D, et al. Arteriolar niches maintain haematopoietic stem cell quiescence. Nature. 2013 Oct 31;502(7473):637–43.

126. Dar A, Goichberg P, Shinder V, Kalinkovich A, Kollet O, Netzer N, et al. Chemokine receptor CXCR4-dependent internalization and resecretion of functional chemokine SDF-1 by bone marrow endothelial and stromal cells. Nat Immunol. 2005 Oct;6(10):1038–46.

127. Mizoguchi T, Pinho S, Ahmed J, Kunisaki Y, Hanoun M, Mendelson A, et al. Osterix marks distinct waves of primitive and definitive stromal progenitors during bone marrow development. Dev Cell. 2014 May 12;29(3):340–9.

128. Liu Y, Strecker S, Wang L, Kronenberg MS, Wang W, Rowe DW, et al. Osterix-cre labeled progenitor cells contribute to the formation and maintenance of the bone marrow stroma. PLoS One. 2013;8(8):e71318.

129. Lacković Z, Buneta Z, Relja M, Cecuk L. [Yugoslav medical science in the Science Citation Index. 2. Relation between input and results]. Lijec Vjesn. 1987 Mar;109(2–3):49–56.

130. Jebson P, Dewar J, White J. An oxygen enrichment attachment for use with humidified air. Thorax. 1974 May;29(3):371–6.

131. Sturgess JM, Minaker E, Mitranic MM, Moscarello MA. The incorporation of L-fucose into glycoproteins in the Golgi apparatus of rat liver and in serum. Biochim Biophys Acta. 1973 Aug 17;320(1):123–32.

132. Dominici M, Le Blanc K, Mueller I, Slaper-Cortenbach I, Marini F, Krause D, et al. Minimal criteria for defining multipotent mesenchymal stromal cells. The International Society for Cellular Therapy position statement. Cytotherapy. 2006;8(4):315–7.

133. Birbrair A, Frenette PS. Niche heterogeneity in the bone marrow. Ann N Y Acad Sci. 2016 Apr;1370(1):82–96.

134. Baccin C, Al-Sabah J, Velten L, Helbling PM, Grünschläger F, Hernández-Malmierca P, et al. Combined single-cell and spatial transcriptomics reveal the molecular, cellular and spatial bone marrow niche organization. Nature Cell Biology. 2020 Jan;22(1):38–48.

135. Schofield R. The relationship between the spleen colony-forming cell and the haemopoietic stem cell. Blood Cells. 1978;4(1–2):7–25.

136. Crane GM, Jeffery E, Morrison SJ. Adult haematopoietic stem cell niches. Nature Reviews Immunology. 2017 Sep;17(9):573–90.

137. Gomes AC, Hara T, Lim VY, Herndler-Brandstetter D, Nevius E, Sugiyama T, et al. Hematopoietic stem cell niches produce lineage-instructive signals to control multipotent progenitor differentiation. Immunity. 2016;45(6):1219–31.

138. Isern J, García-García A, Martín AM, Arranz L, Martín-Pérez D, Torroja C, et al. The neural crest is a source of mesenchymal stem cells with specialized hematopoietic stem cell niche function. Elife. 2014 Sep 25;3:e03696.

139. Itkin T, Gur-Cohen S, Spencer JA, Schajnovitz A, Ramasamy SK, Kusumbe AP, et al. Distinct bone marrow blood vessels differentially regulate haematopoiesis. Nature. 2016 Apr 21;532(7599):323–8.

140. Tokoyoda K, Egawa T, Sugiyama T, Choi B-I, Nagasawa T. Cellular niches controlling B lymphocyte behavior within bone marrow during development. Immunity. 2004 Jun;20(6):707–18.

141. Becker RP, De Bruyn PP. The transmural passage of blood cells into myeloid sinusoids and the entry of platelets into the sinusoidal circulation; a scanning electron microscopic investigation. Am J Anat. 1976 Feb;145(2):183–205.

142. Kusumbe AP, Ramasamy SK, Itkin T, Mäe MA, Langen UH, Betsholtz C, et al. Age-dependent modulation of vascular niches for haematopoietic stem cells. Nature. 2016 Apr 21;532(7599):380–4.

143. Baryawno N, Przybylski D, Kowalczyk MS, Kfoury Y, Severe N, Gustafsson K, et al. A Cellular Taxonomy of the Bone Marrow Stroma in Homeostasis and Leukemia. Cell. 2019 Jun;177(7):1915-1932.e16.

144. Gomariz A, Helbling PM, Isringhausen S, Suessbier U, Becker A, Boss A, et al. Quantitative spatial analysis of haematopoiesis-regulating stromal cells in the bone marrow microenvironment by 3D microscopy. Nat Commun. 2018 Jun 28;9(1):2532.

145. Burgess DJ. Spatial transcriptomics coming of age. Nat Rev Genet. 2019 Jun;20(6):317.

146. Chen W-T, Lu A, Craessaerts K, Pavie B, Sala Frigerio C, Corthout N, et al. Spatial Transcriptomics and In Situ Sequencing to Study Alzheimer's Disease. Cell. 2020 Aug 20;182(4):976-991.e19.

147. Vickovic S, Eraslan G, Salmén F, Klughammer J, Stenbeck L, Schapiro D, et al. High-definition spatial transcriptomics for in situ tissue profiling. Nat Methods. 2019 Oct;16(10):987–90.

148. Batsivari A, Haltalli MLR, Passaro D, Pospori C, Lo Celso C, Bonnet D. Dynamic responses of the haematopoietic stem cell niche to diverse stresses. Nature Cell Biology. 2020 Jan;22(1):7–17.

149. Johnson CB, Zhang J, Lucas D. The Role of the Bone Marrow Microenvironment in the Response to Infection. Front Immunol. 2020;11(585402).

150. Takizawa H, Boettcher S, Manz MG. Demand-adapted regulation of early hematopoiesis in infection and inflammation. Blood. 2012 Mar 29;119(13):2991–3002.

151. Essers MAG, Offner S, Blanco-Bose WE, Waibler Z, Kalinke U, Duchosal MA, et al. IFNalpha activates dormant haematopoietic stem cells in vivo. Nature. 2009 Apr 16;458(7240):904–8.

152. Walter D, Lier A, Geiselhart A, Thalheimer FB, Huntscha S, Sobotta MC, et al. Exit from dormancy provokes DNA-damage-induced attrition in haematopoietic stem cells. Nature. 2015 Apr 23;520(7548):549–52.

153. Nagai Y, Garrett KP, Ohta S, Bahrun U, Kouro T, Akira S, et al. Toll-like receptors on hematopoietic progenitor cells stimulate innate immune system replenishment. Immunity. 2006 Jun;24(6):801–12.

154. Baldridge MT, King KY, Boles NC, Weksberg DC, Goodell MA. Quiescent haematopoietic stem cells are activated by IFN-gamma in response to chronic infection. Nature. 2010 Jun 10;465(7299):793–7.

155. Vainieri ML, Blagborough AM, MacLean AL, Haltalli MLR, Ruivo N, Fletcher HA, et al. Systematic tracking of altered haematopoiesis during sporozoite-mediated malaria development reveals multiple response points. Open Biol. 2016 Jun;6(6).

156. Matatall KA, Jeong M, Chen S, Sun D, Chen F, Mo Q, et al. Chronic Infection Depletes Hematopoietic Stem Cells through Stress-Induced Terminal Differentiation. Cell Rep. 2016 Dec 6;17(10):2584–95.

157. Rashidi NM, Scott MK, Scherf N, Krinner A, Kalchschmidt JS, Gounaris K, et al. In vivo time-lapse imaging shows diverse niche engagement by quiescent and naturally activated hematopoietic stem cells. Blood. 2014 Jul 3;124(1):79–83.

158. Boettcher S, Gerosa RC, Radpour R, Bauer J, Ampenberger F, Heikenwalder M, et al. Endothelial cells translate pathogen signals into G-CSF-driven emergency granulopoiesis. Blood. 2014 Aug 28;124(9):1393–403.

159. Prendergast ÁM, Kuck A, van Essen M, Haas S, Blaszkiewicz S, Essers MAG. IFNα-mediated remodeling of endothelial cells in the bone marrow niche. Haematologica. 2017 Mar;102(3):445–53.

160. Khakpour S, Wilhelmsen K, Hellman J. Vascular endothelial cell Toll-like receptor pathways in sepsis. Innate Immun. 2015 Nov;21(8):827–46.

161. Shi C, Jia T, Mendez-Ferrer S, Hohl TM, Serbina NV, Lipuma L, et al. Bone marrow mesenchymal stem and progenitor cells induce monocyte emigration in response to circulating toll-like receptor ligands. Immunity. 2011 Apr 22;34(4):590–601.

162. Chou DB, Sworder B, Bouladoux N, Roy CN, Uchida AM, Grigg M, et al. Stromal-derived IL-6 alters the balance of myeloerythroid progenitors during Toxoplasma gondii infection. J Leukoc Biol. 2012 Jul;92(1):123–31.

163. Schürch CM, Riether C, Ochsenbein AF. Cytotoxic CD8+ T cells stimulate hematopoietic progenitors by promoting cytokine release from bone marrow mesenchymal stromal cells. Cell Stem Cell. 2014 Apr 3;14(4):460–72.

164. Ivashkiv LB, Donlin LT. Regulation of type I interferon responses. Nat Rev Immunol. 2014 Jan;14(1):36–49.

165. Stark GR, Kerr IM, Williams BRG, Silverman RH, Schreiber RD. How Cells Respond to Interferons. Annual Review of Biochemistry. 1998;67(1):227–64.

166. Gough DJ, Messina NL, Clarke CJP, Johnstone RW, Levy DE. Constitutive type I interferon modulates homeostatic balance through tonic signaling. Immunity. 2012 Feb 24;36(2):166–74.

167. Venkatesh D, Ernandez T, Rosetti F, Batal I, Cullere X, Luscinskas FW, et al. Endothelial TNF receptor 2 induces IRF1 transcription factor-dependent interferon-β autocrine signaling to promote monocyte recruitment. Immunity. 2013 May 23;38(5):1025–37.

168. Yarilina A, Park-Min K-H, Antoniv T, Hu X, Ivashkiv LB. TNF activates an IRF1-dependent autocrine loop leading to sustained expression of chemokines and STAT1-dependent type I interferon-response genes. Nat Immunol. 2008 Apr;9(4):378–87.

169. Paludan SR, Bowie AG. Immune sensing of DNA. Immunity. 2013 May 23;38(5):870–80.

170. Iwasaki A. A virological view of innate immune recognition. Annu Rev Microbiol. 2012;66:177–96.

171. Hertzog PJ, Williams BRG. Fine tuning type I interferon responses. Cytokine Growth Factor Rev. 2013 Jun;24(3):217–25.

172. Pestka S, Krause CD, Walter MR. Interferons, interferon-like cytokines, and their receptors. Immunol Rev. 2004 Dec;202:8–32.

173. Goulard M, Dosquet C, Bonnet D. Role of the microenvironment in myeloid malignancies. Cellular and Molecular Life Sciences. 2018 Apr;75(8):1377–91.

174. Huntly BJP, Gilliland DG. Leukaemia stem cells and the evolution of cancer-stem-cell research. Nat Rev Cancer. 2005 Apr;5(4):311–21.

175. Kiel MJ, Yilmaz OH, Iwashita T, Yilmaz OH, Terhorst C, Morrison SJ. SLAM family receptors distinguish hematopoietic stem and progenitor cells and reveal endothelial niches for stem cells. Cell. 2005 Jul 1;121(7):1109–21.

176. Shanafelt T, Zent C, Byrd J, Erlichman C, LaPlant B, Ghosh A, et al. Phase II Trials of Single Agent Anti-VEGF Therapy for Patients with Chronic Lymphocytic Leukemia (CLL). Leuk Lymphoma. 2010 Dec;51(12):2222–9.

177. Ria R, Melaccio A, Racanelli V, Vacca A. Anti-VEGF Drugs in the Treatment of Multiple Myeloma Patients. J Clin Med. 2020 Jun 6;9(6):1765.

178. Duarte D, Hawkins ED, Akinduro O, Ang H, De Filippo K, Kong IY, et al. Inhibition of Endosteal Vascular Niche Remodeling Rescues Hematopoietic Stem Cell Loss in AML. Cell Stem Cell. 2018 Jan 4;22(1):64-77.e6.

179. Fiedler W, Graeven U, Ergün S, Verago S, Kilic N, Stockschläder M, et al. Vascular endothelial growth factor, a possible paracrine growth factor in human acute myeloid leukemia. Blood. 1997 Mar 15;89(6):1870–5.

180. Passaro D, Di Tullio A, Abarrategi A, Rouault-Pierre K, Foster K, Ariza-McNaughton L, et al. Increased Vascular Permeability in the Bone Marrow Microenvironment Contributes to Disease Progression and Drug Response in Acute Myeloid Leukemia. Cancer Cell. 2017 Sep 11;32(3):324-341.e6.

181. von der Heide EK, Neumann M, Baldus CD. Targeting the leukemic bone marrow microenvironment. Oncotarget. 2017 Oct 27;8(57):96474–5.

182. Geyh S, Oz S, Cadeddu R-P, Fröbel J, Brückner B, Kündgen A, et al. Insufficient stromal support in MDS results from molecular and functional deficits of mesenchymal stromal cells. Leukemia. 2013 Sep;27(9):1841–51.

183. Manshouri T, Estrov Z, Quintás-Cardama A, Burger J, Zhang Y, Livun A, et al. Bone marrow stroma-secreted cytokines protect JAK2(V617F)-mutated cells from the effects of a JAK2 inhibitor. Cancer Res. 2011 Jun 1;71(11):3831–40.

184. Guarnerio J, Mendez LM, Asada N, Menon AV, Fung J, Berry K, et al. A non-cell-autonomous role for Pml in the maintenance of leukemia from the niche. Nat Commun. 2018 Jan 4;9(1):66.

185. The Nobel Prize in Physiology or Medicine 1990 [Internet]. NobelPrize.org. [cited 2020 Nov 23]. Available from: https://www.nobelprize.org/prizes/medicine/1990/thomas/facts/

186. Galleu A, Milojkovic D, Deplano S, Szydlo R, Loaiza S, Wynn R, et al. Mesenchymal stromal cells for acute graft-versus-host disease: response at 1 week predicts probability of survival. British journal of haematology. 2019;185(1):89–92.

187. Wood ME, Vogel V, Ng A, Foxhall L, Goodwin P, Travis LB. Second malignant neoplasms: assessment and strategies for risk reduction. J Clin Oncol. 2012 Oct 20;30(30):3734–45.

188. Kondo H, Searby ND, Mojarrab R, Phillips J, Alwood J, Yumoto K, et al. Total-body irradiation of postpubertal mice with (137)Cs acutely compromises the microarchitecture of cancellous bone and increases osteoclasts. Radiat Res. 2009 Mar;171(3):283–9.

189. Willey JS, Lloyd SAJ, Robbins ME, Bourland JD, Smith-Sielicki H, Bowman LC, et al. Early increase in osteoclast number in mice after whole-body irradiation with 2 Gy X rays. Radiat Res. 2008 Sep;170(3):388–92.

190. Gong B, Oest ME, Mann KA, Damron TA, Morris MD. Raman spectroscopy demonstrates prolonged alteration of bone chemical composition following extremity localized irradiation. Bone. 2013 Nov;57(1):252–8.

191. Mauch P, Constine L, Greenberger J, Knospe W, Sullivan J, Liesveld JL, et al. Hematopoietic stem cell compartment: acute and late effects of radiation therapy and chemotherapy. Int J Radiat Oncol Biol Phys. 1995 Mar 30;31(5):1319–39.

192. Green DE, Rubin CT. Consequences of irradiation on bone and marrow phenotypes, and its relation to disruption of hematopoietic precursors. Bone. 2014 Jun;63:87–94.

193. Rieger K, Marinets O, Fietz T, Körper S, Sommer D, Mücke C, et al. Mesenchymal stem cells remain of host origin even a long time after allogeneic peripheral blood stem cell or bone marrow transplantation. Exp Hematol. 2005 May;33(5):605–11.

194. Abbuehl J-P, Tatarova Z, Held W, Huelsken J. Long-Term Engraftment of Primary Bone Marrow Stromal Cells Repairs Niche Damage and Improves Hematopoietic Stem Cell Transplantation. Cell Stem Cell. 2017 Aug 3;21(2):241-255.e6.

195. Zhou BO, Yu H, Yue R, Zhao Z, Rios JJ, Naveiras O, et al. Bone marrow adipocytes promote the regeneration of stem cells and haematopoiesis by secreting SCF. Nat Cell Biol. 2017 Aug;19(8):891–903.

196. Gencheva M, Hare I, Kurian S, Fortney J, Piktel D, Wysolmerski R, et al. Bone marrow osteoblast vulnerability to chemotherapy. Eur J Haematol. 2013 Jun;90(6):469–78.

197. Zhao M, Perry JM, Marshall H, Venkatraman A, Qian P, He XC, et al. Megakaryocytes maintain homeostatic quiescence and promote post-injury regeneration of hematopoietic stem cells. Nat Med. 2014 Nov;20(11):1321–6.

198. Itkin T, Ludin A, Gradus B, Gur-Cohen S, Kalinkovich A, Schajnovitz A, et al. FGF-2 expands murine hematopoietic stem and progenitor cells via proliferation of stromal cells, c-Kit activation, and CXCL12 down-regulation. Blood. 2012 Aug 30;120(9):1843–55.

199. Hérault A, Binnewies M, Leong S, Calero-Nieto FJ, Zhang SY, Kang Y-A, et al. Myeloid progenitor cluster formation drives emergency and leukaemic myelopoiesis. Nature. 2017 Apr 6;544(7648):53–8.

200. Lucas D, Scheiermann C, Chow A, Kunisaki Y, Bruns I, Barrick C, et al. Chemotherapy-induced bone marrow nerve injury impairs hematopoietic regeneration. Nat Med. 2013 Jun;19(6):695–703.

201. Barrett DM, Teachey DT, Grupp SA. Toxicity management for patients receiving novel T-cell engaging therapies. Curr Opin Pediatr. 2014 Feb;26(1):43–9.

202. Giavridis T, van der Stegen SJC, Eyquem J, Hamieh M, Piersigilli A, Sadelain M. CAR T cell-induced cytokine release syndrome is mediated by macrophages and abated by IL-1 blockade. Nat Med. 2018 Jun;24(6):731–8.

203. Grupp SA, Kalos M, Barrett D, Aplenc R, Porter DL, Rheingold SR, et al. Chimeric antigen receptor-modified T cells for acute lymphoid leukemia. N Engl J Med. 2013 Apr 18;368(16):1509–18.

204. Maude SL, Frey N, Shaw PA, Aplenc R, Barrett DM, Bunin NJ, et al. Chimeric antigen receptor T cells for sustained remissions in leukemia. N Engl J Med. 2014 Oct 16;371(16):1507–17.

205. Bello AB, Park H, Lee S-H. Current approaches in biomaterial-based hematopoietic stem cell niches. Acta Biomaterialia. 2018 May 1;72:1–15.

206. Martin PS, Li S, Nikiforow S, Alyea EP, Antin JH, Armand P, et al. Infused total nucleated cell dose is a better predictor of transplant outcomes than CD34+ cell number in reduced-intensity mobilized peripheral blood allogeneic hematopoietic cell transplantation. 1. 2016 Apr 1;101(4):499–505.

207. Boitano AE, Wang J, Romeo R, Bouchez LC, Parker AE, Sutton SE, et al. Aryl Hydrocarbon Receptor Antagonists Promote the Expansion of Human Hematopoietic Stem Cells. Science. 2010 Sep 10;329(5997):1345–8.

208. Fares I, Chagraoui J, Gareau Y, Gingras S, Ruel R, Mayotte N, et al. Pyrimidoindole derivatives are agonists of human hematopoietic stem cell self-renewal. Science. 2014 Sep 19;345(6203):1509–12.

209. Wagner JE, Brunstein CG, Boitano AE, DeFor TE, McKenna D, Sumstad D, et al. Phase I/II Trial of StemRegenin-1 Expanded Umbilical Cord Blood Hematopoietic Stem Cells Supports Testing as a Stand-Alone Graft. Cell Stem Cell. 2016 Jan 7;18(1):144–55.

210. Yonemura Y, Ku H, Lyman SD, Ogawa M. In Vitro Expansion of Hematopoietic Progenitors and Maintenance of Stem Cells: Comparison Between FLT3/FLK-2 Ligand and KIT Ligand. Blood. 1997 Mar 15;89(6):1915–21.

211. Gattazzo F, Urciuolo A, Bonaldo P. Extracellular matrix: A dynamic microenvironment for stem cell niche. Biochimica et Biophysica Acta (BBA) - General Subjects. 2014 Aug 1;1840(8):2506–19.

212. Discher DE, Mooney DJ, Zandstra PW. Growth Factors, Matrices, and Forces Combine and Control Stem Cells. Science. 2009 Jun 26;324(5935):1673–7.

213. Wilkinson AC, Ishida R, Kikuchi M, Sudo K, Morita M, Crisostomo RV, et al. Long-term ex vivo haematopoietic-stem-cell expansion allows nonconditioned transplantation. Nature. 2019 Jul;571(7763):117–21.

214. LaIuppa JA, McAdams TA, Papoutsakis ET, Miller WM. Culture materials affect ex vivo expansion of hematopoietic progenitor cells. J Biomed Mater Res. 1997 Sep 5;36(3):347–59.

215. Franke K, Pompe T, Bornhäuser M, Werner C. Engineered matrix coatings to modulate the adhesion of CD133+ human hematopoietic progenitor cells. Biomaterials. 2007 Feb;28(5):836–43.

216. Feng Q, Chai C, Jiang X-S, Leong KW, Mao H-Q. Expansion of engrafting human hematopoietic stem/progenitor cells in three-dimensional scaffolds with surface-immobilized fibronectin. J Biomed Mater Res A. 2006 Sep 15;78(4):781–91.

217. Dao MA, Hashino K, Kato I, Nolta JA. Adhesion to fibronectin maintains regenerative capacity during ex vivo culture and transduction of human hematopoietic stem and progenitor cells. Blood. 1998 Dec 15;92(12):4612–21.

218. Chua K-N, Chai C, Lee P-C, Tang Y-N, Ramakrishna S, Leong KW, et al. Surface-aminated electrospun nanofibers enhance adhesion and expansion of human umbilical cord blood hematopoietic stem/progenitor cells. Biomaterials. 2006 Dec;27(36):6043–51.

219. Li Y, Ma T, Kniss DA, Yang ST, Lasky LC. Human cord cell hematopoiesis in three-dimensional nonwoven fibrous matrices: in vitro simulation of the marrow microenvironment. J Hematother Stem Cell Res. 2001 Jun;10(3):355–68.

220. Sharma MB, Limaye LS, Kale VP. Mimicking the functional hematopoietic stem cell niche in vitro: recapitulation of marrow physiology by hydrogel-based three-dimensional cultures of mesenchymal stromal cells. Haematologica. 2012 May;97(5):651–60.

221. Torisawa Y, Spina CS, Mammoto T, Mammoto A, Weaver JC, Tat T, et al. Bone marrow-on-a-chip replicates hematopoietic niche physiology in vitro. Nat Methods. 2014 Jun;11(6):663–9.

222. Choi JS, Mahadik BP, Harley BAC. Engineering the hematopoietic stem cell niche: Frontiers in biomaterial science. Biotechnol J. 2015 Oct;10(10):1529–45.

223. Ferreira MSV, Jahnen-Dechent W, Labude N, Bovi M, Hieronymus T, Zenke M, et al. Cord blood-hematopoietic stem cell expansion in 3D fibrin scaffolds with stromal support. Biomaterials. 2012;33(29):6987–97.

224. Perry JM, He XC, Sugimura R, Grindley JC, Haug JS, Ding S, et al. Cooperation between both Wnt/{beta}-catenin and PTEN/PI3K/Akt signaling promotes primitive hematopoietic stem cell self-renewal and expansion. Genes Dev. 2011 Sep 15;25(18):1928–42.

225. Huang J, Nguyen-McCarty M, Hexner EO, Danet-Desnoyers G, Klein PS. Maintenance of hematopoietic stem cells through regulation of Wnt and mTOR pathways. Nat Med. 2012 Dec;18(12):1778–85.

226. Pinho S, Lacombe J, Hanoun M, Mizoguchi T, Bruns I, Kunisaki Y, et al. PDGFRα and CD51 mark human Nestin+ sphere-forming mesenchymal stem cells capable of hematopoietic progenitor cell expansion. Journal of Experimental Medicine. 2013 Jun 17;210(7):1351–67.

227. Haas S, Hansson J, Klimmeck D, Loeffler D, Velten L, Uckelmann H, et al. Inflammation-Induced Emergency Megakaryopoiesis Driven by Hematopoietic Stem Cell-like Megakaryocyte Progenitors. Cell Stem Cell. 2015 Oct 1;17(4):422–34.

228. Florez MA, Matatall KA, Jeong Y, Ortinau L, Shafer PW, Lynch AM, et al. Interferon Gamma Mediates Hematopoietic Stem Cell Activation and Niche Relocalization through BST2. Cell Rep. 2020 Dec 22;33(12):108530.

229. Goedhart M, Cornelissen AS, Kuijk C, Geerman S, Kleijer M, van Buul JD, et al. Interferon-Gamma Impairs Maintenance and Alters Hematopoietic Support of Bone Marrow Mesenchymal Stromal Cells. Stem Cells Dev. 2018 May 1;27(9):579–89.

230. Helbling PM, Piñeiro-Yáñez E, Gerosa R, Boettcher S, Al-Shahrour F, Manz MG, et al. Global Transcriptomic Profiling of the Bone Marrow Stromal Microenvironment during Postnatal Development, Aging, and Inflammation. Cell Reports. 2019 Dec;29(10):3313-3330.e4.

231. Leimkühler NB, Gleitz HFE, Ronghui L, Snoeren IAM, Fuchs SNR, Nagai JS, et al. Heterogeneous bone-marrow stromal progenitors drive myelofibrosis via a druggable alarmin axis. Cell Stem Cell. 2021 Apr 1;28(4):637-652.e8.

232. Maryanovich M, Zahalka AH, Pierce H, Pinho S, Nakahara F, Asada N, et al. Adrenergic nerve degeneration in bone marrow drives aging of the hematopoietic stem cell niche. Nature Medicine. 2018 Jun;24(6):782–91.

233. Saçma M, Pospiech J, Bogeska R, de Back W, Mallm J-P, Sakk V, et al. Haematopoietic stem cells in perisinusoidal niches are protected from ageing. Nat Cell Biol. 2019 Nov;21(11):1309–20.

234. Ho Y-H, Del Toro R, Rivera-Torres J, Rak J, Korn C, García-García A, et al. Remodeling of Bone Marrow Hematopoietic Stem Cell Niches Promotes Myeloid Cell Expansion during Premature or Physiological Aging. Cell Stem Cell. 2019 Sep 5;25(3):407-418.e6.

235. Sambuceti G, Brignone M, Marini C, Massollo M, Fiz F, Morbelli S, et al. Estimating the whole bone-marrow asset in humans by a computational approach to integrated PET/CT imaging. Eur J Nucl Med Mol Imaging. 2012 Aug;39(8):1326–38.

236. Ono N, Ono W, Mizoguchi T, Nagasawa T, Frenette PS, Kronenberg HM. Vasculature-associated cells expressing nestin in developing bones encompass early cells in the osteoblast and endothelial lineage. Dev Cell. 2014 May 12;29(3):330–9.

237. Ding L, Morrison SJ. Haematopoietic stem cells and early lymphoid progenitors occupy distinct bone marrow niches. Nature. 2013 Mar 14;495(7440):231–5.

238. Hara T, Tanegashima K. CXCL14 antagonizes the CXCL12-CXCR4 signaling axis. Biomol Concepts. 2014 May;5(2):167–73.

239. An W, Mohapatra BC, Zutshi N, Bielecki TA, Goez BT, Luan H, et al. VAV1-Cre mediated hematopoietic deletion of CBL and CBL-B leads to JMML-like aggressive early-neonatal myeloproliferative disease. Oncotarget. 2016 Sep 13;7(37):59006–16.

240. Gregory CD, Devitt A. The macrophage and the apoptotic cell: an innate immune interaction viewed simplistically? Immunology. 2004 Sep;113(1):1–14.

241. Fujisaki J, Wu J, Carlson AL, Silberstein L, Putheti P, Larocca R, et al. In vivo imaging of Treg cells providing immune privilege to the haematopoietic stem-cell niche. Nature. 2011 Jun 8;474(7350):216–9.

242. Li N, Hua J. Interactions between mesenchymal stem cells and the immune system. Cell Mol Life Sci. 2017 Jul;74(13):2345–60.

243. Gao F, Chiu SM, Motan D a. L, Zhang Z, Chen L, Ji H-L, et al. Mesenchymal stem cells and immunomodulation: current status and future prospects. Cell Death Dis. 2016 Jan 21;7:e2062.

244. Strioga M, Viswanathan S, Darinskas A, Slaby O, Michalek J. Same or not the same? Comparison of adipose tissue-derived versus bone marrow-derived mesenchymal stem and stromal cells. Stem Cells Dev. 2012 Sep 20;21(14):2724–52.

245. Koliaraki V, Prados A, Armaka M, Kollias G. The mesenchymal context in inflammation, immunity and cancer. Nature Immunology. 2020 Sep;21(9):974–82.

246. Nowarski R, Jackson R, Flavell RA. The Stromal Intervention: Regulation of Immunity and Inflammation at the Epithelial-Mesenchymal Barrier. Cell. 2017 Jan 26;168(3):362–75.

247. Naik S, Larsen SB, Cowley CJ, Fuchs E. Two to tango: dialogue between immunity and stem cells in health and disease. Cell. 2018 Nov 1;175(4):908–20.

248. Takamura S. Niches for the Long-Term Maintenance of Tissue-Resident Memory T Cells. Front Immunol. 2018;9(01214).

249. Schaumann DHS, Tuischer J, Ebell W, Manz RA, Lauster R. VCAM-1-positive stromal cells from human bone marrow producing cytokines for B lineage progenitors and for plasma cells: SDF-1, flt3L, and BAFF. Mol Immunol. 2007 Mar;44(7):1606–12.

250. Ulyanova T, Scott LM, Priestley GV, Jiang Y, Nakamoto B, Koni PA, et al. VCAM-1 expression in adult hematopoietic and nonhematopoietic cells is controlled by tissue-inductive signals and reflects their developmental origin. Blood. 2005 Jul 1;106(1):86–94.

251. Tajer P, Pike-Overzet K, Arias S, Havenga M, Staal FJT. Ex Vivo Expansion of Hematopoietic Stem Cells for Therapeutic Purposes: Lessons from Development and the Niche. Cells. 2019 Feb 18;8(2):169.

252. Bai T, Li J, Sinclair A, Imren S, Merriam F, Sun F, et al. Expansion of primitive human hematopoietic stem cells by culture in a zwitterionic hydrogel. Nature Medicine. 2019 Oct;25(10):1566–75.

253. Ribeiro-Filho AC, Levy D, Ruiz JLM, Mantovani M da C, Bydlowski SP. Traditional and Advanced Cell Cultures in Hematopoietic Stem Cell Studies. Cells. 2019 Dec 12;8(12):1628.

254. Chen Q. The niche for hematopoietic stem cell expansion: a collaboration network. Cellular & Molecular Immunology. 2017 Oct;14(10):865–7.

255. Glettig DL, Kaplan DL. Extending Human Hematopoietic Stem Cell Survival In Vitro with Adipocytes. Biores Open Access. 2013 Jun;2(3):179–85.

256. Paix A, Antoni D, Waissi W, Ledoux M-P, Bilger K, Fornecker L, et al. Total body irradiation in allogeneic bone marrow transplantation conditioning regimens: A review. Crit Rev Oncol Hematol. 2018 Mar;123:138–48.

257. Reske SN, Bunjes D, Buchmann I, Seitz U, Glatting G, Neumaier B, et al. Targeted bone marrow irradiation in the conditioning of high-risk leukaemia prior to stem cell transplantation. Eur J Nucl Med. 2001 Jul;28(7):807–15.

258. Brehm MA, Racki WJ, Leif J, Burzenski L, Hosur V, Wetmore A, et al. Engraftment of human HSCs in nonirradiated newborn NOD-scid IL2rγnull mice is enhanced by transgenic expression of membrane-bound human SCF. Blood. 2012 Mar 22;119(12):2778–88.

259. Waskow C, Rodewald H-R. Lymphocyte development in neonatal and adult c-Kit-deficient (c-KitW/W) mice. Adv Exp Med Biol. 2002;512:1–10.

260. Waskow C, Paul S, Haller C, Gassmann M, Rodewald H-R. Viable c-Kit(W/W) mutants reveal pivotal role for c-kit in the maintenance of lymphopoiesis. Immunity. 2002 Sep;17(3):277–88.

261. Chen H, Jiang M, Xiao L, Huang H. Single-cell qPCR facilitates the optimization of hematopoietic differentiation in hPSCs/OP9 coculture system. Braz J Med Biol Res. 2018 Mar 15;51(5):e7183.

262. Weisel KC, Moore MAS, Kanz L, Möhle R. Extended in vitro expansion of adult, mobilized CD34+ cells without significant cell senescence using a stromal cell coculture system with single cytokine support. Stem Cells Dev. 2009 Mar;18(2):229–34.

263. Holmes R, Zúñiga-Pflücker JC. The OP9-DL1 system: generation of T-lymphocytes from embryonic or hematopoietic stem cells in vitro. Cold Spring Harb Protoc. 2009 Feb;2009(2):pdb.prot5156.

264. Morgan EF, Barnes GL, Einhorn TA. Chapter 1 - The Bone Organ System: Form and Function. In: Marcus R, Feldman D, Dempster DW, Luckey M, Cauley JA, editors. Osteoporosis. Fourth. San Diego: Academic Press; 2013. p. 3–20.

265. Staines KA, Brown G, Farquharson C. The Ex Vivo Organ Culture of Bone. Methods Mol Biol. 2019;1914:199–215.

266. Pinho S, Frenette PS. Haematopoietic stem cell activity and interactions with the niche. Nat Rev Mol Cell Biol. 2019 May;20(5):303–20.

267. Hoggatt J, Kfoury Y, Scadden DT. Hematopoietic Stem Cell Niche in Health and Disease. Annu Rev Pathol. 2016 May 23;11:555–81.

268. Yu VWC, Scadden DT. Heterogeneity of the bone marrow niche. Curr Opin Hematol. 2016 Jul;23(4):331–8.

8 APPENDIX

8.1 List of abbreviations

Abbreviations	Explanation
BL	Bone lining
BM	Bone marrow
BrdU	Bromodeoxyuridine / 5-bromo-2'-deoxyuridine
CAR cell	CXCL12-abundant reticular cells
CFU-F	Colony-forming unit-fibroblasts
CFU-GEMM	Colony-forming unit − granulocyte, erythroid, macrophage, megakaryocyte
CTFr	Cell Trace Far-red
CTV	Cell Trace Violet
ECM	Extracellular matrix
ELDA	Extreme limiting dilution analysis
Endo	Endothelial cells
FUCCI	Fluorescent Ubiquitination-based Cell Cycle Indicator
GSEA	Gene Set Enrichment Analysis
HSC	Hematopoietic stem cell
HSPC	Hematopoietic stem and progenitor cell
IFITM	Interferon-induced transmembrane
IFN	Interferon
IFN-I	Type I IFN
IFNAR	IFN-α receptor
Ifnar$^{-/-}$	Type-I IFN receptors knockout
iMSC	Inflammation-responding mesenchymal stem cells

IRF9	Interferon regulatory factor 9
ISG	IFN stimulated gene
ISGF3	ISG factor 3
ISRE	IFN stimulated response elements
LT-HSC	Long-term HSC
MDS	Myelodysplastic syndrome
MPN	Myeloproliferative neoplasm
MSC	Mesenchymal stem/stromal cell
PASC	Plastic adherent stromal cells
PB	Peripheral blood
PCA	Principal component analysis
pI:C	Polyinosinic:polycytidylic acid
rMSC	Reinvigorating mesenchymal stem cells
SC	Single cell-RNA-seq.
SCs	Stromal cells
Sca-1	Stem cell antigen 1
SCF	Stem cell factor
Stat$^{-/-}$	Cytoplasmic transcription factor STAT1 knockout
TF	Transcription factors
WT	Wildtype

8.2 List of figures